Aalto University
School of Chemical
Technology

School of Chemical Technology
Degree Programme of Chemical Technology

Mikael Männistö

NEW LEWIS-CELL TYPE MEASUREMENT APPARATUS SETUP AND VALIDATION ALONG WITH NEW ACID GAS ABSORPTION MEASUREMENTS INTO PHASE-CHANGE SOLVENTS

Master's thesis for the degree of Master of Science in Technology submitted for inspection, Espoo, 2 March, 2015.

Supervisor **Professor Ville Alopaeus**

Instructors **D. Sc. (Tech) Petri Uusi-Kyyny**
PhD Hernando Guerrero Amaya

Aalto University
School of Chemical
Technology

Aalto University, P.O. BOX 11000, 00076
AALTO
www.aalto.fi

Abstract of master's thesis

Author Mikael Männistö

Title of thesis New Lewis-cell type measurement apparatus setup and validation along with new acid gas absorption measurements into phase-change solvents

Department Chemical Engineering

Professorship Processes and products **Code of professorship** Kem-42

Thesis supervisor Prof. Ville Alopaeus

Thesis advisor(s) / Thesis examiner(s) D. Sc. (Tech) Petri Uusi-Kyyny and PhD Hernando Guerrero Amaya

Date 2.3.2015 **Number of pages** 109+ 27 **Language** English

Abstract

Gas absorption is very important in the modern world of industry, as there are multiple sources of toxic and hazardous gases involved with it. Absorption is used as a method of carbon capture and to purify these gas streams.

This work aims to provide more insight in to variables closely related to absorption of acid gases in to aqueous alkanolamine solutions. These variables come from phase equilibria, reaction kinetics and mass transfer kinetics. In this work the focus is on reaction kinetics and mass transfer kinetics for both carbon dioxide and hydrogen sulfide in to primary, secondary and tertiary alkanolamines.

A literature survey on existing equipment and the background theory behind the phenomena was conducted. A new apparatus was set up and used inside the laboratory. The new apparatus was first validated and additional data for N-Methyldiethanolamine and carbon dioxide absorption were provided. In addition new data for carbon dioxide and hydrogen sulfide absorption into 2-(diethylamino)-ethanol and 3-(methylamino)-propylamine were provided and analyzed. In the light of the studies provided in this thesis, despite being effective in carbon dioxide capture, the studied composition (5M MAPA + 2M DEEA) of this phase change solvent does not seem viable for hydrogen sulfide absorption. Further studies related to VLLE measurements of carbon dioxide loaded MAPA+DEEA solution in various compositions are suggested to better understand the distribution of the acid gas(es) in the liquid when a phase-split is observed.

Keywords Absorption, MDEA, Methyldiethanolamine, DEEA, 2-(diethylamino)-ethanol, MAPA, 3-(methylamino)-propylamine, sour gas, Hydrogen sulfide, H_2S, Carbon Dioxide, CO_2

Aalto-yliopisto
Kemian tekniikan korkeakoulu

Aalto-yliopisto, PL 11000, 00076
AALTO
www.aalto.fi

Diplomityön tiivistelmä

Tekijä Mikael Männistö

Työn nimi Uuden Lewis-tyyppisen kennon käyttöönotto ja validointi sekä uusien kaasun absorptionopeusmittauksien suorittaminen faasimuunnosliuottimiin

Laitos Kemian tekniikka

Professuuri Prosessit ja tuotteet **Professuurikoodi** Kem-42

Työn valvoja Prof. Ville Alopaeus

Työn ohjaaja(t)/Työn tarkastaja(t) TkT Petri Uusi-Kyyny ja FT Hernando Guerrero Amaya

Päivämäärä 2.3.2015 **Sivumäärä** 109+ 27 **Kieli** Englanti

Tiivistelmä

Kaasun absorptio on modernissa teollistuneessa maailmassa erittäin tärkeä työväline, johtuen useista haitallisten ja myrkyllisten kaasujen lähteistä prosessiteollisuudessa. Absorptiota käytetään näiden kaasuvirtojen puhdistukseen ja hiilidioksidin talteenottoon.

Tässä työssä pyritään lisäämään ymmärrystä niistä muuttujista, jotka vaikuttavat kaasujen absorptioon amiinien vesiseoksiin. Nämä muuttujat koostuvat faasitasapainosta riippuvista tekijöistä, reaktioihin ja aineensiirtoon liittyvistä kineettisistä ominaisuuksista sekä laitteiston suunnitteluun vaikuttavista hydrodynaamisista ominaisuuksista. Työ painottuu hiilidioksidin ja rikkivedyn reaktioihin ja aineensiirtoon liittyvän kinetiikan mittauksiin primäärisissä, sekundäärisissä ja tertiäärisissiä amiiniliuoksissa.

Kirjallisuustutkimuksessa paneudutaan absorptioon vaikuttavin ilmiöihin. Kokeellinen osa koostuu laitteiston käyttöönotosta sekä validoinnista N-metyylidietanoliaminiliuoksilla. Lisäksi uutta mittausdataa tuotettiin ja analysoitiin hiilidioksidin absorptiosta N-methyylidietanoliamiiniin sekä hiilidioksidin ja rikkivedyn absorptiosta uusiin faasimuunnosliuoittimiin. Faasimuunnosliuoittimina käytettiin 2-(dietyyliamino)-etanolia ja 3-(metyyliamino)-propyyliaminia. Saatujen tulosten valossa tutkittu faasimuunnosliuottimen konsentraatio ei vaikuta toimivalta ratkaisulta rikkivedyn poistoon sellaisenaan. Lisätutkimukseksi ehdotetaan rikkivedyn ja hiilidioksidin VLLE mittauksia hiilidioksidilla ladattuun faasimuunnosliuottimeen useissa eri liuotinkonsentraatioissa.

Avainsanat Absorptio, MDEA, Metyylidietanoliamiini, DEEA, 2-(dietyyliamino)-etanoli, MAPA, 3-(methylamino)-propylamiini, hapan kaasu, rikkivety, H_2S, hiilidioksidi, CO_2

Foreword

Experiments for this master's thesis were completed at the Chemical Engineering research group at Aalto University School of Chemical Technology in Finland during May 2014 – November 2014.

I wish to thank both my advisors D. Sc (Tech) Petri Uusi-Kyyny and PhD Hernando Guerrero Amaya for the help and guidance they offered with the experiments and issues faced during the work. I also wish to thank my supervisor Prof. Alopaeus for many useful comments and the guidance offered during the thesis. In addition to this, Prof. Dominique Richon offered much valuable knowledge to better understand the topic.

I would also thank my family, friends and the colleagues at the lab for their support and company and especially M.Sc. (Tech) Alexandr Ostonen for helping make this thesis possible. I also wish to express gratitude to Elif, my girlfriend of the time and my parents for their faith in me and their unending support. Last but not least, I wish to offer thanks to Erasmus Student Network for the balance & friendships it offered during this hard work through all the interesting and motivating voluntary work.

Lastly I want to thank the Finnish Funding Agency for Innovation TEKES, Neste Oil, Neste Jacobs and UPM for the funding in the project that made this thesis possible.

Table of Contents

Literature Part

1 Introduction 1
2 Chemicals related to sour gas absorption 2
2.1 Hydrogen sulfide (H_2S) 3
2.1.1 Health and Safety 3
2.1.2 Uses in industry 4
2.2 Carbon dioxide (CO_2) 5
2.3 Methyldiethanolamine (MDEA) 6
2.4 2-(diethylamino)-ethanol (DEEA) 7
2.5 3-(methylamino)-propylamine (MAPA) 8
3 Theory of absorption 8
4 Phase Equilibria 10
5 Kinetics of mass transfer and reactions 12
5.1 CO_2 Mass transfer kinetics 13
5.2 CO_2 Reaction kinetics 16
5.2.1 CO_2 Reaction with MDEA 16
5.2.2 CO_2 Reaction with MAPA 18
5.2.3 CO_2 Reaction with DEEA 20
5.2.4 CO_2 Reaction with DEEA + MAPA 21
5.3 H_2S Mass transfer kinetics 22
5.4 H_2S Reaction kinetics 26
5.4.1 H_2S Reaction with MDEA 26
5.4.2 H_2S Reaction with MAPA 27
5.4.3 H_2S Reaction with DEEA 28
5.4.4 H_2S Reaction with DEEA+MAPA 29
5.5 N_2O Mass transfer kinetics 30
6 Physical properties 31
6.1 Methyldiethanolamine (MDEA) 31
6.2 2-(diethylamino)-ethanol (DEEA) 33
6.3 3-(methylamino)-propylamine (MAPA) 35
6.4 Aqueous solutions of MAPA and DEEA 36
7 Processes and Phase Change Solvents 38
7.1 Demixing amines 39

7.2 Applications in gas purification 41
7.2.1 Typical Absorption Process 42
7.2.2 DMX^{TM} process 43
7.2.3 HySWEET process 43
8 Published research equipment and methods for kinetic measurements 44
8.1 Autoclave & Cell 44
8.2 Wetted Wall Columns 46
8.3 Wetted Sphere Apparatus 49
8.4 Laminar Jet Apparatus 50

Experimental Part

9 Instruments and measurements 51
9.1 Experimental apparatus 51
9.1.1 Volume of the gas feed tank (GFT) 55
9.1.2 Volume of the cell 56
9.2 Measurements and validation with CO_2 58
9.2.1 Measurements with MDEA+CO_2 58
9.2.2 Measurements with MDEA+N_2O 64
9.2.3 Measurements with MAPA+DEEA+CO_2 65
9.3 Measurements with MAPA+DEEA+H_2S 68
10 Analysis of results 70
10.1 MDEA+CO_2 70
10.2 MDEA+N_2O 81
10.3 MAPA+DEEA+CO_2 82
10.4 MDEA vs MAPA+DEEA in CO_2 capture 91
10.5 DEEA+MAPA+H_2S 93
10.6 MAPA+DEEA, H_2S vs CO_2 96
11 Ideas for further research and improvements 99
11.1 Ideas for further research 99
11.2 Improvement ideas for the equipment 100
12 Conclusions 102
References 104
Appendix A. Calibration data for the PT1 UNIK 5000 sensor I
Appendix B. Calibration data for the PT2 UNIK 5000 sensor III
Appendix C. Calibration data for PT100 units TT1 and TT2 V

Appendix D. Calibration data for the Huba Control pressure transducer..... VII
Appendix E. Calibration data for Trafag NAH 6A series pressure transducer..... IX
Appendix F. Gas Feed Tank volume measurements XI
Appendix G. Measurement Cell volume measurements XV
Appendix H. Raw results of all measurements …….….. Supplementary file

List of Symbols and Abbreviations

5D2M = Solution of 5M DEEA and 2M MAPA used in the experiments
A = interfacial area [m^2]
Am = generic abbreviation for any amine in a solution
AMP = 2-amino-2-methyl-1-propanol
β = the slope of pressure decrease curve for the initial decrease of pressure
$C_{j,i}$ = interfacial concentration of component j in liquid film [$mol \cdot m^{-3}$]
$C_{j,bulk}$ = bulk concentration of component j in liquid film [$mol \cdot m^{-3}$]
C_i = the concentration of component i in the liquid phase of the studied system [$mol \cdot m^{-3}$]
$C_{i,Total}$ = the total concentration of component i in the liquid phase of the studied system [$mol \cdot m^{-3}$]
CO_2 = carbon dioxide
DEEA = 2-(diethylamino)-ethanol
DEA = diethanolamine
DETA = diethylenetriamine
DIPA = diisopropylamine
D_{Ag} = diameter of the agitator / mixer [m]
D_{Cell} = diameter of the cell [m]
D_i= diffusion coefficient of component I [$m^2 \cdot s^{-1}$]
E = enhancement factor
EPA = US Environmental Protection Agency
H_i = Henry's law coefficient for component i [$Pa \cdot m^3 \cdot mol^{-1}$]
H' = experimental Henry's law coefficient [atm]
H'_0 = Henry's law coefficient in pure water [$atm \cdot dm^3 \cdot mol^{-1}$]
H_2S = hydrogen sulfide
k_L = liquid mass transfer coefficient [$m \cdot s^{-1}$]
k_G = gas mass transfer coefficient [$m \cdot s^{-1}$]
k_{ov} = the overall reaction coefficient for the system [s^{-1}]
k_i = the kinetic reaction coefficient for reaction i [$m^3 \cdot (mol \cdot s)^{-1}$]
K_i = the equilibrium constant for reaction i
MAPA = 3-(methylamino)-propylamine
MDEA = methyldiethanolamine
MDH = Minnesota Department of Health
MEA = monoethanolamine
M_i = molar weight of the component i [$g \cdot mol^{-1}$]
N = rotation speed of the mixer [s^{-1}]
N_i = the rate of absorption for component i [$mol \cdot (m^2 \cdot s)^{-1}$]
N_2O = nitrous oxide
OSHA = Occupational Safety & Health Administration
ΔP_{CO_2} = the change in the partial pressure of component i [Pa]
P_{total} = total pressure of the system [Pa]
$P_{measured}$ = pressure of the system measured at given time [Pa]
$P_{initial}$ = pressure of the system measured prior to gas injection [Pa]
P_i = partial pressure of component i [Pa]
R = molar gas constant [$J \cdot (mol \cdot K)^{-1}$]
R_i = denotes a carbon chain or other molecule in a compound

Re = Reynolds Number
r_i = reaction rate of component i [$mol \cdot s^{-1}$]
Sc = Schmidt number
Sh = Sherwood number
t = time [s]
T = temperature [K]
TEA = Triethanolamine
Vg = gas space volume in the system [m^3]
V^E is the excess molar volume [$cm^3 \cdot mol^{-1}$]
w_i = the mass fraction of component i
WHO = World Health Organization
x_i = molar fraction of component i in liquid phase
y_i = molar fraction of component i in gas phase
ρ_i = density of the component or mixture I [$kg \cdot m^{-3}$]
μ_i = the viscosity of the solution i [$kg \cdot (m \cdot s)^{-1}$]
α_i = the loading of the amine [$mol(sour\ gas) \cdot mol(amine)^{-1}$]

1 Introduction

In the modern world of industry we have an ever increasing problem, exhaust gases and their effect on our planet. Solutions to this problem have been provided through different methods such as improving the processes to provide less waste flows and exhaust gases and trying to first develop and then improve processes to treat these waste streams as well as process raw material streams such as natural gas. One of the processes developed for this purpose has been the absorption of acidic gases into various solvents. These gases can be present in anywhere from process industry streams to natural gas reserves. In the absorption process the largest single operating cost comes from the desorption process for the gas or the regeneration process for the solvent in use. This step is usually very energy intensive and therefore costly.

To improve the regeneration step, experiments that provide insight in to the behavior of different solvents when in contact with the acid gases in the streams are required. This data consists of phase equilibrium data, absorption kinetic data and reaction kinetic data. The focus of our experiments was the absorption kinetics and the enhancement of that absorption through the reaction kinetics. With these experiments we can find solvents that have much smaller regeneration costs. One such discovered solvent is Methyldiethanolamine (MDEA), which has been in use for quite some time in the industrial processes already. Modern solvents for the same purpose have now gained increased interest, as they can have an ability to form a split of two liquid layers, a gas rich and gas lean layer, when loaded with acid gases. This provides the possibility of regenerating only one of these phases, which greatly reduces the liquid flow inside the desorption column and consequently the costs of the unit operation. In these cases the absorbent is usually made of two components. One that has fast absorption kinetics but low maximum loading and the other with slow kinetics but high maximum loading. This allows for fast kinetics at the interface layer and then a transfer from the interface layer to liquid in the bulk.

The goal of this thesis was to prepare and use a new experimental apparatus, a Lewis type cell, for the laboratory and set up all the measurement equipment related to it. The cell designed by Professor Dominique Richon allows studies of gas absorption in various conditions. After setting up the equipment it was validated with CO_2 absorption into aqueous Methyldiethanolamine by comparing obtained results with reliable literature data. When adequate validation results were obtained, the target solvents of this thesis, 2-(dimethylamino)-ethanol (DEEA) and 3-(methylamino)-propylamine (MAPA) were tackled. Aqueous mixture of these solvents forms a liquid-liquid split when loaded with high amounts of CO_2.

In order to better analyze the behavior of H_2S absorption into the solvent consisting of DEEA and MAPA, investigation of this solvents behavior with CO_2 was required. A study on when the formation of the liquid-liquid phase split occurs in regard to the amine loading (moles of CO_2 per moles of Amine) and temperature of the solution as well as the effect the split has on the absorption rate of CO_2 into the solution was performed. After analyzing the effects of temperature and loading on the split with CO_2, we were interested in whether similar split occurs with H_2S.

2 Chemicals related to sour gas absorption

Compounds of interest were the acidic gases for which absorption is currently studied, carbon dioxide (CO_2) and hydrogen sulfide (H_2S). Their absorption was studied in to three different aqueous amines and their aqueous mixtures. The amines in use were N-Methyldiethanolamine (MDEA), 2-(diethylamino)-ethanol (DEEA) and 3-(methylamino)-propylamine (MAPA). In the next chapters these compounds will be explored further by studying their sources, health effects and what kind of effect they have on our daily lives.

2.1 Hydrogen sulfide (H_2S)

Hydrogen sulfide (CAS# 7783-06-4) is a gas abundant in industry and nature. It is toxic, flammable and has a characteristic smell of rotten eggs. Most of the flue gases in industry contain H_2S and the need for better removal processes increases as the industry inadvertently producing it spreads and grows. It is also found in natural gas deposits as a contaminant along with other sulfur compounds and CO_2 (Cadours et al., 2012) as well as obtained as a product from the Hydrodesulfurization (HDS) process when producing sulfur free fuels.

World Health Organization (WHO) has estimated that in year 2000 only 10% of the global sources of H_2S were man related and rest were natural. Natural sources include organic matter decomposition, hot springs and volcanos where as human related sources include oil refineries and pulp and paper production as well as natural gas drilling sites. (WHO, 2000) Some natural gas deposits have been estimated to include up to 50% H_2S (Argirova et al., 1981).

2.1.1 Health and Safety

Hydrogen sulfide is a gas heavier than air, therefore it accumulates in closed low-laying spaces such as sewage and cellars. The major method of exposure for man is through lungs, which is why proper safety gear is important when handling the gas. It is hazardous at low concentrations and immediately dangerous to life already at 300 ppm and it can only take a few breaths to be fatal. The gas does numb the sense of smell quite fast, already at 100-150 ppm, therefore proper sensors to analyze gas content in air are important in spaces where it is handled. (OSHA, 2005) In Europe the exposure limits have been set in a directive in 2009 for constant exposure. They are 5 ppm for 8 hours of constant exposure and 10 ppm for an exposure of 15 minutes. (European Commission, 2009)

Surveys on the quality of air are done regularly in cities around Finland. One such measurement has been conducted yearly by the city of Imatra to analyze what influences the air quality in this part of Finland. It among other things has included a measurement device near a pulp and paper factory in Svetogorsk in Russia since

1990. There have been some years in which this measurement has not been carried out, but from the data available we can see that the emissions have declined since 2007 as the plant implemented a new gas purification process. The guideline value in Finland is 10 ppm. The average values for H_2S emissions have not surpassed this value since 2006. The daily guideline value has however been surpassed in 2013, 2011 and 2009. During the year 2013 values surpassing the hourly guideline value were recorded for 3.8% of the whole measurement time. Peak emissions were as high as 44 ppm. (Ahlqvist et al., 2014) The average content of hydrogen sulfide in air has been estimated to be about 0.3 ppm (Argirova et al., 1981). The report by Ahlqvist et al. proves that the gas purification processes are vital for industry and their improvement is still needed. Even though the values have dropped from the hourly mean averages of 1998-2006, which were up to 12 ppm, improvement is still needed as the emissions still surpass the guideline values nearly every year.

In addition to natural gases and industrial flue gases, H_2S is also produced when refining crude oil, for which the sulfide content in U.S. Energy Information Administration's measurements has grown from the 0.9% present in 1980's to 1.44% found in today's deposits (U.S. Energy Information Administration, 2014). This can be related to the global increase in fuel needs that has forced the oil industry to move to deposits that contain more sulfur. This logically leads to higher sulfide based emissions from the refining processes, which can be then seen as increasing SO_2 and H_2S emissions. This yet again proves the need for enhancing the current processes for the treatment of these gases.

2.1.2 Uses in industry

The demand for natural gas for various purposes increases every year (Sweeney, 2014). Highest increase in USA can be credited to electric power generation. To meet the demand the producers turn to gas fields that contain higher H_2S content. In the United States removal of hydrogen sulfide from the acidic natural gas is usually (95% of the cases) done by absorption to amines (EPA, 1995).

Hydrogen sulfide is used as a synthesis gas for many different compounds, including sulfur dioxide, an integral component in sulfuric acid synthesis, as well as in the synthesis of dimethyl-sulfide, which is used in oil industry and dimethyl sulfoxide, which is used in organic chemistry as a solvent. In addition it is used as a raw material in the Claus-process to convert it to elemental sulfur. (Weil et al., 2006)
Problems with hydrogen sulfide are not limited to just toxicity, environmental regulations and bad smell. It also is very corrosive and causes challenges in equipment design and potential dangerous situations in their usage as well as in the gas storage (Baker Hughes Incorporated, 2011). Growing amount of hydrogen sulfide as well as its obvious health hazards and use as a raw product create a clear need for efficient methods to capture the gas and purify these streams for less hazardous release.

2.2 Carbon dioxide (CO_2)

Carbon dioxide (CAS# 124-38-9) is an odorless and colorless gas that is toxic in high concentrations and causes potential environmental damage through the greenhouse effect. Prolonged exposure (multiple hours) to high concentrations (over 5000 ppm) of CO_2 cause headache, dizziness, nausea and other symptoms (MDH, 2013). Carbon dioxide is a normal part of the carbon cycle and as such it is a gas that is released from many natural sources such as the combustion of organic matter, wildfires and volcanic gases. The gas is also removed from the atmosphere by many natural methods, such as forests and plants that use it in their photosynthesis cycle and through absorption into oceans. However as industrial processes have become more common in the last few centuries, so have the energy needs. They have been met by burning coal or other carbon based fuels, which directly release carbon dioxide in to the air and thus upset the normal carbon cycle.

It has been reported by Environmental Protection Agency in U.S. (2014) that about 82% of all U.S. greenhouse gas emissions in 2012 were CO_2. The same report also lists the main sources that emit the gas in U.S., which are electricity production, transportation and industry. At the same time it is reported that in U.S. the management of forests and non-agricultural land has created a positive offset for the

carbon dioxide removal from the atmosphere, meaning that up to 15% more CO_2 is captured than is produced inside the borders of the country. Amongst the examples of CO_2 emission reduction the carbon capture and sequestration is mentioned, which includes the absorption of the gas in to a suitable solvent. (EPA, 2014)

The existence of climate change has been clearly shown in many reports (Crowley, 2000, Falkowski et al., 2000), and it can, amongst other things, lead to a sea level rise up to 1.9m in 21st century (Solomon et al., 2009) if the worst case scenario would come to pass. It is therefore essential that new methods of carbon capture are researched and old methods are improved upon as much as possible. To this goal, gas absorption of flue gases is an important research topic that has received much attention. Different absorbents, such as Methyldiethanolamine (Mandal and Bandyopadhyay, 2006, Pacheco and Rochelle, 1998, Pani et al., 1997a, Weiland et al., 1993), 3-(methylamino)-propylamine (Voice et al., 2013, Arshad et al., 2014) and 2-(diethylamino)-ethanol (Arshad et al., 2014, Vaidya and Kenig, 2007b), have been researched and studied by many teams across the world.

2.3 Methyldiethanolamine (MDEA)

Methyldiethanolamine (CAS# 105-59-9) is a tertiary amine compound illustrated in figure 1.

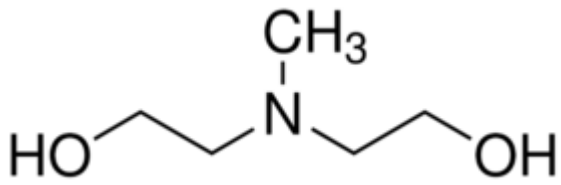

Figure 1. Methyldiethanolamine molecule (Sigma-Aldrich Co. LLC., 2014a)

It has been categorized to be an irritant to eyes and skin. MDEA is mostly used as a synthesis block for multiple chemical compounds as well as a sweetening chemical in oil-, gas- and chemical industries. Mixtures of MDEA and water are currently widely used in industry as one of the absorption media for gas sweetening. As such, it has a lot of research and measurement data available in literature.

2.4 2-(diethylamino)-ethanol (DEEA)

DEEA (CAS# 100-37-8) is an amine with two ethyl groups and an ethanol group. It is a yellow liquid and miscible in water. A structure for the molecule is illustrated in figure 2**.**

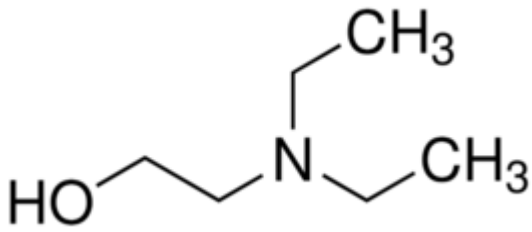

Figure 2. 2-(diethylamino)-ethanol molecule (Sigma-Aldrich Co. LLC., 2014b)

It is an irritant to eyes, skin and respiratory system and it can cause nausea and vomiting. There is an occupational exposure limit in effect from Centers for Disease Control and Prevention in United States for 50 $mg \cdot m^{-3}$ over an eight-hour workday. (Centers for Disease Control and Prevention, 2007) Suppliers recommend the use of full face respirators, gloves and other protective equipment. DEEA is mainly used as a corrosion inhibitor. Other applications include lubricants and pharmaceutical industries. (BASF - The Chemical Company, 2014, Sigma-Aldrich Co. LLC., 2014b) DEEA is synthesized through a reaction between diethylamine and ethylene oxide, which both can be obtained from ethanol. Diethylamine is synthesized from ethanol and ammonia and ethylene oxide is made from oxidation of ethylene, which is synthesized from dehydration of ethanol. As ethanol can be produced from renewable raw materials, the solvent can be considered to be “green”, which of course adds extra value to its use. (Sutar et al., 2013)

2.5 3-(methylamino)-propylamine (MAPA)

MAPA (CAS# 6291-84-5) is a diamine compound illustrated in figure 3.

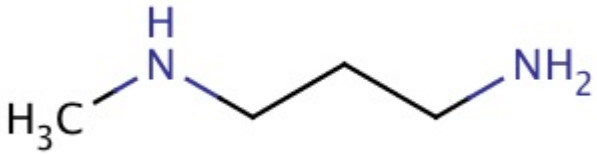

Figure 3. 3-(methylamino)-propylamine molecule (Santa Cruz Biotechnology, 2014)

MAPA contains a primary and a secondary amine group, which gives it interesting properties as an absorbent. It is considered to be flammable, hazardous to health if swallowed and corrosive to skin. It is also poisonous if inhaled. This leads to the need of using protective equipment such as respirators and protective gloves or other protective clothing when handling of this amine. One research team has noted that MAPA degrades rapidly when in contact with oxygen, making it potentially difficult to use with flue gases (Voice et al., 2013).

3 Theory of absorption

Absorption is the process of diffusing a compound from a gas phase carrier to a liquid phase carrier. It is used for example in the recovery of ammonia or the removal of sulfur dioxide from flue gases. (Geankoplis, 2008) A gas absorption process generally consists of an absorption column, a couple of heat exchangers and a desorption column. Normally the more energy demanding step with the process is desorption, as it requires high regeneration temperatures. The process can be illustrated with the simple flow diagram shown in figure 4.

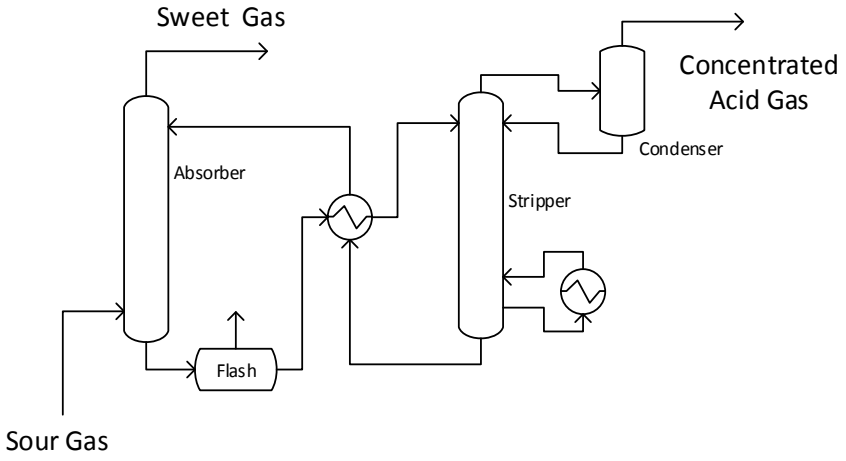

Figure 4. Typical Absorber/Stripper system for gas absorption

When designing an absorption column, a large amount of data is needed. This data consists of the phase equilibrium data (vapor-liquid equilibrium or liquid-liquid equilibrium) between the components (deviation from equilibrium causes the driving force), the reaction and absorption kinetics involved within the absorption process (enhancement of rate of absorption) and the hydrodynamics involved in the physical design (interface area and flow rates) of an absorption process. These are governed by physical properties and diffusion coefficients of the components involved, as well as the known reactions that these compounds have with each other.

In recent years there has been development towards such absorbents, which form a liquid-liquid split at certain temperatures or loadings. These compounds are known as phase-change solvents or demixing amines and will be covered in detail in chapter 7.1. Usually the absorbent in these cases is made of two components with varying kinetics towards the absorbing gas.

In the next chapters basics of phase equilibrium measurements are briefly discussed and reaction kinetics will be explained in detail. In addition the relevant compounds will be covered for their specific physical properties.

4 Phase Equilibria

The mass transfer between gas and liquid is based on the deviation from phase equilibrium. The driving force can be further explained, as the difference in partial pressure between the equilibrium partial pressure of the absorbed component in the liquid phase and the actual partial pressure of that component in the gas phase. The correlation used to show the relation between the liquid molar fraction of the absorbing component and its equilibrium vapor pressure is usually Henry's law as shown in equation (**1**).

$$\frac{P_A}{[Pa]} = \frac{H_A}{[Pa]} * x_A \tag{1}$$

Experimental coefficients for Henry's law have been defined for multiple different compounds in literature. The error in the correlation usually increases as the molar fraction and/or the partial pres sure of the compound increases (Geankoplis, 2008). Henry's law also works for the absorption cases where enhancement of absorption rate through a reaction is involved, as it only shows the relationship between the partial pressure of the component and its molecular concentration in the liquid phase.

With large concentrations, the diffusion through the interface layer and the change in the diffusion rate as the gas pressure decreases must be taken in to consideration. As the pressure gradient decreases, so does the driving force of diffusion. This can usually be witnessed with a change in the slope of the diffusion rate when a certain critical concentration is reached.

Molar fraction in vapor phase can roughly be estimated with equation (2).

$$y_A = \frac{P_A}{P_{total}} \tag{2}$$

To make use of this equation, the pressure of the inert components that do not contribute to the absorption process must be measured before introducing the absorbing compound(s). These inert components can include inert gases, pressure of the vaporized solvent or other sources of pressure in the absorber. This way the partial pressure of the absorbing component can be deducted from the total pressure measured during the process.

In the liquid phase this molecular gas component is dissolved as ions through reactions that depend on the solution. Glasscock (1990) illustrated the difference between a water solution and an alkanolamine solution as the absorbent in his doctoral thesis. Illustrations he used are shown in figure 5.

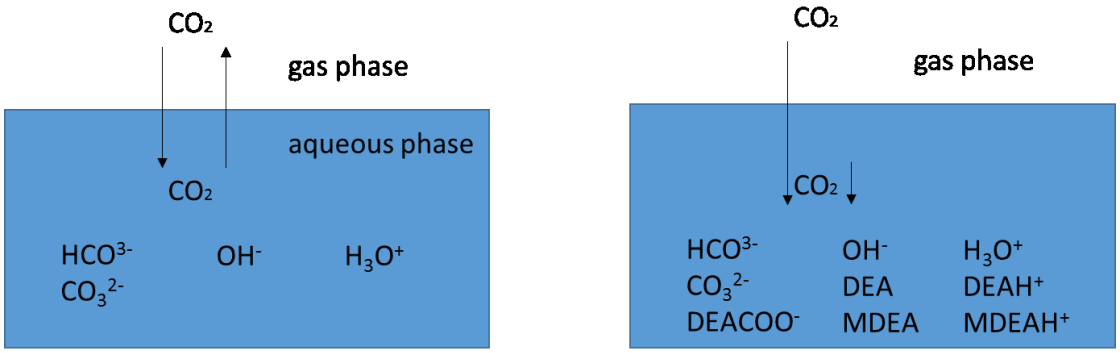

Figure 5. Species involved in absorption with water solution (left) and alkanolamine solution (right) (Glasscock, 1990)

In the figure we see that in water the equilibrium reaction is controlled by reactions (I) to (III).

$$H_2O \Leftrightarrow H^+ + OH^- \quad \text{(I)}$$

$$CO_{2(aq)} + OH^- \Leftrightarrow HCO_3^- \quad \text{(II)}$$

$$CO_3^{2-} + 2H_2O \Leftrightarrow HCO_3^- + H_2O + OH^- \quad \text{(III)}$$

In an alkanolamine solution however, the reactions include different interactions with the amine compounds. Glasscock (1990) used diethanolamine and methyldiethanolamine as examples. In this illustration the equilibrium would be

governed by reactions shown before and additional reactions (IV) to (VI) (Mandal and Bandyopadhyay, 2006).

$$CO_{2(aq)} + H_2O + MDEA \Leftrightarrow MDEAH^+ + HCO_3^- \quad \text{(IV)}$$

$$MDEA + H^+ \Leftrightarrow MDEAH^+ \quad \text{(V)}$$

$$CO_{2(aq)} + DEA \Leftrightarrow DEACOO^- + H^+ \quad \text{(VI)}$$

The reactions in alkanolamine solutions cause enhancement of absorption through reaction kinetics discussed in the next chapter. This is usually taken in to consideration in absorption calculations by the use of enhancement factor.

5 Kinetics of mass transfer and reactions

The mass transfer from gas to liquid is usually simplified to a two-film theory of mass transfer seen in figure 6.

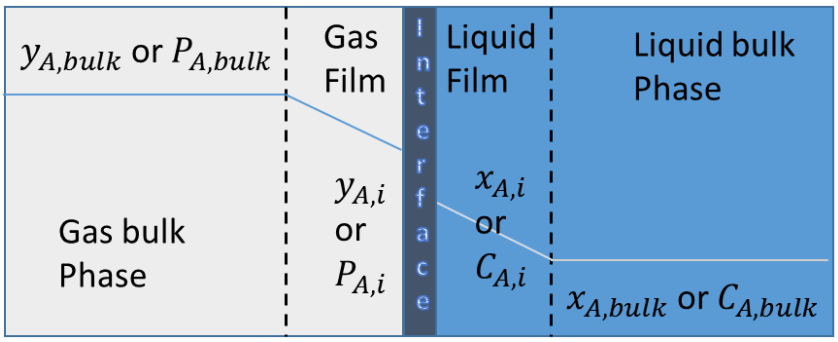

Figure 6. Two-Film Model in Mass Transfer

The mass transfer phenomenon (diffusion) assumes a difference between the liquid bulk and liquid film layers and equilibrium between the two film layers on both sides of the interface. Usually the diffusion resistance is not between the films, but rather between a film and its bulk layer. In absorption to alkanolamine solution, the resistance is usually only contributed to the liquid layer and an assumption for zero resistance in gas phase is made.

To make calculations easier, some assumptions can be made. Such assumptions are equimolar diffusion, in which equal amounts of components diffuse from one phase to the other and vice versa, or the assumption of stagnant or non-diffusing component, where only one component diffuses through a stagnant layer of the other component. (Geankoplis, 2008)

The reactions seen in the right part of figure 5 decrease the concentration of the absorbed component as it reacts with other components and thereby decrease the equilibrium partial pressure and increase the driving force. This leads to higher absorbed gas amount as the equilibrium partial pressure is kept further away from the saturation partial pressure and it is known as the enhancement of absorption. The enhancement factor is a way to explain the effect a reaction kinetics have on the equilibrium between the gas and the amine solvent it absorbs in to. The bulk and interfacial liquid concentration for the gas are dependent on reaction kinetics in these cases.

5.1 CO_2 Mass transfer kinetics

Kinetics for the absorption process typically assume that the slowest and rate determining step is the absorption from gas to liquid. For this assumption Pani et al. (1997a) used the following equation

$$\frac{dP_{CO_2}}{dt} = -\frac{R \cdot T}{V_G} \cdot k_L \cdot A \cdot E \cdot C_{CO_2,i} \qquad (3)$$

The partial pressure of CO_2 can be expressed by calculating the difference between the partial pressures of inert components and the total pressure in the measuring cell at given time. This equation however assumes, that as long as there is any CO_2 left in the interface the absorption continues. This is usually not the case but some equilibrium is reached. However they only take in to account the first 10 kPa pressure drop and evaluate the absorption based on this. Initial pressure is determined prior to gas injection. After this the carbon dioxide is introduced and pressure drop vs

time logged in the system. The partial pressure of carbon dioxide can be then expressed with the equation (4)

$$P_{CO_2} = P_{measured} - P_{initial} \quad (4)$$

The interfacial concentration of carbon dioxide is obtained from a molar scale Henry's law equation

$$P_{CO_2} = H_{CO_2} \cdot C_{CO_2,interface} \quad (5)$$

If equation (3) is then simplified so, that all the terms that are independent of pressure are grouped up under one variable and integrated, a linear logarithmic correlation between the partial pressure of CO_2 and time is obtained. Pani et al. (1997a) specifically noted, that as long as the pressure decrease from P_0 to $P_{measured}$ is below 10 kPa the values for Henry's law coefficient, enhancement factor and liquid side transfer coefficient should stay stable and the correlation can be used without further adjustment to their change over time. After simplification and integration the correlation is as shown in equation (6) (Pani et al., 1997a)

$$\ln\left(\frac{P_{measured} - P_{initial}}{P_{measured,0} - P_{initial}}\right) = -b * t \quad (6)$$

where b contains pressure independent variables and is given by equation (7).

$$b = \frac{R \cdot T}{V_G \cdot H_{CO_2}} \cdot k_L \cdot A \cdot E \quad (7)$$

For the Henry's law constant Pani et al. (1997a) used a correlation by Al-Ghawas et al. (1989). The mass transfer coefficient in liquid phase was calculated using a correlation based on dimensionless numbers. The correlation is shown in equations (8) - (11). This correlation is validated and further developed in chapters 9.2.2 and 10.2.

$$\mathrm{Re} = \frac{\rho_{\mathrm{solution}} \cdot \mathrm{N} \cdot \mathrm{D}_{\mathrm{Ag}}^2}{\mu_{\mathrm{solution}}} \quad (8)$$

$$\mathrm{Sc} = \frac{\mu_{\mathrm{solution}}}{\rho_{\mathrm{solution}} \cdot \mathrm{D}_{\mathrm{CO_2}}} \quad (9)$$

$$\mathrm{k_L} = \frac{\mathrm{Sh} \cdot \mathrm{D}_{\mathrm{CO_2}}}{\mathrm{D}_{\mathrm{Cell}}} \quad (10)$$

$$\mathrm{Sh} = 0.34 \cdot \mathrm{Re}^{\frac{2}{3}} \cdot \mathrm{Sc}^{\frac{1}{3}} \quad (11)$$

Diffusion coefficient for CO_2 (D_{CO_2}) in aqueous MDEA was calculated using a set of correlations devised by Versteeg and Swaaij (1988). They proposed a correlation for estimating the diffusion of CO_2 in water and a correlation that then estimated the diffusion in an aqueous alkanolamine solution from that. These correlations were created for a Lewis cell and should therefore be accurate enough for the measurements presented in this work. They are shown in equations (12) and (13).

$$\mathrm{D}_{\mathrm{CO_2}} = 2.35 * 10^{-6} \cdot \mathrm{e}^{-\frac{2119}{T}} \quad (12)$$

$$\left(\mathrm{D}_{\mathrm{CO_2}} \cdot \mu_{\mathrm{Amine\ solution}}^{0.8}\right)_{\mathrm{Amine\ solution}} = \left(\mathrm{D}_{\mathrm{CO_2}} \cdot \mu_{\mathrm{Water}}^{0.8}\right)_{\mathrm{Water}} \quad (13)$$

For equation (13) the amine viscosity was estimated with the correlation by Al-Ghawas et al. (1989).

It was also of interest to study the mass transfer in an absorbent composed of aqueous mixtures of DEEA and MAPA, as it forms a liquid-liquid split, and to determine if the split has any effect in the transfer rate of CO_2 to the absorbent. Correlations have been suggested for the solubility of CO_2 in to DEEA and its aqueous solutions by Vaidya and Kenig (2007b).

In their research Arshad et al. (2013, 2014) have published gas solubility measurements in different concentrations of DEEA and MAPA in water as well as a ternary DEEA/MAPA/H_2O against which our results can be compared.

5.2 CO_2 Reaction kinetics

In this chapter the reaction kinetics for CO_2 with MDEA, MAPA and DEEA are investigated. The chapters present the different reactions that undergo in a solution containing these species as well as some reaction rate equations related to these. Correlations and calculation bases are presented for use in measurement result analysis.

5.2.1 CO_2 Reaction with MDEA

Pani et al. (1997a) suggested that fast hydrogen bonding of water with a tertiary amine would increase the reactivity of water with dissolved CO_2. This reaction is expressed as shown in reactions (VII) and (VIII).

$$R_1R_2R_3N + H_2O \Leftrightarrow R_1R_2R_3N \cdot H_2O \quad \text{(VII)}$$

$$CO_2 + R_1R_2R_3N \cdot H_2O \rightarrow R_1R_2R_3NH^+ + HCO_3^- \quad \text{(VIII)}$$

They assumed reaction (VII) to be in equilibrium and reaction (VIII) to be in pseudo-stationary state and nearly instant, resulting in a zero concentration at any given time for the component $R_1R_2R_3N{\cdot}H_2O$. This mechanism is also supported by other earlier research by Donaldson and Nguyen (1980). Pani et al. (1997a) propose a reaction rate expression shown in equation (14) for solutions with water concentrations higher than that of MDEA.

$$r = k \cdot C_{MDEA} \cdot C_{CO_2} \quad (14)$$

It has also been suggested by Pacheco and Rochelle (1998) that the solubility would be expressed by Henrys law and the reaction would follow the kinetics shown in reaction (IX) and equation (15). (Pacheco and Rochelle, 1998)

$$CO_{2(aq)} + H_2O + MDEA \Leftrightarrow MDEAH^+ + HCO_3^- \quad \text{(IX)}$$

$$r_{MDEA} = k_{VIII} \cdot C_{CO_2} \cdot C_{MDEA} - \frac{k_{VIII}}{K_{VIII}} \cdot C_{HCO_3^-} \cdot C_{MDEAH^+} \quad (15)$$

These models are essentially the same, except that Pacheco and Rochelle seemingly better take in to account the reversibility of the reaction between CO_2 and MDEA. They however do not specify the reactions as Pani et al. did, so it is possible that they made the same pseudo-stationary assumption and just refer to the reversibility of the reaction (VII).

If the enhancement factor from equation (7) is above 3, Pani et al. (1997a) propose that the reaction is in the fast regime of absorption, in which they propose a film theory by Brian et al. (1961), which assumes that a single irreversible reaction between CO_2 and MDEA is responsible for the enhancement of absorption as shown in reaction (IX)

$$C_{MDEA,i} = C_{MDEA,Total} \cdot \left(1 - \frac{P_{CO_2}}{H_{CO_2} \cdot C_{MDEA,Total}} \cdot \left(\frac{D_{CO_2}}{D_{MDEA}} \right)^{\frac{1}{2}} \cdot (E - 1) \right) \qquad (16)$$

By using this equation at the point when the pressure drop from initial is 5 kPa, with the Henry's law coefficient from Al-Ghawas et al. (1989) and the diffusion coefficients CO_2 (equations (12) and (13)) and MDEA (equation (57)), as well as the total concentration of MDEA in the solution we can calculate the interfacial concentration of MDEA.

Kinetics similar to those devised by Pacheco and Rochelle (1998) (reaction (IX)) have also been suggested by another laboratory. They investigated simultaneous absorption of H_2S and CO_2 in to MDEA and diethanolamine. (Mandal and Bandyopadhyay, 2006)

Pani et al. (1997a) also regressed their results for the overall transfer coefficient of absorption to find the constants in the Arrhenius equation for the reaction rate coefficient. They estimated the reaction rate using equation (14) and used equation

(16) for interfacial MDEA concentration with a model for the enhancement factor in fast region absorption shown in equation (17).

$$E = \frac{1}{k_L} \cdot \left(k_{ov} \cdot D_{CO_2}\right)^{\frac{1}{2}} \tag{17}$$

where they defined the overall reaction rate coefficient and liquid side mass transfer coefficient as

$$k_{ov} = k \cdot C_{MDEA,i} \tag{18}$$

$$k_L = \frac{Sh}{D_{Cell}} \cdot D_{CO_2} \tag{19}$$

and where Sherwood number was obtained as shown earlier in equations (8) to (11)

Their regression provided them with a correlation for the overall reaction rate coefficient and the constants for the Arrhenius equation.

$$k_{ov} = 13.5 + 0.934 \cdot \ln\left(C_{MDEA,i}\right) - \frac{5454}{T} \tag{20}$$

$$k = 4.68 * 10^5 \cdot e^{-\frac{5461}{T}} \tag{21}$$

Solving equation (18) for the kinetic reaction constant allows us to compare their results with our cell results and thereby validate our cells functionality. We can also compare our calculated reaction rate coefficient to their Arrhenius equation and our overall reaction rate coefficient to their values.

5.2.2 CO_2 Reaction with MAPA

MAPA has one primary and one secondary amine group and should therefore react through the carbamate formation reaction path. As it has two amine groups, they will actually form two distinct carbamates, however there is no way to find out which of the two carbamates is formed with the equipment in use.

Monteiro et al. (2013b) assumed, that as the loadings were very low (0.01 mol CO_2·(mol Amine)$^{-1}$), the results they got would have been representative of the primary amine group's reaction in MAPA. They proposed the absorption rate of CO_2 to follow the two film theory and therefore it is possible to correlate it as shown in equation (22).

$$N_{CO_2} \cdot A = \frac{P_{CO_2}}{\frac{1}{A \cdot k_G} + \frac{H_{CO_2}}{E \cdot A \cdot k_L}} = \frac{P_{CO_2}}{\frac{1}{A \cdot k_G} + \frac{H_{CO_2}}{A \cdot \sqrt{k_{ov} \cdot D_{CO_2}}}} \quad (22)$$

This correlation is dependent on the gas- and liquid side mass transfer coefficients, the current partial pressure of CO_2 and the area of interface as well as the Henry's law coefficient and enhancement factor caused by the chemical reaction. As all these are experimentally assessable, they suggest the use of this equation to determine the observed reaction rate coefficient. It has to be noted that this equation does not take in to account the fact, that the flux will reach zero prior to the partial pressure reaching zero. This however does not cause any problems, as the reaction already assumes a constant enhancement factor, an assumption that is only viable in the beginning of the absorption (assumed to be the first 10 kPa drop in pressure). It was previously discussed, that in the absence of other gases than CO_2 in the vapor phase, the resistance for absorption should be only in the liquid layer. This would simplify the reaction equation to a form shown below

$$N_{CO_2} \cdot A = \frac{P_{CO_2}}{\frac{H_{CO_2}}{E \cdot A \cdot k_L}} = \frac{P_{CO_2}}{\frac{H_{CO_2}}{A \cdot \sqrt{k_{ov} \cdot D_{CO_2}}}} \quad (23)$$

They proposed the rate of reaction to follow the rate equation (24), which is basically the same as for MDEA earlier.

$$-r_{CO_2} = k_{ov} \cdot C_{CO_2} = k \cdot C_{Amine} \cdot C_{CO_2} \quad (24)$$

In their studies Hartono and Svendsen (2009) propose similar kinetics for DETA, which reacts in the same manner as MAPA. They used an in-house Matlab code to determine the reaction rate coefficients. Their flux equation is very similar to that of equation (22)

$$N_i = \frac{1}{\frac{1}{k_L \cdot \sqrt{1 + \frac{k_{ov} \cdot D_i}{k_L^2}}} + \frac{R \cdot T}{H_i \cdot k_G}} \Delta C_{i,interface} \quad (25)$$

Similar reaction kinetics were also proposed by Sutar et al. (2013) for some diamines. They split the reaction in to two distinct reactions, a zwitterion formation reaction and a base catalysis reaction to carbamate formation as shown in (X) and (XI)

$$AmH + CO_2 \Leftrightarrow AmH^+COO^- \quad (X)$$

$$AmH^+COO^- + B \rightarrow AmCOO^- + BH^+ \quad (XI)$$

This reaction path could also be suitable for MAPA and CO_2 reaction, as it was suggested to follow a base catalysis reaction path earlier.

5.2.3 CO_2 Reaction with DEEA

Absorption of CO_2 in to DEEA has been studied by a few laboratories. DEEA was studied by Monteiro et al. (2013a) and they have used the electrolyte-NRTL model to estimate activities in the reaction between CO_2 and DEEA. The modelling was done using Aspen plus e-NRTL model. They also optimized some of the e-NRTL parameters for DEEA.

DEEA has also been studied by Sutar et al. (2013). Their article focuses on the reaction between DEEA and CO_2 and the enhancement of that reaction through a few promoters. They propose the reaction path to follow base catalysis as seen in (XII).

$$R_1^2R_2N + CO_2 + H_2O \overset{k_{R_1R_2N}}{\Longleftrightarrow} R_1^2R_2N^+H + HCO_3^- \quad \text{(XII)}$$

This reaction looks very similar to earlier reaction (IX). They further suggest that the reaction would follow a path shown in (XIII) and (XIV), instead of the suggested hydrogen bonding based path for MDEA in (VII) to (IX) earlier.

$$R_1^2R_2N + CO_2 \Leftrightarrow R_1^2R_2N^+COO^- \quad \text{(XIII)}$$

$$R_1^2R_2N^+COO^- + H_2O \Leftrightarrow R_1^2R_2N^+H + HCO_3^- \quad \text{(XIV)}$$

They define the reaction rate for DEEA to also consist of the reaction between CO_2 and water as shown in (XV) and (XVI).

$$CO_2 + OH^- \overset{k_{OH^-}}{\Longleftrightarrow} HCO_3^- \quad \text{(XV)}$$

$$CO_2 + H_2O \overset{k_{H_2O}}{\Longleftrightarrow} HCO_3^- + H^+ \quad \text{(XVI)}$$

They therefore correlate the reaction rate to be dependent on all of these as seen in equation (26)

$$r_{DEEA} = \left(k_{XV} \cdot C_{H_2O} + k_{XV} \cdot C_{OH^-} + k_{XV} \cdot C_{DEEA}\right) \cdot C_{CO_2} \quad (26)$$

5.2.4 CO_2 Reaction with DEEA + MAPA

With the reactions shown in chapters 5.2.2 and 5.2.3 as well as the promoter effect discussed in Sutar et al. (2013), it is possible to propose a reaction rate equation for CO_2 and MAPA+DEEA. The reaction rate was suggested by Pinto et al. (2014b) to initially be dependent on the fast reaction between MAPA and CO_2 until all MAPA has reacted in the liquid. After this the liquid-liquid split should be visible and the reaction speed would drop as the reaction between DEEA and CO_2 is considerably slower. However as both DEEA and MAPA reactions are equilibrium reactions, there is molecular CO_2 available in the MAPA phase and therefore it would act as a

promoter for the reaction between DEEA and CO_2. This would suggest that the reaction with DEEA+MAPA+CO_2 be initially dominated by rate equation (24) and later by rate equation (26).

5.3 H_2S Mass transfer kinetics

Pani et al (1997b) studied H_2S absorption in to aqueous MDEA. They suggested using Henry's law as before to correlate the interfacial H_2S concentration in the liquid phase. They however faced an issue with the Henry's law constant as the coefficient has not been determined for H_2S. Therefore they proposed that a correlation by van Krevelen and Hoftjizer (1948) would be used. However they also note, that this equation is highly dependent on the dissociation degree of the different contributing salts and might not be entirely trustworthy.

They calculated the diffusion coefficient of MDEA through the flux of H_2S in to the liquid. The flux was calculated through total pressure vs time data by

$$\frac{N_{H_2S} \cdot R \cdot T \cdot A}{V_G} = -\frac{dP_{Total}}{dt} = -\beta \tag{27}$$

It is assumed that the slope is taken after a 10 kPa drop in pressure as was done in their previous article (Pani et al., 1997a). It is unclear if they still used the correlation by van Krevelen and Hoftjizer to estimate Henry's law coefficients, but as it was not available and is suggested to be unreliable in any case, more research was made to find an available correlation for the Henry's law coefficient. A correlation was proposed by Rinker and Sandall (2000) for the solubility of H_2S in aqueous alkanolamines. The correlation could prove problematic when used with aqueous MAPA+DEEA solutions as they consist mostly of amines and have about 20 w-% of water. However this is the best correlation available. It is dependent on the mole fraction of solvent added to water and it is shown in equations (28) and (29).

$$\frac{H'}{H'_0} = 1 - (0.917 - 0.0334 \cdot M_i) \cdot x_i \tag{28}$$

$$\frac{H'}{[atm]} = \frac{H}{\left[\frac{atm*dm^3}{mol}\right]} \cdot \frac{\rho_{solution}}{\left[\frac{g}{dm^3}\right]} \cdot \sum_i^2 \left(\frac{w_i}{M_i}\right) \quad (29)$$

Henry's law coefficients in pure water can be calculated from a correlation by Kamps et al. (2001) shown in equation (30).

$$\frac{H_0'}{\left[\frac{MPa*kg}{mol}\right]} = A + \frac{B}{T} + C \cdot \ln(T) + D \cdot T \quad (30)$$

Coefficients A-D are available in table 1.

Table 1. Coefficients for Henry's law correlation in pure water

i	*A*	*B*	*C*	*D*	*T(K)*
CO_2	192.876	-9624.41	-28.7488	$14.4074 \cdot 10^{-3}$	273-473
H_2S	340.305	-13236.8	-55.0551	$59.5651 \cdot 10^{-3}$	273-423

With this estimation for Henry's law, the solubility of H_2S in different alkanolamine solutions can be calculated.

Pani et al. (1997b) calculated the diffusion coefficient for the amine, in their case MDEA, through a second flux equation devised from the stagnant boundary layer model (Liss and Slater, 1974), equilibrium equation for the different components as well as Fick's law for mass transfer for the species involved.

$$K_{eq} = \frac{C_{MDEAH^+} \cdot C_{HS^-}}{C_{MDEA} \cdot C_{H_2S}} \quad (31)$$

They assumed a near complete H_2S atmosphere and therefore no gas resistance in mass transfer. With the equilibrium equation (31) and some assumptions regarding diffusivities of the different ionic species they could create a flux equation (32) for H_2S. The third term in this equation models the enhancement of the absorption in the system. For the equilibrium constants of equation (31) they used a correlation by Kent and Eisenberg shown in equation (33).

$$N_{H_2S} = k_L \cdot \left(C_{H_2S,i} - C_{H_2S,bulk}\right) \cdot \left[1 + \frac{D_{MDEA}}{D_{H_2S}} \cdot \frac{\Omega}{C_{H_2S,i}}\right] \quad (32)$$

$$K_{eq} = e^{A + \frac{B}{\frac{T}{[F]}} + \frac{C}{\left(\frac{T}{[F]}\right)^2} + \frac{D}{\left(\frac{T}{[F]}\right)^3} + \frac{E}{\left(\frac{T}{[F]}\right)^4}} \quad (33)$$

where

$$\Omega = \frac{1}{2}\left[\left(C_{H_2S,i} \cdot K_{eq}\right)^2 + 4C_{H_2S,i} \cdot K_{eq} \cdot C_{MDEA,bulk}\right]^{\frac{1}{2}} - \frac{1}{2}K_{eq} \cdot C_{H_2S,i} \quad (34)$$

$$C_{H_2S,b} = \alpha_{H_2S,initial} \cdot C_{MDEA,Total} \quad (35)$$

The correlation by Kent and Eisenberg (1976) does not include MDEA in the original work, and Pani et al. (1997b) do not report the constants (A to E) they used for equation (33) but they however do provide the values they used for the equilibrium constants as 44.6 for 296 K and 19.3 for 343 K. An equation was found from Kamps et al. (2001) for the equilibrium constants and is presented in the reaction kinetics between H_2S and MDEA in Chapter 5.4.1.

From this flux equation, with the help of a correlation for H_2S diffusivity in water and the equilibrium constants, the diffusion coefficient for MDEA could be calculated. The correlation used for H_2S diffusion coefficient was developed by Haimour and Sandall (1987) for a temperature range of 288 K-303 K.

$$\frac{D_{H_2S}}{\left[\frac{cm^2}{s}\right]} = \frac{1.91 * 10^{-9} \cdot T}{\left(\frac{\mu}{\left[\frac{g}{cm * s}\right]}\right)^{0.74}} \quad (36)$$

However as the temperature range of the correlation by Haimour and Sandall (1987) does not encompass our entire temperature range. Tamimi et al. (1994) have continued the research of Haimour and Sandall and improved the diffusion coefficient equation to include temperatures between 293 and 368 K. Their data

range covers the temperatures used in our experiments, but their correlation does not seem to provide the values claimed and has large error (~50%) in high temperature (368 K). Therefore it was necessary to create a correlation from their collective data suitable for our use. We used the data available in Tamimi et al. (1994) for both their and Haimour and Sandall (1987) measurements. The correlation is shown in equation (37).

$$\frac{D_{H_2S}}{\left[\frac{cm^2}{s}\right]} = \frac{2.1999 * 10^{-9} \cdot T}{\left(\frac{\mu}{\left[\frac{g}{cm * s}\right]}\right)^{0.725}} \tag{37}$$

It can be further corrected by taking in to account the change in viscosity caused by adding amines to the solution. Correlation by Haimour and Sandall (1987) and our correlation are displayed in figure 7 in more detail.

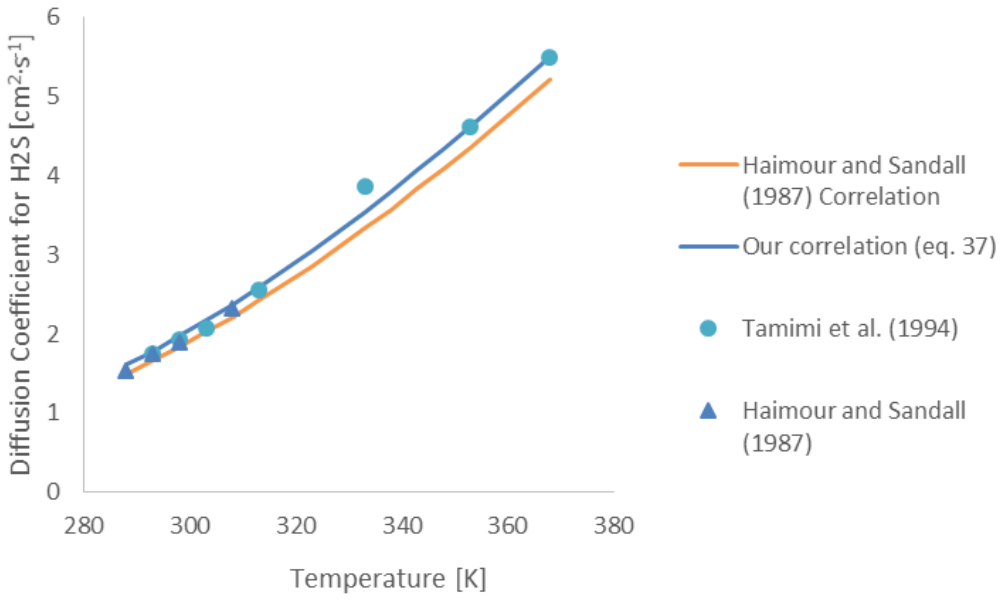

Figure 7. Haimour and Sandall (1987) and our correlation with measurement points

Calculated RSQ for our correlation and the correlation of Haimour and Sandall (1987) versus the measurement points from both Hamour and Sandall and Tamimi et al. (1994) were 0.992556 and 0.992337 respectfully, however there is a large

deviation in the higher temperature range with Hamour and Sandall correlation. As can be seen in the figure, our model represents the data better and could be used in the later calculations.

The mass transfer coefficient for H_2S was calculated by Pani et al. (1997b) using the same method described in 5.1 for CO_2. The equipment used for correlation calculation was the same Lewis-type cell as was used earlier in their articles (Pani et al., 1997a, 1997b). It consisted of two Rushton mixers, one for gas and one for liquid and vortex baffles on the liquid space. They used a slightly different multipliers in equation (11). Their updated correlation for H_2S is shown in equation (38).

$$\mathrm{Sh} = 0.25 \cdot \mathrm{Re}^{0.63} \cdot \mathrm{Sc}^{0.42} \quad (38)$$

5.4 H_2S Reaction kinetics

This chapter presents the available literature data on H_2S reaction kinetics with MDEA, MAPA and DEEA as well as some other amines that can be related to these. It also provides the preliminary means to estimate the enhancement caused by the reaction for the absorption and analyze the measurement results provided by the analysis equipment used.

5.4.1 H_2S Reaction with MDEA

For the flux equation (32) for H_2S the equilibrium constants are needed. Pani et al. (1997b) used a correlation by Kent and Eisenberg (1976). However as the original research article by Kent and Eisenberg did not include constants for MDEA and they were not reported by Pani et al. (1997b), a model for the equilibrium constants developed by Kamps et al. (2001) was used. Their research consisted of H_2S and CO_2 absorption in to MDEA and aqueous solutions of MDEA. They propose the reactions involved with H_2S to be

$$H_2S \Leftrightarrow HS^- + H^+ \quad \text{(XVII)}$$

$$HS^- \Leftrightarrow S^{2-} + H^+ \quad \text{(XVIII)}$$

$$H_2O \Leftrightarrow H^+ + OH^- \quad \text{(XIX)}$$

$$MDEAH^+ \Leftrightarrow MDEA + H^+ \quad \text{(XX)}$$

They created a correlation for the equilibrium constants for these reactions along with regressed parameters. Their correlation is valid in the temperature range of this thesis and is shown below in equation (39).

$$\ln(K_R) = A + \frac{B}{T} + C * \ln(T) + D * T + \frac{E}{T^2} \quad (39)$$

in which the constants A-E are reported in table 2.

Table 2. Constants for equation (39).

reaction	*A*	*B*	*C*	*D*	*E*	*T(K)*
(XVII)	461.716	-18034.7	-78.072	$9.1982 \cdot 10^{-2}$	-	273-548
(XVIII)	-214.559	-406.004	33.889	$-5.411 \cdot 10^{-2}$	-	273-498
(XIX)	140.932	-13445.9	-22.477	-	-	273-498
(XX)	-79.474	-819.7	10.9756	-	-	278-422

With equation (34) and correlation (39), we can now solve equation (32) and find out the flux of H_2S. It is worth noting however, that the equilibrium constant received this way is considerably lower than the one used by Pani et al. (1997b). The value given by this correlation for 296 K is 34.66 whereas Pani et al. used 44.6 in their calculations.

5.4.2 H_2S Reaction with MAPA

Direct literature articles studying MAPA and H_2S are unfortunately not available. However as MAPA contains both primary and secondary amine groups, its reaction should be similar to other compounds with these groups. Solubility of H_2S in diisopropanolamine (DIPA), a secondary amine, has been studied by Mazloumi et al. (2012) and the reaction equation they propose can be used for the secondary amine group in MAPA. However there is still the primary amine group that needs to be

addressed. This could be done by comparing it to monoethanolamine (MEA), which is also a primary amine, and by assuming that they would therefore react similarly. Reaction between MEA and H_2S was studied by Godini and Mowla (2008) who propose a reaction equilibrium equation that can be used as well for the primary amine group of MAPA. The reaction equilibrium equations for the primary group is shown in reaction (XXI) and the secondary group are shown in reactions (XXII) and (XXIII).

$$MEA + H_2S \overset{K_{eq,MEA}}{\Longleftrightarrow} MEAH^+ + HS^- \quad \text{(XXI)}$$

$$H_2S + H_2O \overset{K_{eq,H_2S}}{\Longleftrightarrow} H_3O^+ + HS^- \quad \text{(XXII)}$$

$$H_2O + DIPAH^+ \overset{K_{eq,DIPAH^+}}{\Longleftrightarrow} H_3O^+ + DIPA \quad \text{(XXIII)}$$

These equations can be further written for MAPA as follows

$$MAPA + H_2S \overset{K_{eq,XXIII}}{\Longleftrightarrow} MAPAH^+ + HS^- \quad \text{(XXIV)}$$

$$H_2S + H_2O \overset{K_{eq,XXIV}}{\Longleftrightarrow} H_3O^+ + HS^- \quad \text{(XXV)}$$

$$H_3O^+ + MAPA \overset{K_{eq,XXV}}{\Longleftrightarrow} H_2O + MAPAH^+ \quad \text{(XXVI)}$$

Study of the equilibrium constants of these reactions would provide the necessary data to calculate the flux equation presented earlier in equations (32) and (34).

5.4.3 H_2S Reaction with DEEA

The reaction with DEEA and H_2S is similar to that of and H_2S and MDEA as both of the amines are classified as tertiary. Earlier we have seen, in reaction equations (XVII) to (XX) from Pani et al. (1997b), how MDEA reacts with hydrogen sulfide. From these equations we can devise similar equations for DEEA as seen below

$$H_2S \overset{k_{eq,XXVI}}{\Longleftrightarrow} HS^- + H^+ \quad \text{(XXVII)}$$

$$HS^- \overset{k_{eq,XXVII}}{\Longleftrightarrow} S^{2-} + H^+ \quad \text{(XXVIII)}$$

$$H_2O \overset{k_{eq,XXVIII}}{\Longleftrightarrow} H^+ + OH^- \quad \text{(XXIX)}$$

$$DEEAH^+ \overset{k_{eq,XXIX}}{\Longleftrightarrow} DEEA + H^+ \quad \text{(XXX)}$$

Study of the equilibrium constants of these reactions would provide the necessary data to calculate the flux equation presented earlier in equations (32) and (34).

5.4.4 H_2S Reaction with DEEA+MAPA

The reactions (XXIV) to (XXVI) seen earlier in chapter 5.4.2 and (XXVII) to (XXX) seen in earlier chapter 5.4.3 can be used to model the whole system with DEEA and MAPA. There is however an apparent lack for the equilibrium constants of these reactions, which means we do not have the thermodynamic equilibrium data required for the use of equations (32) and (34) in estimation of flux. Further study of these equilibrium reactions is required for accurate analysis of results.

However the H_2S ionization in the aqueous alkanolamine can be described with equations (XVII), (XVIII) and (XIX). After the transfer to the liquid phase, the amine would start to react with the formed ions as seen in reaction equations (XXIII), (XXIV), (XXVI) and (XXX) and consequently decrease the H_2S concentration in the interface layer thus moving the actual concentration further from equilibrium. This in turn will increase the driving force of the absorption and increase the amount of H_2S diffusing to the liquid phase and thus increase the total loading of H_2S against the whole amine concentration.

Because accurate analysis with the earlier presented flux equations is not possible, the measurement results for absorption are provided. They are analyzed with equation (40) for rate of absorption.

$$N_{CO_2} = \frac{\Delta P_{CO_2} \cdot V_G}{T \cdot R} \quad (40)$$

This method however does not allow for the determination of the reaction coefficients for CO_2 within the solution.

5.5 N_2O Mass transfer kinetics

For the verification aforementioned mass transfer correlations (equations (8) - (11)), some measurements with Nitrous oxide are required. Nitrous oxide is used when developing mass transfer correlations for carbon dioxide in amine solutions, as its molecular structure is very similar to CO_2 but the absorption is purely molecular and does not include reactions. The mass transfer kinetics of nitrous oxide are straightforward. In the absorption process the phenomena is purely kinetic and does not contain any reactions that would enhance the absorption.

For our equations (8) - (11), a measurement for N_2O absorption in to MDEA is required. To calculate and verify coefficients of equation (11), some new calculations need to be presented. Equation (41) shows the calculation method used for mass transfer coefficient calculation. For this equation the flux of gas is required. The path to calculate the flux is shown in equations (42) to (47).

$$k_L = \frac{N_{N_2O}}{A \cdot \Delta C_{N_2O}} \tag{41}$$

$$C_{N_2O} = C_{N_2O,i} - C_{N_2O,bulk} \tag{42}$$

$$C_{N_2O,bulk} = \alpha_{N_2O} \cdot C_{MDEA,Total} \tag{43}$$

$$\alpha_{N_2O} = \frac{n_{N_2O,liquid}}{n_{MDEA,Total}} \tag{44}$$

$$n_{N_2O,liquid} = n_{N_2O,gas\ intial} - n_{N_2O,gas\ current} \tag{45}$$

$$n_{N_2O,gas} = \frac{P_{N_2O} \cdot V_G}{R \cdot T} \tag{46}$$

$$N_{N_2O} = \frac{\left(P_{N_2O,initial} - P_{N_2O,current}\right) \cdot V_G}{R \cdot T} \tag{47}$$

With the calculated mass transfer coefficient from equation (41), it is possible to iterate coefficients for equation (11) and thereby verify the correlation suggested by Pani et al. (1997a, 1997b)

6 Physical properties

This chapter will present correlations for physical properties of the solvents and their aqueous mixtures used within this work.

6.1 Methyldiethanolamine (MDEA)

As can be seen in the earlier correlations for mass transfer and reaction kinetics, the different physical properties of compounds are vital for the understanding of the whole absorption process. MDEA has considerable amount of data available about different properties related to absorption. Physical properties of the aqueous mixtures have been correlated by Al-Ghawas et al. (1989). Their work includes the density and viscosity correlations as well as correlations for Henry's law coefficients and the diffusion coefficients of CO_2 and N_2O in MDEA.

Density of aqueous MDEA can be modeled with equation (48)

$$\frac{\rho_{MDEA}}{\left[\frac{g}{ml}\right]} = K_1 + K_2 * T + K_3 * T^2 \tag{48}$$

Viscosity of the aqueous solution of MDEA can be modeled with equation (49)

$$\ln\left(\frac{\mu_{MDEA}}{[cP]}\right) = K_4 + \frac{K_5}{T} + K_6 * T \tag{49}$$

Henry's law coefficient for nitrous oxide in the solution can be modeled with equation (50).

$$\ln\left(\frac{H_{N_2O}}{\left[\frac{atm * dm^3}{mol}\right]}\right) = K_7 + \frac{K_8}{T} + \frac{K_9}{T^2} \quad (50)$$

Henry's law coefficient for carbon dioxide in the solution can be modeled with equation (51).

$$\ln\left(\frac{H_{CO_2}}{\left[\frac{atm * dm^3}{mol}\right]}\right) = K_{10} + \frac{K_{11}}{T} + \frac{K_{12}}{T^2} \quad (51)$$

Diffusion coefficient for nitrous oxide in aqueous MDEA can be modeled with equations (52) and (53) and diffusion coefficient for CO_2 in the solution with equations (54) and (55).

$$\frac{D_{N_2O}}{\left[\frac{cm^2}{s}\right]} * \frac{\left[\frac{\mu}{\left[\frac{g}{cm * s}\right]}\right]^{K_{13}}}{T} = K_{14} \quad (52)$$

$$\frac{D_{N_2O}}{\left[\frac{cm^2}{s}\right]} = K_{15} + K_{16} * T + K_{17} * T^2 \quad (53)$$

$$\frac{D_{CO_2}}{\left[\frac{cm^2}{s}\right]} * \frac{\left[\frac{\mu}{\left[\frac{g}{cm * s}\right]}\right]^{K_{18}}}{T} = K_{19} \quad (54)$$

$$\frac{D_{CO_2}}{\left[\frac{cm^2}{s}\right]} = K_{20} + K_{21} * T + K_{22} * T^2 \quad (55)$$

All the equations above use variables K_i for which the values are obtained from

$$K_i = k_{i,1} + k_{i,2} * w_M + k_{i,3} * w_M^2 + k_{i,4} * w_M^3 \quad (56)$$

The values for constants $k_{i,j}$ are found from table 3.

Table 3. Constants $k_{i,j}$ for Al Ghawas et al. (1989) correlations

i	*j*			
	1	2	3	4
1	$7.15929 \cdot 10^{-1}$	$3.95951 \cdot 10^{-1}$	$9.27974 \cdot 10^{-1}$	$-7.94931 \cdot 10^{-1}$
2	$2.13799 \cdot 10^{-3}$	$-1.98173 \cdot 10^{-3}$	$-3.87553 \cdot 10^{-3}$	$3.04228 \cdot 10^{-3}$
3	$-4.00972 \cdot 10^{-6}$	$3.07038 \cdot 10^{-6}$	$3.58483 \cdot 10^{-6}$	$-2.70947 \cdot 10^{-6}$
4	$-1.95214 \cdot 10^{1}$	$-2.33979 \cdot 10^{1}$	$-3.12363 \cdot 10^{1}$	$3.61735 \cdot 10^{1}$
5	$3.91273 \cdot 10^{3}$	$4.85880 \cdot 10^{3}$	$8.47705 \cdot 10^{3}$	$-8.35776 \cdot 10^{3}$
6	2.11220E-02	$3.33890 \cdot 10^{-2}$	$2.77980 \cdot 10^{-2}$	$-4.03670 \cdot 10^{-2}$
7	$-2.76708 \cdot 10^{1}$	$-2.51807 \cdot 10^{1}$	$2.94904 \cdot 10^{2}$	$-4.85183 \cdot 10^{2}$
8	$2.08156 \cdot 10^{4}$	$1.62930 \cdot 10^{4}$	$-1.86665 \cdot 10^{5}$	$3.03313 \cdot 10^{5}$
9	$-3.42241 \cdot 10^{6}$	$-2.59343 \cdot 10^{6}$	$2.95727 \cdot 10^{7}$	$-4.74632 \cdot 10^{7}$
10	2.01874	$-2.37638 \cdot 10^{1}$	$2.90092 \cdot 10^{2}$	$-4.80196 \cdot 10^{2}$
11	$3.13549 \cdot 10^{3}$	$1.54931 \cdot 10^{4}$	$-1.83987 \cdot 10^{5}$	$3.00562 \cdot 10^{5}$
12	$-8.13702 \cdot 10^{5}$	$-2.48081 \cdot 10^{6}$	$2.92013 \cdot 10^{7}$	$-4.70852 \cdot 10^{7}$
13	$2.87082 \cdot 10^{-1}$	1.63080	2.18355	
14	$1.15431 \cdot 10^{-8}$	$-4.38688 \cdot 10^{-8}$	$6.10493 \cdot 10^{-8}$	
15	$-1.87003 \cdot 10^{-4}$	$-9.28977 \cdot 10^{-4}$	$2.90751 \cdot 10^{-3}$	
16	$1.17495 \cdot 10^{-6}$	$5.47369 \cdot 10^{-6}$	$-1.81176 \cdot 10^{-5}$	
17	$-1.66913 \cdot 10^{-9}$	$-8.08740 \cdot 10^{-9}$	$2.79727 \cdot 10^{-8}$	
18	1.00481	$-7.43677 \cdot 10^{-2}$	$-4.65263 \cdot 10^{-2}$	
19	$5.47115 \cdot 10^{-10}$	$1.76598 \cdot 10^{-9}$	$3.16239 \cdot 10^{-9}$	
20	$2.46851 \cdot 10^{-4}$	$-1.00629 \cdot 10^{-3}$	$2.87762 \cdot 10^{-3}$	
21	$-1.99813 \cdot 10^{-6}$	$5.98956 \cdot 10^{-6}$	$-1.73422 \cdot 10^{-5}$	
22	$4.13889 \cdot 10^{-9}$	$-8.99012 \cdot 10^{-9}$	$2.56824 \cdot 10^{-8}$	

The diffusion coefficient for the amine in water has been correlated by Snijder et al. (1993) but was found to be inaccurate. Their published data was used to develop a correlation for the diffusion coefficient as is shown in equation (57)

$$D_{MDEA} = e^{8.065-\left(\frac{2502.961}{T}\right)-2.4772*10^{-4}*C_{MDEA}} \quad (57)$$

6.2 2-(diethylamino)-ethanol (DEEA)

The densities of DEEA and aqueous solutions of DEEA can be estimated through correlations by Pinto et al. (2014a). The correlations work well with the aqueous

solutions and provide only a small error that increases as temperature increases, however the error reaches only 0.19% at 353 K. Correlation for pure DEEA is shown in equation (58) and the correlation for aqueous solutions of DEEA is shown in equation (59).

$$\frac{\boldsymbol{\rho_{DEEA}}}{\left[\frac{\boldsymbol{g}}{\boldsymbol{cm^3}}\right]} = \boldsymbol{D_1} * \boldsymbol{T^2} + \boldsymbol{D_2} * \boldsymbol{T} + \boldsymbol{D_3} \tag{58}$$

$$\frac{\mathbf{1}}{\frac{\boldsymbol{\rho_{mix,aq}}}{\left[\frac{\boldsymbol{g}}{\boldsymbol{cm^3}}\right]}} = \frac{\boldsymbol{V^E} + \boldsymbol{x_{DEEA}} * \left(\frac{\boldsymbol{M_{DEEA}}}{\frac{\boldsymbol{\rho_{DEEA}}}{\left[\frac{\boldsymbol{g}}{\boldsymbol{cm^3}}\right]}}\right) + \boldsymbol{x_{Water}} * \left(\frac{\boldsymbol{M_{Water}}}{\frac{\boldsymbol{\rho_{Water}}}{\left[\frac{\boldsymbol{g}}{\boldsymbol{cm^3}}\right]}}\right)}{\boldsymbol{x_{DEEA}} * \boldsymbol{M_{DEEA}} + \boldsymbol{x_{Water}} * \boldsymbol{M_{Water}}} \tag{59}$$

$$V^E = x_{DEEA} * x_{Water} * \sum_n A_n * (1 - 2 * x_{Water})^{n-1} \tag{60}$$

Terms A_n used in equation (60) depend on temperature as shown in equation (61)

$$A_n = a_n + b_n * T \tag{61}$$

for which the constants a_n and b_n for DEEA are available in table 4.

Table 4. Constants for equation (61)

a_1	b_1	a_2	b_2	a_3	b_3
-11.2847	$1.2653 \cdot 10^{-2}$	6.6899	$-1.2813 \cdot 10^{-2}$	-5.1906	$8.7350 \cdot 10^{-3}$

A viscosity correlation for pure DEEA has been proposed by DiGuilio et al. (1992) as is shown in equation (62).

$$\frac{\boldsymbol{\mu_{DEEA}}}{[\boldsymbol{mPa} * \boldsymbol{s}]} = \boldsymbol{e}^{\boldsymbol{b_1} + \frac{\boldsymbol{b_2}}{\boldsymbol{T} - \boldsymbol{b_3}}} \tag{62}$$

where b_i are available in table 5.

Table 5. Constants for equation (62)

b_1	b_2	b_3
-4.2337	884.19	141.15

6.3 3-(methylamino)-propylamine (MAPA)

Densities of MAPA and aqueous solutions of MAPA have been correlated by Pinto et al. (2014a) to follow a Redlich-Kister equation. The correlation for aqueous solutions has a similar error as that of DEEA and it reaches a maximum of 0.24% (at 333.15 K) in the temperature range used in this work. The error increases significantly after this temperature and for 353.15 K it is already 1.3%. Density correlation for pure MAPA is shown in equation (63) and the correlation for aqueous MAPA is shown in equation (64).

$$\frac{\rho_{MAPA}}{\left[\frac{g}{cm^3}\right]} = D_1 * T^2 + D_2 * T + D_3 \tag{63}$$

$$\frac{1}{\frac{\rho_{mix,aq}}{\left[\frac{g}{cm^3}\right]}} = \frac{V^E + x_{MAPA} * \left(\frac{M_{MAPA}}{\frac{\rho_{MAPA}}{\left[\frac{g}{cm^3}\right]}}\right) + x_{Water} * \left(\frac{M_{Water}}{\frac{\rho_{Water}}{\left[\frac{g}{cm^3}\right]}}\right)}{x_{MAPA} * M_{MAPA} + x_{Water} * M_{Water}} \tag{64}$$

$$V^E = x_{MAPA} * x_{Water} * \sum_n A_n * (1 - 2 * x_{Water})^{n-1} \tag{65}$$

Terms A_n used in equation (65) depend on temperature as shown earlier in equation (61), for which the constants a_n and b_n for MAPA are available in table 6.

Table 6. Constants for equation (65)

a_1	b_1	a_2	b_2	a_3	b_3
-7.8636	$-4.02 \cdot 10^{-3}$	10.4062	$-2.101 \cdot 10^{-2}$	-4.7552	$1.4846 \cdot 10^{-2}$

A viscosity correlation for aqueous MAPA solutions has been proposed by Liao et al. (2014) and is shown in equation (66).

$$\frac{\mu}{[\mathrm{mPas}]} = e^{D_0 + \frac{D_1}{T} + \frac{D_2}{T^2}} \tag{66}$$

, where D_i is from

$$D_i = d_{i,0} + d_{i,1} * x_{MAPA} + d_{i,2} * x_{MAPA}^2 \tag{67}$$

, where the constants $d_{i,j}$ can be seen from table 7.

Table 7. Constants for equation (67)

i	*j*		
	0	*1*	*2*
0	7.731	$-6.644 \cdot 10^3$	$1.277 \cdot 10^6$
1	33.93	$-3.163 \cdot 10^4$	$8.64 \cdot 10^6$
2	-852.7	$5.377 \cdot 10^5$	$-8.956 \cdot 10^7$

6.4 Aqueous solutions of MAPA and DEEA

The fairly recent interest in the solvent system of MAPA and DEEA means that there is not much kinetic research available. There are some studies in regard to different properties of this combination by other research teams. Measurements for VLE with MAPA/DEEA, MAPA/H_2O and DEEA/H_2O have been published and regressed for UNIQUAC parameters by Hartono et al. (2013), which can be used to model the VLE, activity coefficients, excess enthalpies and freezing point depressions of this system.

The heat of absorption was measured by Arshad et al. (2013) and they found that when a DEEA/MAPA/H_2O solvent is used, the heat of absorption at the usual absorption temperatures (around 313.15 K) is considerably lower than that of MEA.

It is between 95 and 50 kJ·mol^{-1} CO_2 at a loading of 0 to 0.8 mol CO_2·(mol Amine)$^{-1}$ respectively, whereas for MEA, it is approximately 83 kJ·(mol CO_2)$^{-1}$ in the same temperatures, independent from loading. The heat of absorption drops below that of MEA around 0.3 mol CO_2·(mol Amine)$^{-1}$ loading. Similar trend is visible for the higher temperature (around 393.15 K) usually seen with desorption as the heat of absorption is between 105 and 45 kJ·(mol CO_2)$^{-1}$ seen at 0 to 0.3 mol CO_2·(mol Amine)$^{-1}$ loading respectively, whereas MEA has values around 110 kJ·(mol CO_2)$^{-1}$ independent from loading. The phase split between these amines happens so, that the gas rich phase consists of most of the MAPA and some DEEA depending on the loading of the solution. The behavior suggests that the regeneration costs of the CO_2 rich phase should be considerably lower than with conventional solvents if only the CO_2 bound in DEEA is regenerated. Liquid-liquid split in the amines is illustrated in figure 8.

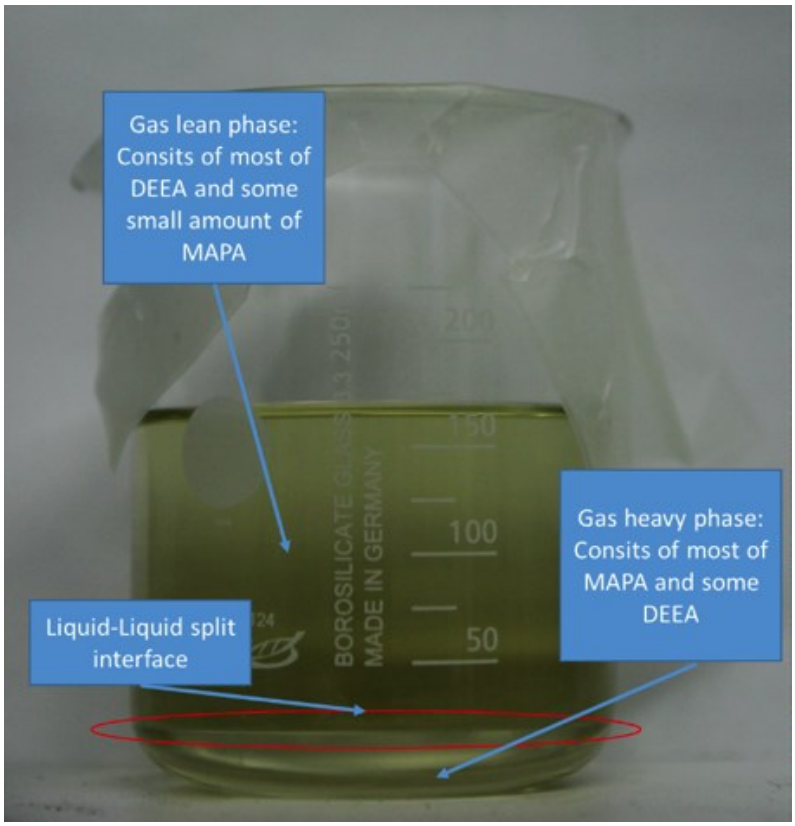

Figure 8. MAPA/DEEA/H_2O Liquid-Liquid split

The density of MAPA+DEEA binary mixtures has been studied by Wang et al. (2013). They correlated the density of this mixture with the equation (64), replacing water with DEEA. However they used more A_n parameters for equation (65) than Pinto et al. (2014a) did for aqueous mixtures of the single amines. These parameters are available in table 8.

Table 8. Constants for equation (65) for MAPA+DEEA

T (K)	A_0 [$cm^3 \cdot mol^{-1}$]	A_1 [$cm^3 \cdot mol^{-1}$]	A_2 [$cm^3 \cdot mol^{-1}$]	A_3 [$cm^3 \cdot mol^{-1}$]
283.15	-1.463	0.051	-0.038	-0.665
293.15	-1.682	0.03	0.003	-0.423
303.15	-1.896	0.061	-0.056	-0.330
313.15	-2.129	0.160	-0.126	-0.354
323.15	-2.366	0.237	-0.187	-0.338
333.15	-2.605	0.303	-0.261	-0.308
343.15	-2.851	0.381	-0.356	-0.256
353.15	-3.059	0.408	-0.376	-0.314
363.15	-3.302	0.421	-0.429	-0.201

As the solution used in this work consists of only 20 wt% water, it is assumed that the volume can be assessed with binary density model of MAPA and DEEA as well as pure water density.

7 Processes and Phase Change Solvents

There are a few different commercially licensed processes in use that use a combination of amine solvents that forms a phase split. This phase split can be caused by critical CO_2 loading or in some cases with a temperature difference in the system. Critical loading is used by both DMX™ (Raynal et al., 2011) and HySWEET (Cadours et al., 2012) process methods. The core concept behind the phase split amine solvents is explained in addition to the typical absorption process and the aforementioned DMX™ and HySWEET processes.

7.1 Demixing amines

As was previously briefly mentioned, the energy intensive part of any absorption process is the desorption. This is usually due to the high volume of liquid required for good gas absorption and purification in the absorption column. When this liquid is regenerated, it is heated to high temperatures (for example 393.15 K) to reduce the saturation pressure of the gas. This then causes the gas to desorb from the liquid and a nearly pure gas stream of acid gas is received. Solvent amount is dependent on the amount of sour gas that can be loaded and unloaded from the solvent in the process. This is referred to the cyclic capacity.

In the desorption step the energy requirements for a normal absorption process can be as high as 3.7 $GJ\cdot(t\ CO_2)^{-1}$, depending on the volume of the absorbent (Raynal et al., 2011). One of the goals in recent research has been that of finding solutions that form a liquid-liquid split at certain loadings in the effort to decrease the costs of regeneration of the solvent. This has led to a study of different mixtures of absorbents. These mixtures are referenced to as demixing amines or phase-changing solvents. They allow for the regeneration of only one phase, high in acid gas concentration, while the other, gas lean phase, is recycled back in to the absorber without stripping. As was earlier mentioned, in these cases the absorbent is usually made of two components. One that has fast absorption kinetics but low maximum loading (for example MAPA) and the other with slow kinetics but high maximum loading (for example DEEA).

When a critical concentration in the absorbent is reached, it will start to form a split of gas rich and gas-lean layers. The gas rich layer will increase in volume as absorption proceeds until the targeted loading is reached. Then the absorbent is fed to a decanter. Heavy phase from decanter is fed to the desorber where it is heated and regenerated and a pure gas stream is obtained. The light phase is circulated to a mixing tank for mixing with the regenerated heavy phase. After being cooled down the regenerated amine mixture is then mixed with the lean phase from the decanter. (Liebenthal et al., 2013) The general schematic of such a process is shown in figure 9.

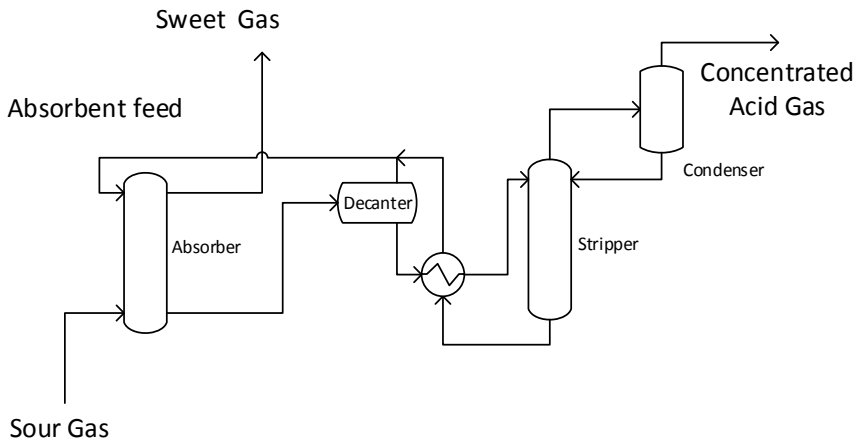

Figure 9. Two liquid phase absorption process

Some solutions have already been researched with a goal to improve energy efficiency of CO_2 capture. Measurements with aqueous alkyl piperidine mixtures and CO_2 were reported by Ballerat-Busserolles et al (2013). Absorption of CO_2 in to MAPA and DEEA and their mixtures was researched by Arshad et al. (2014, 2013).

They found that DEEA has a low heat of absorption, holding at ~60 kJ·(mol CO_2)$^{-1}$ from a loading of 0 mol CO_2·(mol amine)$^{-1}$ until loading reaches 0.9 mol CO_2·(mol amine)$^{-1}$, at which point it drops rapidly, reaching ~10 kJ·(mol CO_2)$^{-1}$ at a loading of 1.3 mol CO_2·(mol amine)$^{-1}$. They also noted that it has a high cyclic capacity for CO_2 meaning that it can absorb a lot of CO_2 in a low temperature (i.e. 313.15 K), but when the temperature is increased the loading drops considerably. The problem, they say, is that while DEEA can absorb high amounts, the absorption kinetics (flux of gas to liquid) are low and can therefore lead to a large size of the absorber. The slow kinetics are due to the tertiary amine configuration and the steric hindrance caused by the groups.

MAPA on the other hand has a fast absorption rate and a high loading at various temperatures. It also has a high heat of absorption, which can lead to large energy costs in regeneration. The reaction kinetics however are fast, and this could lead to a reasonably sized absorber. When these two are combined in to a mixed solvent, the

behavior is first similar to that of MAPA: the reaction kinetics are fast but as all of MAPA is loaded with CO_2, the kinetics become more similar to those of DEEA, meaning slower absorption rates. There is a liquid-liquid split at certain CO_2 loadings. The initial behavior and critical loading is claimed to be dependent on the concentrations of MAPA in the solution. Heats of absorption in the mixtures of DEEA and MAPA are lower than monoethanolamine (MEA), the solvent they compared their research to.

When the solvent pair MAPA+DEEA is used with CO_2, the acid gas rich phase consists initially of MAPA as it has faster reaction rate towards CO_2. The acid gas-lean phase works as a kind of a buffer for DEEA, since the reaction kinetics with it are slower but the maximum loading is higher. As the absorption proceeds further, the buffer phase, consisting mostly of DEEA, transfers in to the CO_2 rich phase. This happens due to the saturation of MAPA, which then works as an activator for the reaction with DEEA and CO_2. (Pinto et al., 2014b)

There is a question that rises from this behavior of MAPA+DEEA solvents: What happens to the kinetic rate in an absorption tower when gas is absorbed in to a solvent over a long period of time. Will the kinetics stay close to those of MAPA or will they behave like DEEA? It would be of interest to study these compounds in an actual absorption column to see their behavior when the solvent is regenerated at the same time and fed back to the system.

7.2 Applications in gas purification

Glasscock (1990) covered a wide range of different gas absorption technologies in his doctoral thesis. It included processes to absorb CO_2 using hot potassium carbonate solutions, ammonia solutions and different amines as a reactive absorption media and water and special physical solvents as physical absorption media. He states that hot potassium carbonate solutions are mostly used in ammonia plants were temperatures and partial pressures of CO_2 reach such high values that amine solutions are not viable. He also makes a note that ammonia is not highly used due to its corrosiveness and problematic process flow schemes compared to those of

alkanolamine and hot potassium based processes. It can however be suitable for removal of CO_2 at low initial partial pressures. Next a typical process for gas absorption is explained and a few novel processes are introduced.

7.2.1 Typical Absorption Process

The typical process for absorption of CO_2 or H_2S from an acidic gas stream consists of an absorber, a desorber, a few heat exchangers, few pumps and of course a liquid solvent that absorbs the acidic gas as was discussed earlier. Alkanolamine based gas treatment processes have been in use since 1930, when R.R. Bottoms patented a process for the use of triethanolamine (TEA) in gas treatment. After his patent many other alkanolamines were evaluated and studied for the same use. (Kohl and Nielsen, 1997)

The process has been described in many books and is being researched by multiple research centers and groups, all trying to improve the energy efficiency and decrease costs related to the process. The high costs from desorption have been also been battled by using an inert gas as the stripping gas when regenerating the solvent. This is often more economical than using just heat to remove the gas. (Kriebel, 2008)

Usually the gas enters an absorption tower from the bottom and exists from top while the solvent is fed from top and exits from bottom. The towers can have either plates or some random or structured packaging in them to increase the mass transfer area between the gas and the liquid. There are varying versions of the plate designs used in the different absorption columns depending on the gas loading and other process variables. Most towers containing random packaging will have Raschig rings, Pall rings, Berl saddles or Intalox packaging in them. Structured packaging has usually higher efficiency than the random packaging types as the ratio of free space towards packaging is set in the structure. Typical packages in this style are Mellapack and Kerpak by Sulzer. There are also application specific specially tailored packaging available. In the top of the tower there is usually a water wash to remove the remainders of amines from the gas flow before it exits from the tower. The gas rich solvent is then pumped to a desorption tower through heat exchangers and then the

acidic gas is removed from the solvent through an up flowing steam flow. The removed acidic gas is then ready for compression while the regenerated solution is ready to be fed back to the absorption tower. (TGM, 2010, Kriebel, 2008)

7.2.2 DMX™ process

IFP Energies nouvelles (Raynal et al., 2011) has developed a process that uses a phase changing solvent to absorb CO_2 from flue gases. The process is focused at reducing the regeneration energy costs of the amine absorbent by creating a CO_2 rich and a CO_2 lean phase. The goal is very similar to the research goals in this thesis for H_2S and CO_2 as well as to the research done by others (Arshad et al., 2013, Arshad et al., 2014, Ballerat-Busserolles et al., 2013) for CO_2. It is reported that the energy costs for regeneration would be decreased from 3.7 GJ·(ton CO_2)$^{-1}$ to 2.3 GJ·(ton CO_2)$^{-1}$ with the new absorbent solution they call DMX-1. They also report that the process was in a pilot plant state in 2011 and was aiming to move to large scale pilot validation later. (Raynal et al., 2011) Unfortunately the solvent used is not described further in any detail. Existence of such processes shows that there is however a possibility to use such novel solvent solutions to largely improve upon the traditional absorption process.

7.2.3 HySWEET process

The HySWEET process was developed for Total S.A. by Cadours et al. (2012) and had its first industrial test in 2007, at an installation that was due to be shut down, and the first commercial license for the process was sold on 2010. The benefits of this process are the simultaneous removal of CO_2, H_2S and mercaptans from acid gas streams as well as a low hydrocarbon absorption and a good energy efficiency.

The process uses a hybrid solvent, which combines the chemical capacity of an amine and the physical properties of thiodiglycol. In their implementations of the process in France, up to 8-15% lower energy consumption was observed when compared to a “conventional” MEA based amine process. They also claim an advantage with the process in relation to simplicity; it is similar to amine processes

in configuration. They therefore propose that it should be possible to retrofit their process to current amine units and upgrade them to improve the efficiency of unwanted component removal. (Cadours et al., 2012) The process has had interest from different companies, including GASCO in Abu Dhabi and Technip and Prosernat. Since 2008, half of Lacq's production has been treated with these units and the four years between the articles release and the installation of the units show that the process is stable and has very good improvements including mercaptan removal and energy efficiency decrease. (Cadours et al., 2012)

8 Published research equipment and methods for kinetic measurements

To discover what other research methods are used to study behavior effecting gas absorption, a literature survey was conducted. During the study it was discovered that the research in to this field is mostly conducted in experimental columns, cells or in a Laminar Jet Sphere Apparatus developed for the purpose. The information on some methods and equipment used to analyze absorption with amines is introduced in this chapter.

8.1 Autoclave & Cell

An autoclave has been used by Kennard and Meisen (1984) to study the phase equilibrium of CO_2 in to DEA. The apparatus could handle temperatures ranging from room temperature to about 400 °C and pressures up to 13 MPa. Their studies however encompassed a temperature range that is more reasonable for amine solutions, ranging from 100 to 205 °C and a pressure range of 70 to 4000 kPa. Estimation of the absorbed gas amount was done with similar methods used in our work: measuring the total pressure before gas introduction and then again after the equilibrium had set. However they do not provide any online pressure vs time data. Their apparatus is shown in figure 10.

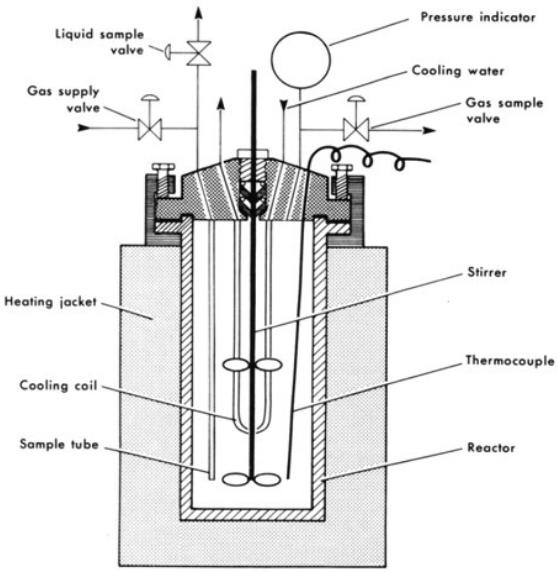

Figure 10. Autoclave used by Kennard and Meisen (Kennard and Meisen, 1984)

A Hastelloy cell has been used by a team in France (Ferrando et al., 2008) to study H_2S and CO_2 absorption and its phase equilibrium and to provide data needed to model it using the electrolyte-NRTL model. The cell could withstand pressures up to 100 bar and temperatures between 323.15 K and 473.15 K. In their setup the storage tanks for H_2S and CO_2 are thermostated to reduce the error caused by temperature changes in the cell when feeding gas with a different temperature. The schematic of their experimental setup is shown in figure 11.

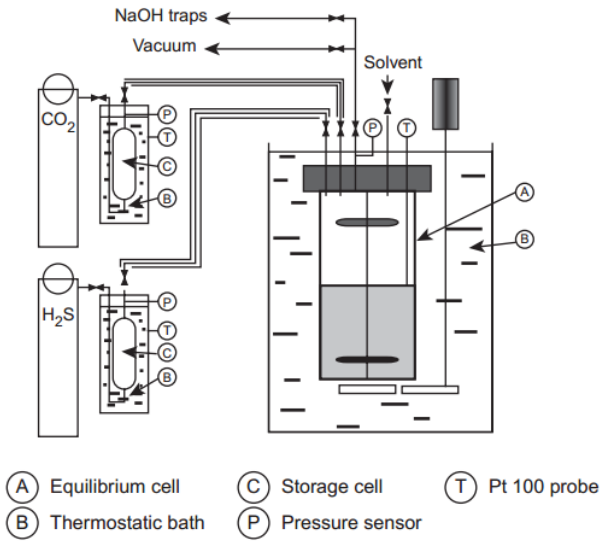

Figure 11. Hastelloy cell used by Ferrando et al. (2008)

A stirred glass cell similar to the setup used by Pani et al. (1997a, 1997b) was also employed by Sutar et al. (2013) in their studies on kinetics of activated DEEA solutions for CO_2 capture. Their cell was designed for a pressure of 202.6 kPa. Experiments were done in 303 K and the DEEA concentration was 2.5 M. They varied the concentration of promoters, piperazine, ethanolamine or 1,6-hexamethylamine, in the range of 0.1-0.5 M. Pressure change was logged against time and analyzed for kinetic data. Their design differs from ours by having only a single mixer shaft instead of two shafts and motors. Allowing only a single stirring speed to be set for both liquid and gas phases. Figure 12 illustrates the experimental setup used by the research group.

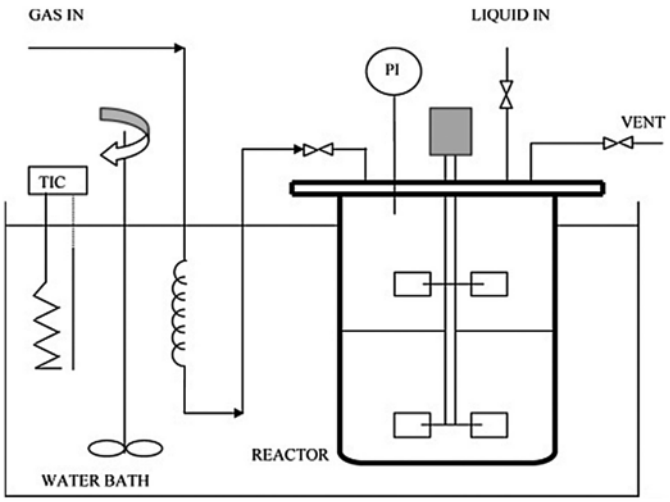

Figure 12. Experimental setup used by Sutar et al. (2013)

8.2 Wetted Wall Columns

Wetted wall columns are proposed to be extensively used due to their ability to evaluate the absorption process and its coefficients on the surface of a real packaging (Chen et al., 2011). One research team has used a wetted wall column in their research of simultaneous absorption of CO_2 and H_2S (Mandal and Bandyopadhyay, 2006). They used a temperature range of 293-313 K and an aqueous solution of 3 mol amine (MDEA+DEA)·dm^{-3}. Concentrations of the two amines ranged from a 2.8 mol MDEA·dm^{-3} + 0.2 mol DEA·dm^{-3} to 0.2 mol MDEA·dm^{-3} + 2.8 mol DEA·dm^{-3}. H_2S content in the absorbent solution was determined with an autotitrator and CO_2 content was determined by acidulating the whole sample, measuring total pressure of

the gas in it and subtracting the H_2S amount from that. The experimental setup is shown in figure 13.

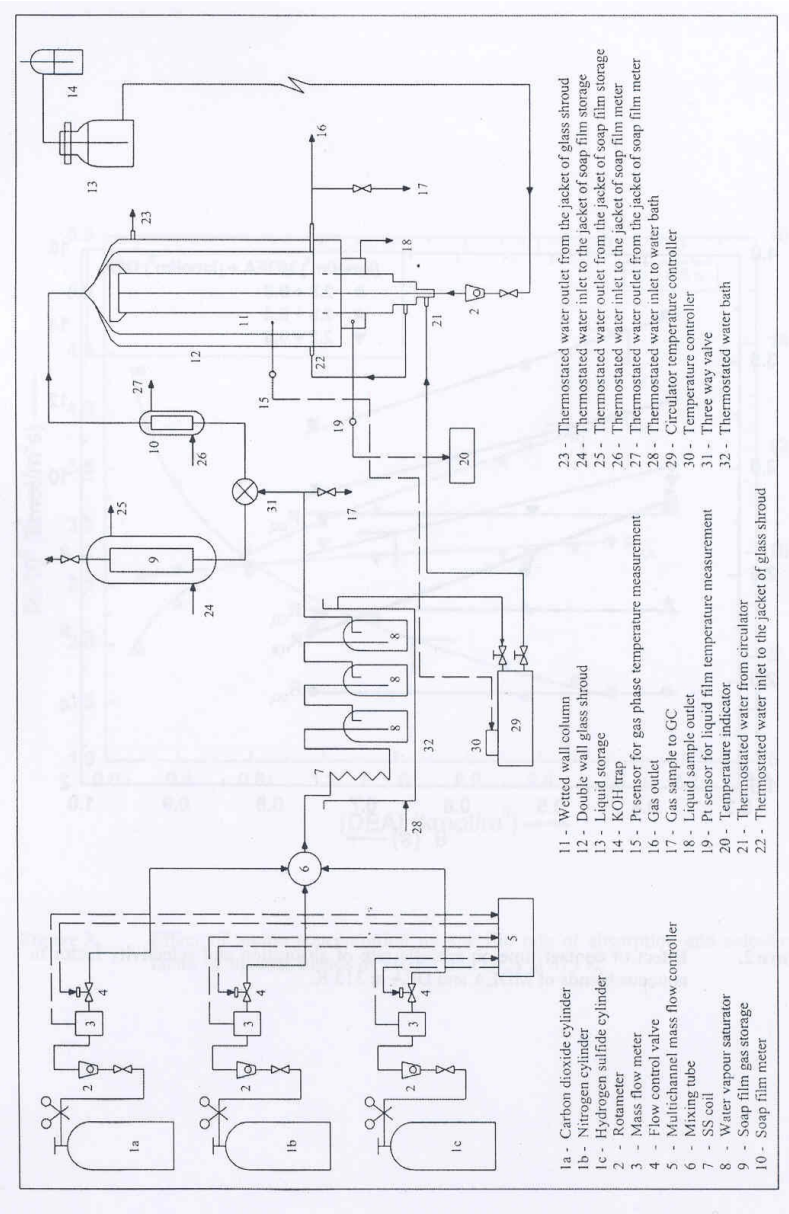

Figure 13. Experimental setup used by Mandal and Bandyopadhyay (2006).

A similar apparatus was used by Chen et al. (2011) to study CO_2 capture by MAPA. Chen et al. kept the system pressure regulated between 200-700 kPa and temperature between 40-100 °C. They screened solvents such as diglycolamine, 2-amino-2methyl-propane, MAPA, and MDEA/piperazine with varying concentrations. Voice et al. (2013) used MAPA concentrations between 8-9 M, MEA concentrations around 7 M and piperazine concentrations of 8 M. The system pressure was regulated in the same pressure range of 200-700 kPa as used in Chen et al. (2011)

measurements. The experimental setup used by both is shown in figure 14 and the wetted wall column is shown in more detail in figure 15.

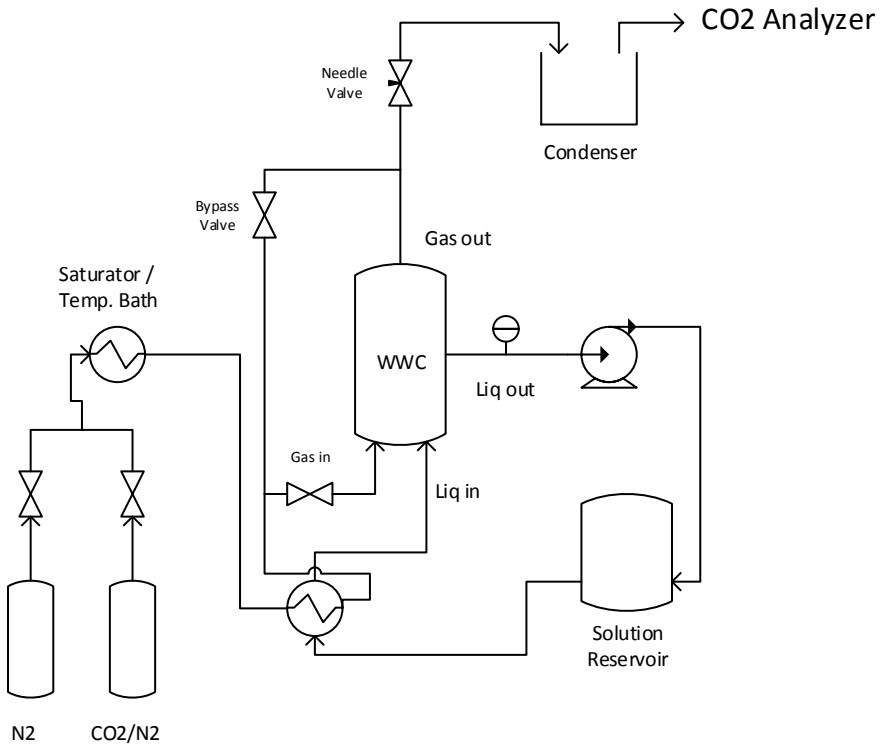

Figure 14. Experimental setup used by Chen et al. (2011) and Voice et al. (2013).

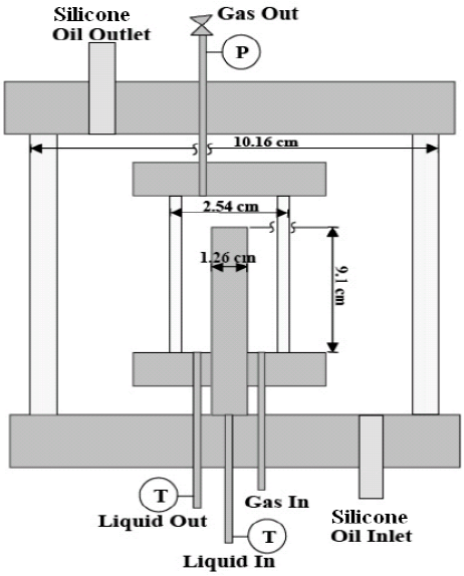

Figure 15. Detailed view of the Wetted Wall Column used by Chen et al. (2011) and Voice et al. (2013).

8.3 Wetted Sphere Apparatus

Another type of equipment developed for the study of absorption is the Wetted Sphere Apparatus. It uses the same principle as wetted wall columns and the equipment consists of a glass cell between two metal flanges and a metal ball within the glass encasement. The ball is supported by a feeding pipe, which feeds the liquid through the ball to the top of it and then the liquid slowly falls down the sides creating a film surface. The radius of the sphere can be varied. There are studies made on CO_2 absorption with MDEA, DEA, DIPA and AMP with activators by multiple authors. (Vaidya and Kenig, 2007a, Seo and Hong, 2000) The apparatus is shown in figure 16.

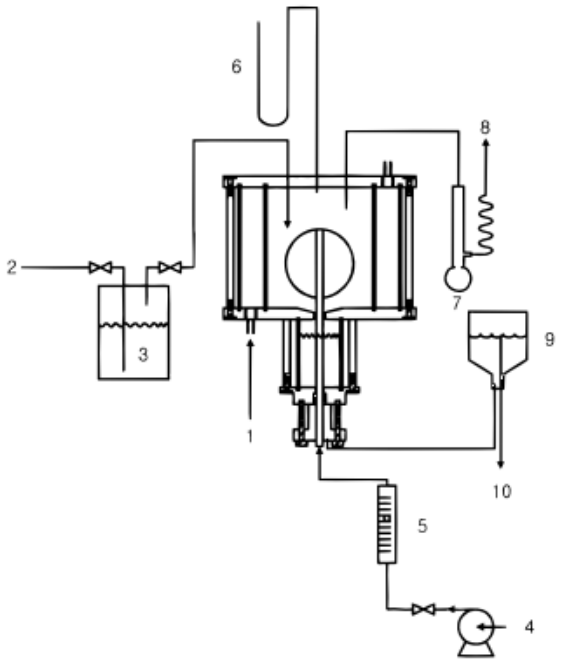

Figure 16. Wetted Sphere Apparatus as seen in (Seo and Hong, 2000). The different equipment are denoted as 1: Cooling water feed, 2: gas supply feed, 3: saturator, 4: Liquid tank feed, 5: rotameter for liquid flow, 6: Manometer for equipment pressure, 7: soap bubble meter, 8: gas vent to fume hood, 9: liquid level controller and 10: drainage connection.

There has also been a study done with the use of a hemispherical connector, which is essentially the same as the wetted sphere apparatus but instead of a full sphere a hemisphere is used. The liquid creates a surface on the flat top of the sphere and then cascades down the sides, forming a liquid film in to which the gas can absorb. The benefit gained from this structure is that the surface rippling in the lower part of the sphere is reduced. (Vaidya and Kenig, 2007a)

8.4 Laminar Jet Apparatus

Laminar jet apparatus consists of a glass cylinder which is enclosed by a jacket. Within the cylinder there are two pipes, one for feeding the liquid and one for collecting it. A liquid jet is shot out from a small cylindrical hole in the feed pipe positioned above the collector. This jet has a very small diameter and it passes through the absorbent gas. The gas absorbs in to the liquid and the liquid is then collected by a small capillary hole in the second tube below it and analyzed. The drawback of the method is that the interface area is very strictly controlled by the cell geometry and cannot be varied highly. There has also been some research done to improve the nozzle from which the liquid is shot out of, in an attempt to improve the accuracy of obtained data. (Vaidya and Kenig, 2007a, Aboudheir et al., 2003, 2004) The experimental setup used by Aboudheir et al. (2004) is shown in figure 17.

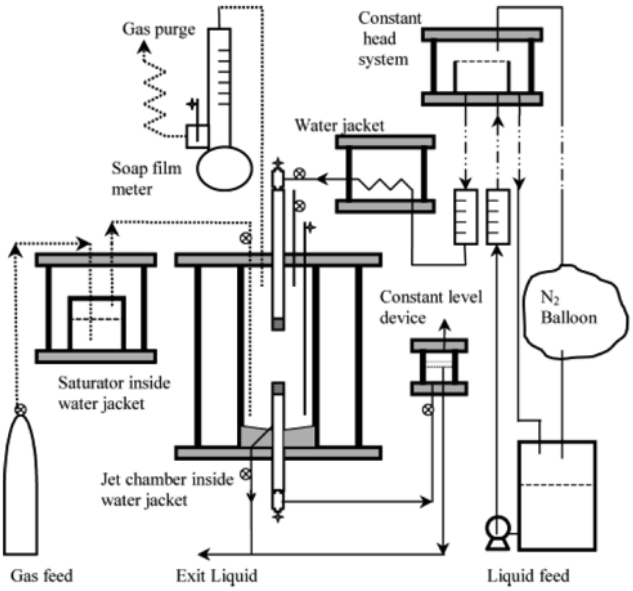

Figure 17. Laminar jet apparatus as used by Aboudheir et al.

Gas concentration is controlled by total pressure in the system rather than by introducing some inert gas to lower the partial pressure of absorbent. This is done to prevent uncertainties in the gas side transfer coefficient. There are studies done in CO_2 absorption in MDEA, DEA and MEA by various authors in a narrow range of 20-70 °C. (Vaidya and Kenig, 2007a)

9 Instruments and measurements

9.1 Experimental apparatus

The experimental apparatus consists of a Lewis cell designed by D. Richon, a gas feed tank, a vacuum pump and a thermostatic bath to control the temperature of the cell. The cell has a PT100 probe for temperature measurement and a UNIK 5000 pressure transducer with a 0 to 250 kPa range connected to it. This latter unit had a reported accuracy of 0.2 % of full range (±500 Pa).

The cell consists of a glass cylinder with an inner diameter of 0.06 m, a bottom and top flange and two magnetically driven 6-bladed Rushton type mixers. Flanges and turbines are made from stainless steel and have sapphire bearings on both ends. The Rushton mixers have a diameter of 0.05m. Lower part of the cell has four baffles made from PVC to prevent vortexes in the liquid. The sapphire bearings for the mixers are embedded in PVC in the middle of the cell and in the steel in top and bottom parts. The cell construction is shown in figure 18 and a picture of the actual cell is shown in figure 19.

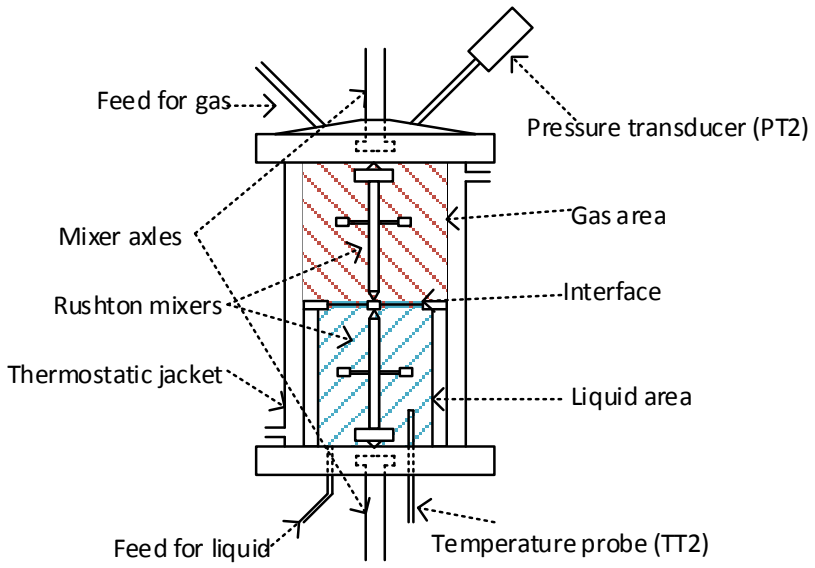

Figure 18. The Lewis type cell used in this work

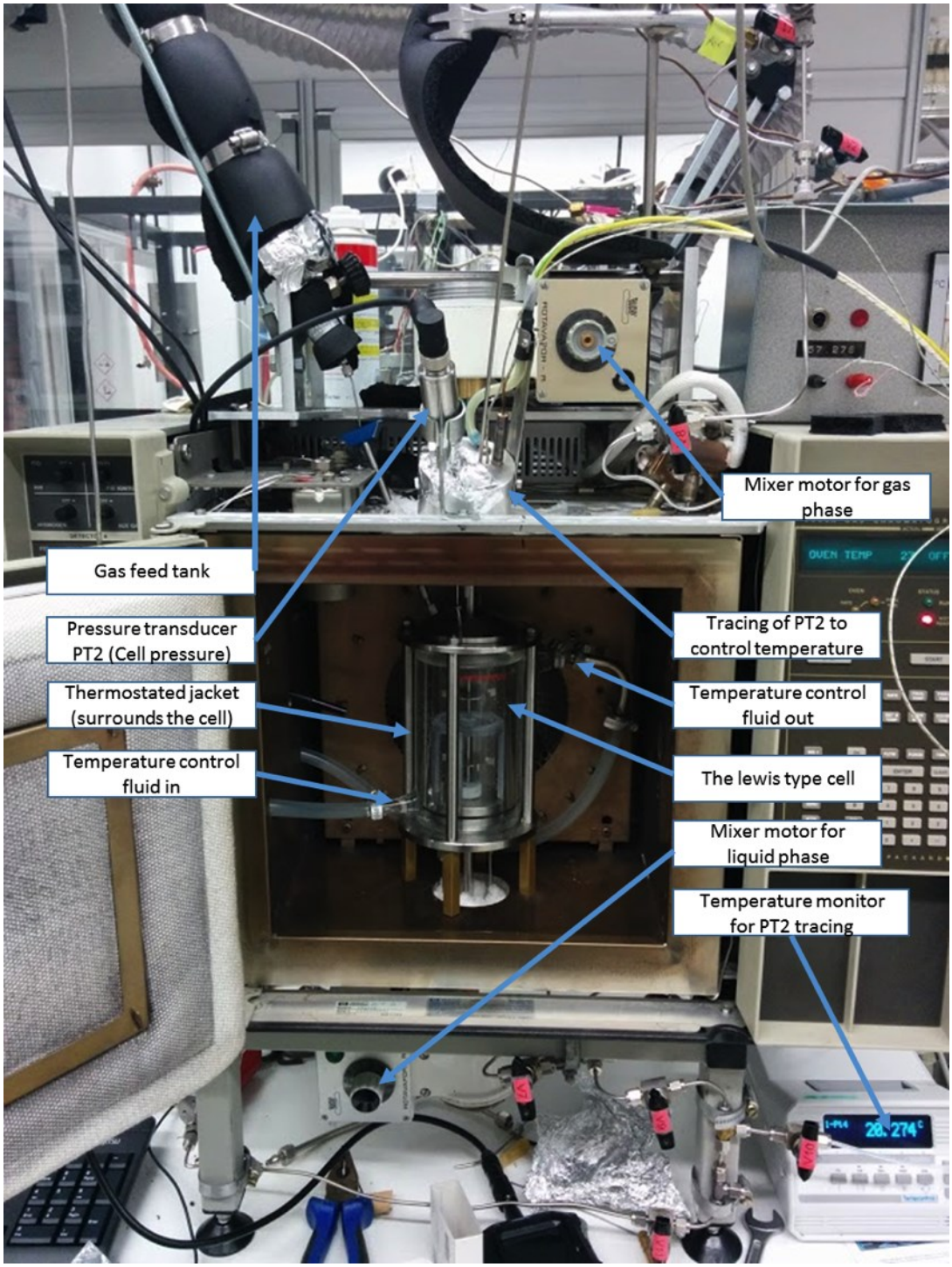

Figure 19. The measurement Apparatus including the Lewis type cell with pressure transducer, mixers, temperature transducers and the oven as well as the temperature control jacket.

The mixer shafts are driven with two rotavapor motors. The rotation speeds for top and bottom shafts in different speed settings were measured using a handheld rotation speed tachometer. The speeds in different settings and the Reynolds numbers for these speeds for pure water as calculated with (8) are available in table 9. These

values are measured without the heating caused by long term use and the subsequent changes in the rotation speed. There was an observed deviation of ±10 rpm caused by the heating of the mixers. Due to the changes in the rotation speeds at different settings and therefore additional measurements were carried out at the beginning and the end of the measurement runs. The area for interface between gas and liquid in the cell was calculated geometrically to be 14.28 cm^2 ± 0.01 cm^2.

Table 9. Rotation speeds and Reynolds numbers for mixers

Top			*Bottom*		
Setting	rpm	Reynolds	Setting	rpm	Reynolds
1	22	1001	1	110	5006
2	25	1138	2	114	5188
3	39	1775	3	151	6872
4	63	2867	4	173	7874
5	100	4551	5	194	8829
6	146	6645	6	211	9603
7	190	8647	7	226	10286
8	206	9376	8	232	10559
9	215	9785	9	236	10741

The pressure transducer was originally connected using a capillary line from the cell. However after the 9th validation run it was noticed that the capillary has condensation during the measurement even though it is thermostated a few degrees higher than the measurement temperature. This would suggest the existence of cold spots in the capillary despite tracing. This was evident in the stair-type graph visible in validation runs 8 and 9 as seen later in figure 27 and figure 28. To reduce the effect of these cold spots, the capillary line was upgraded to a larger inner diameter tube and the problem of inaccurate pressure was solved. The transducer was calibrated using a MC2 Beamex calibration device that had previously been calibrated in the Centre for Metrology and Accreditation in Finland. The unit had a reported error of ± 150 Pa. Calibration data for the sensor is available in Appendix A. The temperature probe was calibrated in house using a probe that was also calibrated in the Center for Metrology and Accreditation. This calibration data is available in Appendix C.

The gas-feeding tank had originally a PT100 temperature probe and a UNIK 5000 pressure transducer with a 0 to 250 kPa range connected to it. Reported accuracy for the transducer was 0.2 % of the full range (±500 Pa). Validation runs 1 to 3 were made with the original UNIK 5000 unit. The pressure transducer in the GFT was changed to a Huba Control 692-series pressure transducer after these three validation runs to allow for higher pressure in GFT. Huba unit was calibrated for a range of 100 kPa to 600 kPa and with a reported accuracy of 0.4 % of full range (±2400 Pa). A UNIK 5000 transducer was ordered with a range of 0-600 kPa to replace the Huba Control transducer. A leak was also noticed later in the Huba Control unit and this was replaced with a Trafag NAH6.0A unit. This unit had a reported accuracy of 0.3 % of full range (±1800 Pa). The Huba unit was used in validation runs 4 to 10 and the Trafag unit was used in validation runs 11 and 12 as well as all the N_2O and MAPA+DEEA measurements. The original UNIK 5000 transducer calibration data is available in Appendix B and the calibration data for the temperature probe is available in Appendix C. The Huba Control transducer calibration data is available in Appendix D. Trafag calibration data is available in Appendix E. For H_2S studies the setup was altered slightly to allow the venting of H_2S into a buffer solution of NaOH. The experimental setup is illustrated in figure 20 for CO_2 and in figure 21 for H_2S.

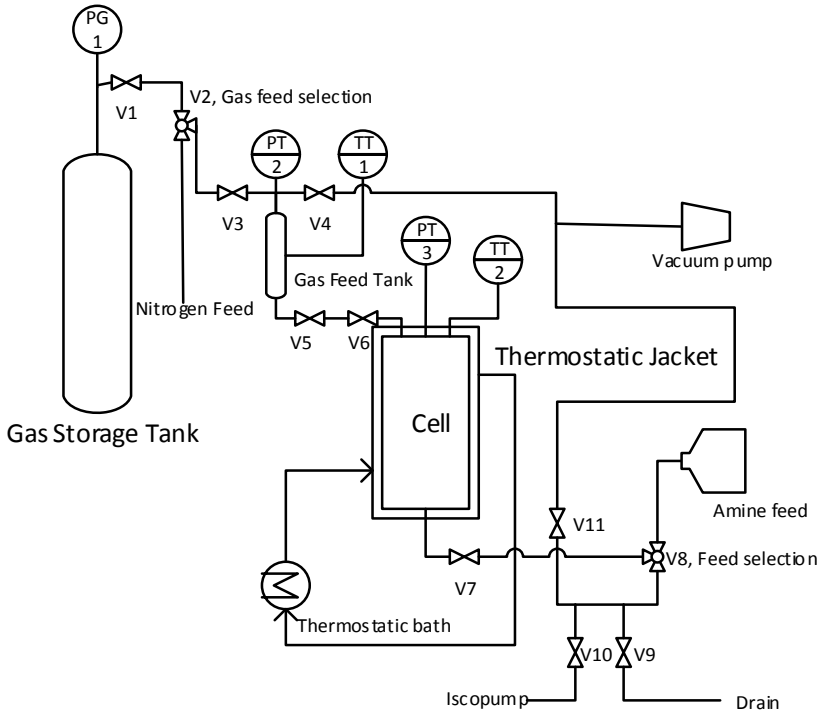

Figure 20. Experimental apparatus for CO_2 studies

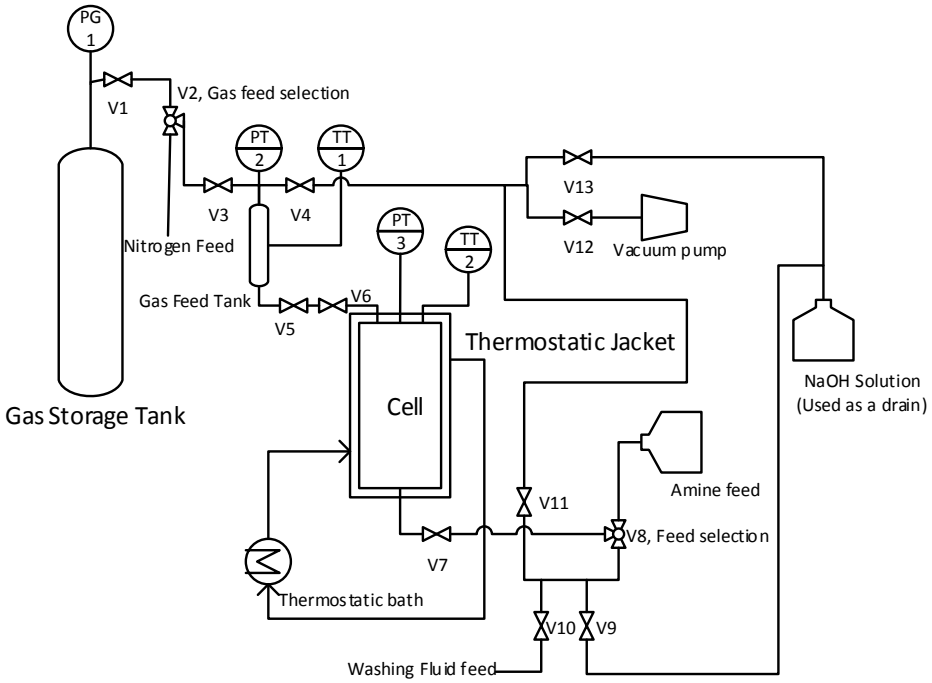

Figure 21. Experimental apparatus for H_2S studies

9.1.1 Volume of the gas feed tank (GFT)

The volume of the tank was determined by loading it with water using an Isco 260D syringe pump loaded with degassed water. It was connected to the tank as shown in figure 22.

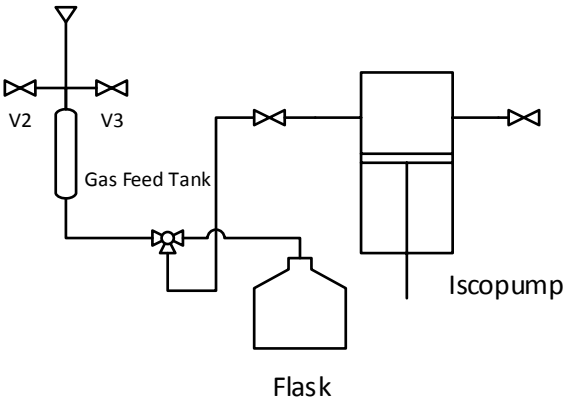

Figure 22. Volume measurement of GFT

The water was pumped in to the cell from below while the PT2 pressure transducer was disconnected and V2 and V3 closed. When the first drop of water was ejected

from PT2 mounting line, the tank was assumed to be full. The experiment was repeated eight times. A Thompson Tau test (Dieck, 2007) was done to check the data and four measurements were discarded. Resulting volume for the GFT was 160.6 ml ± 0.3 ml. The measurement data can be seen in Appendix F.

Due to a need to pressurize the GFT to a higher pressure than 2.5 bar, the transducer was changed to a Huba Control unit. However in the runs with it some discrepancies were noticed and found to be caused by a leak within the transducer. A unit from Trafag was fitted to replace the transducer. After the change to the Trafag unit, the volume of the GFT was redetermied using a 25 cm^3 gas bomb. The volume of the bomb had been previously determined using the degassed water method. The bomb was pressurized to ~800 kPa and connected to the GFT from V3. The valve was opened and pressure change in the system logged. This experiment was repeated 9 times and the data was analyzed with Thompson Tau test. The volume was found to be 161.6 ml ± 0.6 ml. Measurement data are available in Appendix F.

9.1.2 Volume of the cell

The volume of the cell was first determined by loading it with water using an Isco 260D syringe pump. The procedure is similar to that of the GFT volume measurement and can be seen in figure 23.

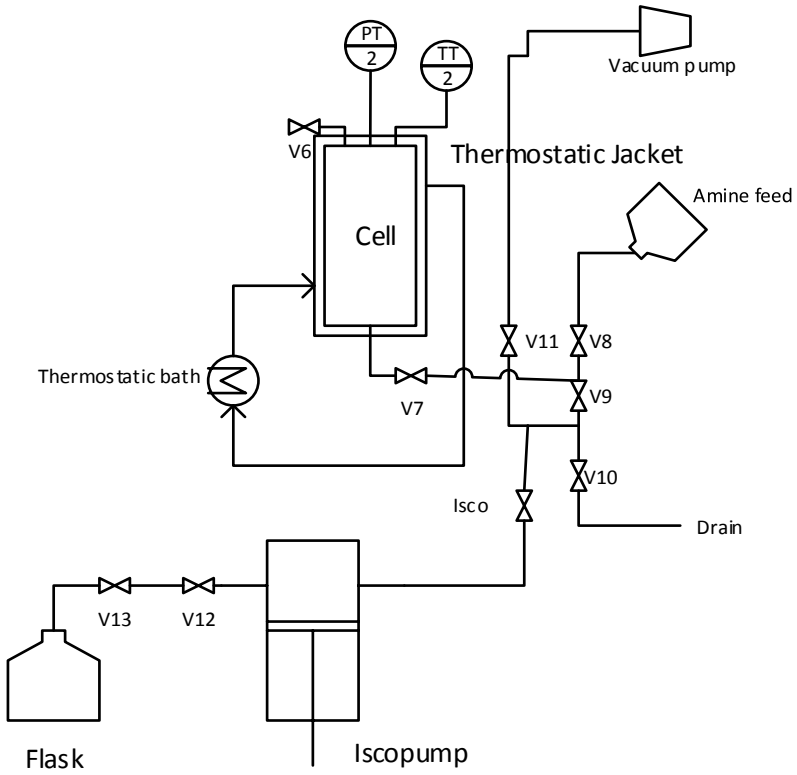

Figure 23. Volume measurement of the Cell

The water degassed in vacuum and connected to V12. V12 was opened and V13-V12 connection vacuumed. After this, the valve for the Isco-pump was closed and V13 opened. Degassed water was allowed to freely flow on to the Isco-pump syringe. After filling the water, V12 and V13 were closed. Cell was vacuumed prior to water injection. Water was fed to the cell with V11, V9 and V6 closed and valve for the Isco-pump and V7 open with V8 set to feed from pump. When pressure in the cell reached 1 bar it was assumed that the cell was full and the pressure increase was caused by the pump pushing water in to the full cell and the pressure transducer. The experiment was repeated three times and the volume was found to be 316.4 ml ± 1.4 ml. Measurement results are reported in Appendix F.

Due to the variance in the measurement carried out with the iscopump and degassed water, a test was also conducted using nitrogen gas. First the gas feeding tank (GFT) was filled with N_2 and pressurized to higher pressure. Then the cell was vacuumed and temperatures for both GFT and cell were allowed to equalize. Afterwards some of the N_2 gas was released to the cell and pressure changes in both GFT and cell were

recorded. From the pressure change in the GFT the moles of N_2 were calculated and with the transferred gas amount and pressure change in the cell the volume of the cell was calculated. This experiment was repeated ten times and the volume found for the cell was found to be 317.5 ml ± 0.3 ml. Measurement results are reported in Appendix F.

9.2 Measurements and validation with CO_2

The solutions were prepared gravimetrically on a Mettler Toledo XP2004S comparator analysis scale with a reported accuracy of 0.1 mg. The MDEA used was obtained from Aldrich (Lot #11819DC) and had a 99+% purity. De-ionized water was prepared in-house by a reverse osmosis system. MAPA was obtained from Fluka (Lot #BCBH5559V) and had a 97+% purity. DEEA was obtained from Aldrich (Lot #SHBC6167V) and had a 99,5+% purity. In their articles Pani et al. (1997a, 1997b) have correlated the mass transfer coefficient of CO_2 in to MDEA as shown in equations (8) to (11). Due to the differences in our measurement values and theirs we decide to make sure that the correlation is suitable as is on our equipment. This was done with the analogy between N_2O and CO_2. The gases were ordered from AGA and N_2O had a purity of 99% and CO_2 had a purity of 99.99%. N_2O is similar in its physical absorption behavior to CO_2. Small errors in the pressure values obtained from transducers lead to such small error bars in the pressure vs time figures that they are not visible in them (±500 Pa).

9.2.1 Measurements with MDEA+CO_2

Validation runs were made with a 10 w-% MDEA solution. The solution was prepared by first weighting the 250 ml round bottom flask, then adding approximately 20 g of the amine solution to the flask. After this the scale was stabilized and them approximately 180 g of de-ionized water was added. The flask was weighted again before and after a vacuum cork was fitted. After this the solution was degassed in an ultrasonic bath with vacuum. The flask was weighted again and all weight lost was assumed to have been water. The prepared solutions and their

compositions are shown in table 10. Measurement conditions for validation runs are shown in table 11. All measurement results are available in Appendix H.

Table 10. Validation Solutions

	Validation 1	*Validation 2*	*Validation 3*	*Validation 4 - 6*	*Validation 7*
m(flask) [g]	106.36	106.35	106.35	106.34	106.34
m(+Am) [g]	126.38	126.36	126.35	126.33	126.32
m(+H2O) [g]	306.90	306.83	306.43	306.58	306.29
m(+cork) [g]	529.34	527.22	499.16	499.30	498.99
m(degassed) [g]	527.93	527.22	498.25	497.99	498.29
m(after fill) [g]	360.10	359.93	327.42	328.13	330.08
V(filled) [cm^3]	166.71	166.18	169.69	168.72	167.09
[MDEA] [M]	0.84	0.84	0.84	0.84	0.84
w(MDEA)	0.10	0.10	0.10	0.10	0.10
	Validation 8	*Validation 9*	*Validation 10*	*Validation 11*	*Validation 12*
m(flask) [g]	106.33	106.34	106.34	106.34	106.34
m(+Am) [g]	126.40	126.35	126.52	126.36	126.33
m(+H2O) [g]	307.39	306.27	308.71	306.60	306.27
m(+cork) [g]	500.10	498.99	501.43	499.30	498.98
m(degassed) [g]	499.31	497.78	500.15	498.75	498.04
m(after fill) [g]	330.63	319.01	324.54	321.99	321.50
V(filled) [cm^3]	167.56	177.57	174.43	175.59	175.35
[MDEA] [M]	0.84	0.85	0.84	0.84	0.84
w(MDEA)	0.10	0.10	0.10	0.10	0.10

Table 11. Measurement conditions for Validation runs

Run #	*Initial Pressure [Pa]*	*C_{MDEA} [$\cdot 10^{-1}$ mol·dm^{-3}]*	*Stirring speed [min^{-1}]*	*$T_{average}$ [K]*	*Vg [$\cdot 10^{-4}$ m^3]*	*Vl [$\cdot 10^{-4}$ m^3]*
1	3119	8.4376	133	296.0	1.5346	1.7234
2	3333	8.3770	133	301.1	1.5399	1.7351
3	3987	8.4253	116	300.8	1.5048	1.7234
4	2916	8.4316	100	295.9	1.5144	1.7234
5	2916	8.4316	100	295.9	1.5144	1.7351
6	2916	8.4316	100	296.0	1.5144	1.7234
7	2907	8.4171	104	295.9	1.5308	1.7351
8	2553	8.4082	105	296.1	1.5261	1.7234
9	4979	8.4526	133	317.9	1.4259	1.7351
10	9158	8.4225	105	318.3	1.4574	1.7234
11	9556	8.4143	120	318.2	1.4457	1.7351
12	2873	8.4329	106	296.3	1.4481	1.7326

Before feeding the amine the cell and the GFT were first vacuumed using an Edwards vacuum pump. Then valves 11, 9 and 7 were closed and a flush for GFT done. Valve 4 was closed and GFT filled with CO_2 and valve 4 opened again. This was repeated three times to flush any air or contaminants out of the gas tank. After this valves 9 and 11 were opened. Then the amine bottle was connected using an Ultra-Torr connector by Swagelok and valve 8 opened, then the feed line for amine was vacuumed. Then valves 11 and 9 were closed and the valve 7 and the valve on the amine bottle opened to let amine flow to the cell. Amine was fed in to the cell. First measurements were done so, that the liquid level was not specifically set. To see how the liquid level affects the absorption rate, tests were made with different liquid levels on the interface. First the liquid was fed only to the lowest liquid level on the interface (Validation runs 7 & 8) and later to the top of the liquid level on interface (see figure 24). After feeding the amine, the flask was weighted to find the exact amount fed to cell.

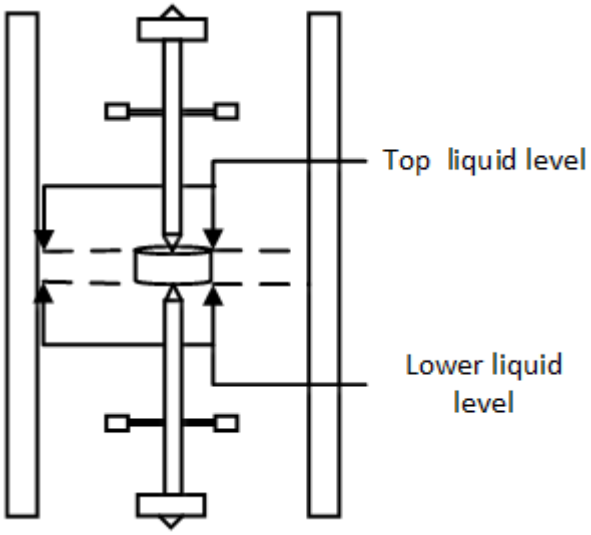

Figure 24. Lower and higher liquid levels in the cell

The first three validation runs are shown in figure 25. The initial runs were done in low pressure due to the possibility of cell glass walls cracking under pressure. Temperature in run 1 was 296 K and in 2 and 3 it was 301 K.

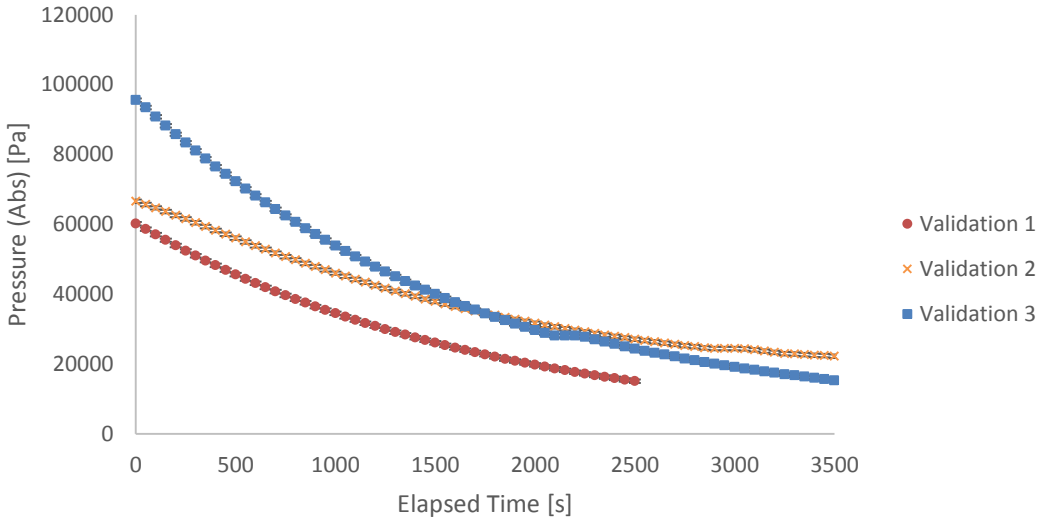

Figure 25. First three validation runs

The first runs were compared with the set of literature data obtained from Pani et al (1997a). Their measurements contain one dataset in the 296 K and it was used as comparison. The comparison of their dataset to our measurements is shown in figure 26.

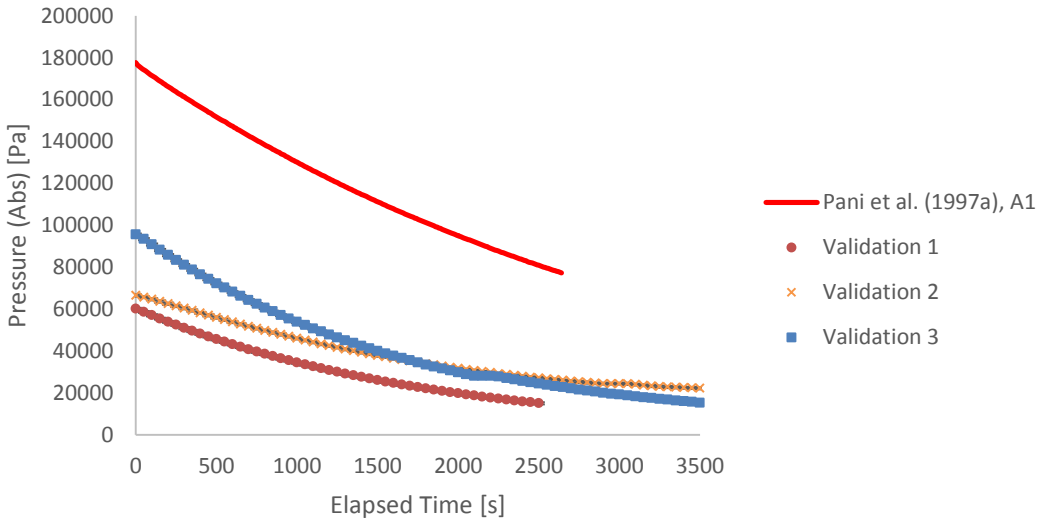

Figure 26. Literature VS Validation runs

The slope of runs one and three is quite similar to the data found from literature. However as the pressure is not as high as in the literature dataset, the measurements

are not adequate to analyze validity of the research apparatus. Therefore it was decided to do additional runs with same MDEA composition and a 1.8 bar pressure.

Validation runs 4 to 8 were made in 296 K and are shown in figure 27. Validation 8 shows the condensation problem noticed in the early measurements.

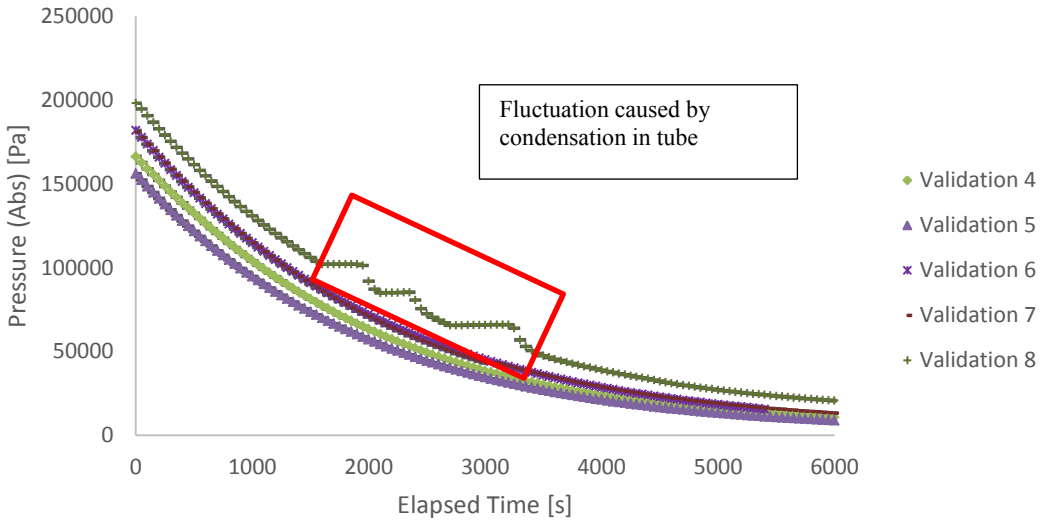

Figure 27. Validation runs 4 to 8

After the steps and condensation in Validation 8 were noticed, the temperature tracing was added to the pressure transducer line and the next measurement in 318 K was ran. It can be seen in figure 28.

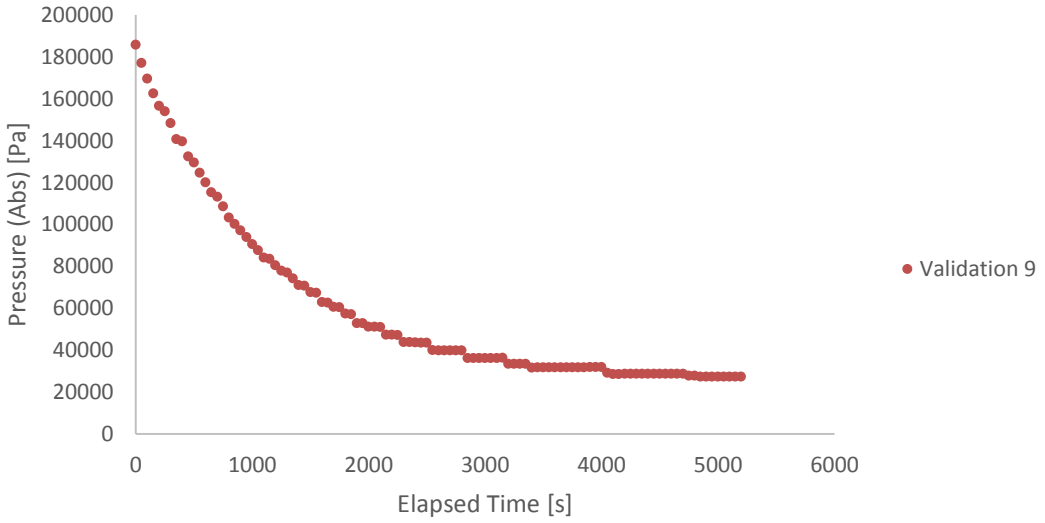

Figure 28. Validation run 9

Despite the line being traced and heated to a few degrees higher than the actual measurement temperature, there was condensation that caused jumps in the pressure value. The connection was therefore exchanged to a larger diameter tube that allowed for better accuracy. This solved the condensation problem and we were able to obtain smooth data. Two more runs were made in 318 K and they are shown in figure 29.

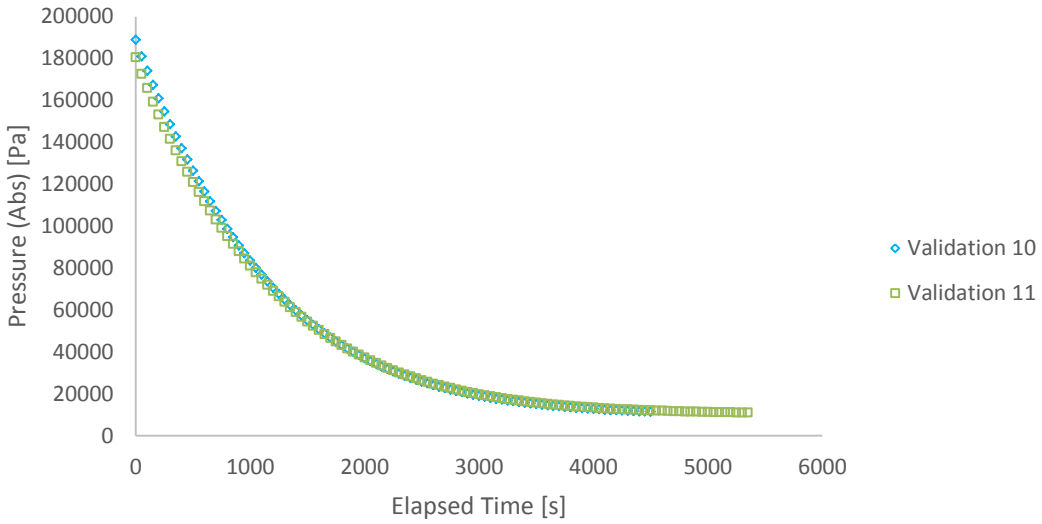

Figure 29. Validation runs 10 and 11

After the promising looking runs, we decided to do one more run in 298 K to verify earlier results. This run is shown in figure 30.

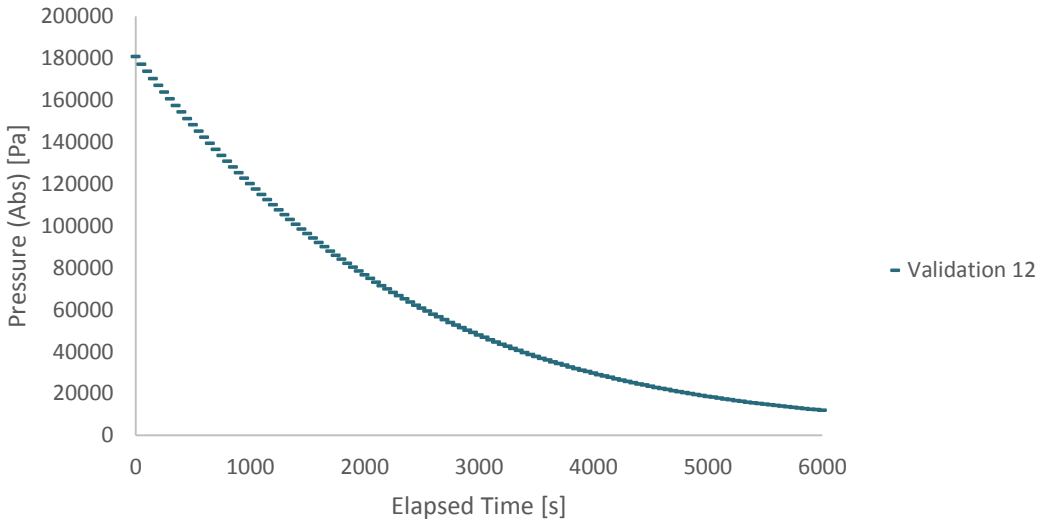

Figure 30. Validation run 12

9.2.2 Measurements with MDEA+N_2O

For our validation experiments we used the correlation shown in equations (8) to (11) as proposed by Pani et al. (1997a, 1997b). To test its applicability to our cell, measurements with N_2O and MDEA were made. Six experimental runs with MDEA, 3 runs with 10 w-% solution (figure 31) and 3 runs with 20 w-% solution (figure 32) were performed. Solutions were prepared as explained earlier. Temperatures were varied between 296 K and 318 K. All raw results are available in Appendix H. Measurement conditions for the runs are available in table 12.

Table 12. Measurement conditions for MDEA+N_2O experiments

Run #	*Initial Pressure [Pa]*	*C_{MDEA} [mol·dm^{-3}]*	*Stirring speed [min^{-1}]*	*$T_{average}$ [K]*	*V_g [·10^{-4} m^3]*	*V_l [·10^{-4} m^3]*
1	3311	0.84299	130	298.4	1.4662	1.7145
2	4727	0.84225	115	305.1	1.4785	1.7023
3	11437	0.89958	125	318.2	1.4554	1.7254
4	4662	1.6695	114	305.1	1.4702	1.7105
5	9214	1.6847	120	318.2	1.4647	1.7161
6	9212	1.6695	120	298.1	1.4934	1.6873

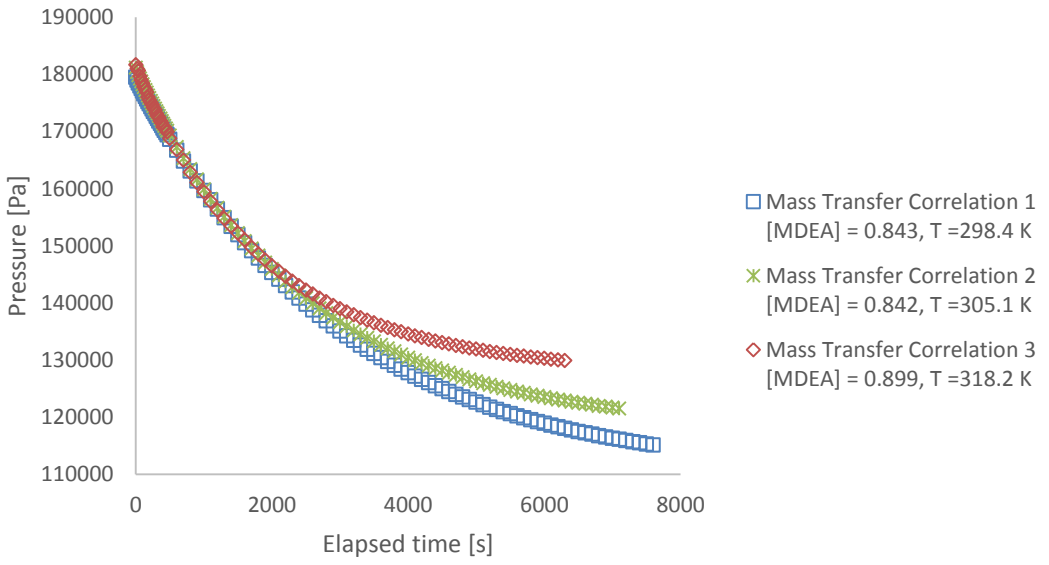

Figure 31. Pressure graph for N2O+MDEA (10 w-%)

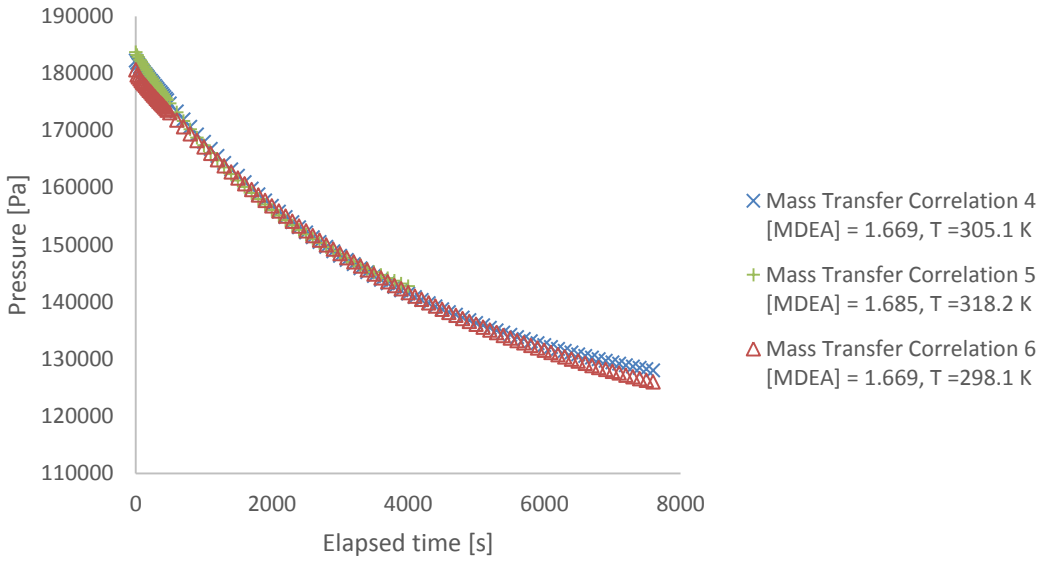

Figure 32. Pressure graph for N2O+MDEA (20 w-%)

9.2.3 Measurements with MAPA+DEEA+CO_2

Two runs were made with aqueous solution of DEEA and MAPA. The solution contained 5M of DEEA and 2M of MAPA (further referenced as 5D2M) as has been previously used by Arshard et al. (2014). Solutions were prepared gravimetrically as explained earlier. First run was made at 318 K. It consisted of 15 consequent absorptions. 2nd run was made at 308 K and consisted of 17 subsequent absorptions. Data from the 1st run can be seen in figure 33 and figure 34 and data from the 2nd run can be seen in figure 35 and figure 36. Figures for the first run show a slower rate of absorption at the beginning of each run because there was no stirring active until all the gas had been transferred from feed tank to cell. All raw results are available in Appendix H. Measurement conditions for the first run are available in table 13 and the second one in table 14.

Table 13. Measurement conditions for the first MAPA+DEEA+CO_2 run

Initial Pressure	8387	[Pa]	Pressure before CO_2 loading
[Amine]	6.9880	[mol·dm^{-3}]	Amine concentration
Stirring speed	125	[min^{-1}]	Speed of liquid stirrer
T	318.0	[K]	Average experiment temperature
V_g	0.145422	[·10^{-3} m^3]	Volume of the gas space in the cell
V_l	0.172653	[·10^{-3} m^3]	Volume of the liquid in the cell

Table 14. Measurement conditions for the second MAPA+DEEA+CO_2 run

Initial Pressure	3815	[Pa]	Pressure before CO_2 loading
[Amine]	6.91881	[mol·dm^{-3}]	Amine concentration
Stirring speed	130	[min^{-1}]	Speed of liquid stirrer
T	308.0	[K]	Average experiment temperature
V_g	0.143529	[·10^{-3} m^3]	Volume of the gas space in the cell
V_l	0.174546	[·10^{-3} m^3]	Volume of the liquid in the cell

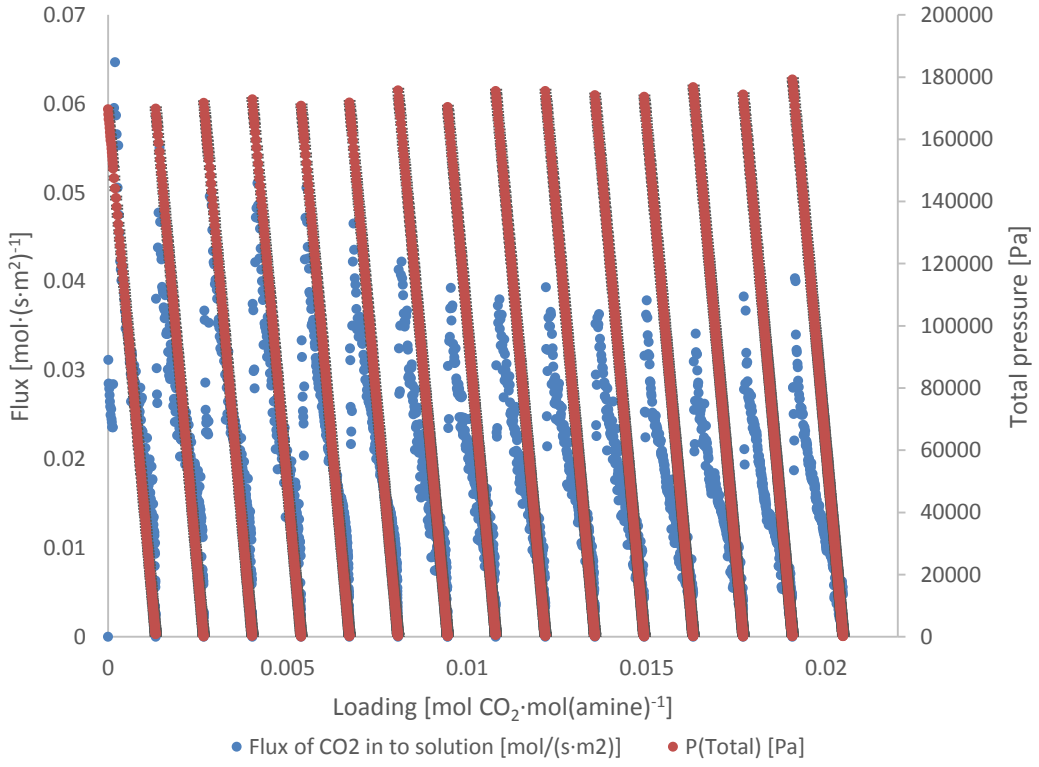

Figure 33. Flux of CO_2 and Pressure of CO_2 as a function of amine loading in the 1st run at 318 K

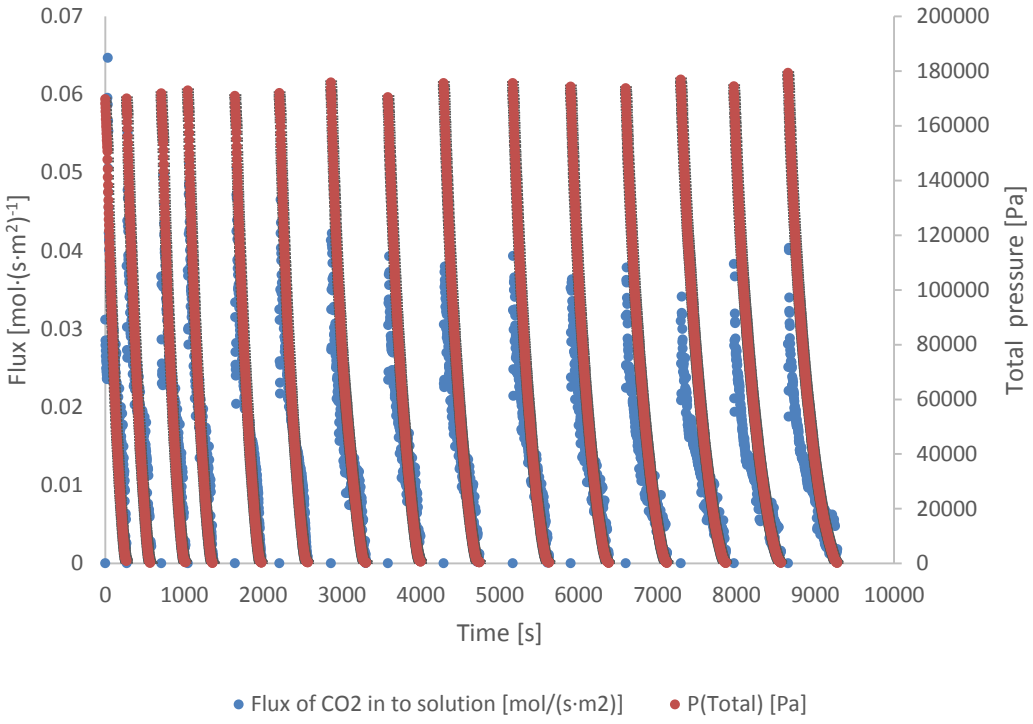

Figure 34. Flux of CO_2 and Pressure of CO_2 as a function of elapsed time in the 1st run at 318 K

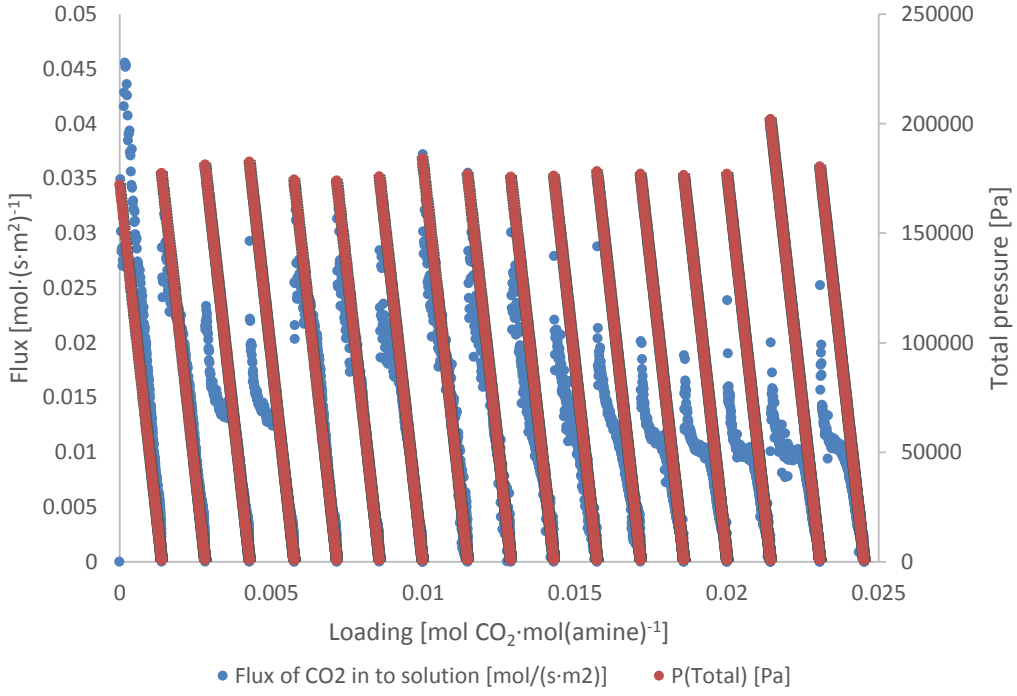

Figure 35. Flux of CO_2 and Pressure of CO_2 as a function of amine loading in the 2nd run at 308 K

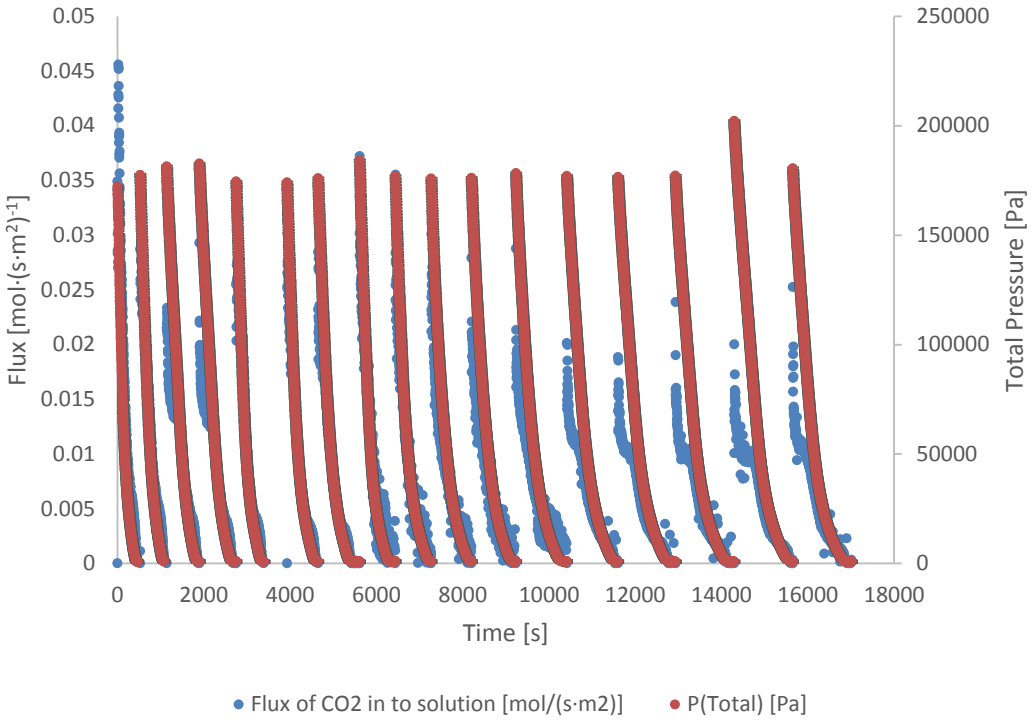

Figure 36. Flux of CO_2 and Pressure of CO_2 as a function of elapsed time in the 2nd run at 308 K

9.3 Measurements with MAPA+DEEA+H_2S

For the measurements of hydrogen sulfide absorption rate, the 5D2M solution was used as for CO_2. Solution was prepared gravimetrically as before. Measurements were made in 319 K. The solution was loaded in to the cell and hydrogen sulfide was fed in. There were 24 feeds of H_2S with a single amine feed. Total pressure after each feed was around 200 kPa and the pressure decrease vs time was logged. The measurement results are shown in figure 37 against loading and in figure 38 against time. All raw results are available in Appendix H. Measurement conditions for the run are available in table 15.

Table 15. Measurement conditions for the MAPA+DEEA+H_2S experiment

Initial Pressure	8469	[Pa]	Pressure before H_2S loading
[Amine]	6.988	[mol·dm^{-3}]	Amine concentration
Stirring speed	100	[min^{-1}]	Speed of liquid stirrer
T	319.0	[K]	Average experiment temperature
V_g	145.96	[·10^{-6} m^3]	Volume of the gas space in the cell
V_l	172.11	[·10^{-6} m^3]	Volume of the liquid in the cell

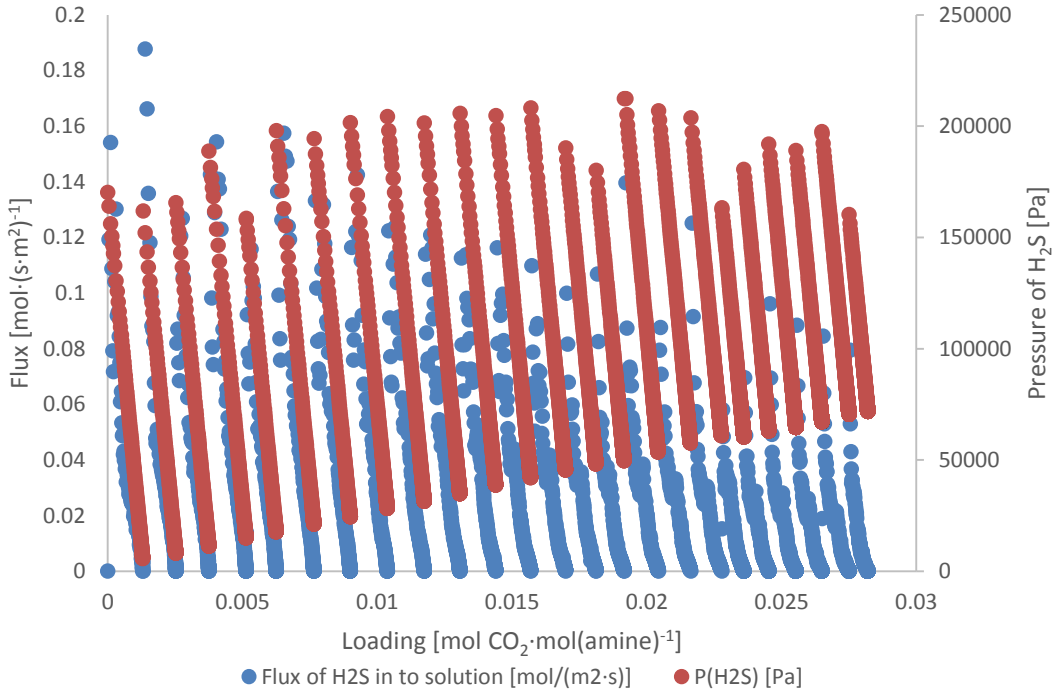

Figure 37. Flux of H_2S and Pressure of H_2S as a function of amine loading at 319 K

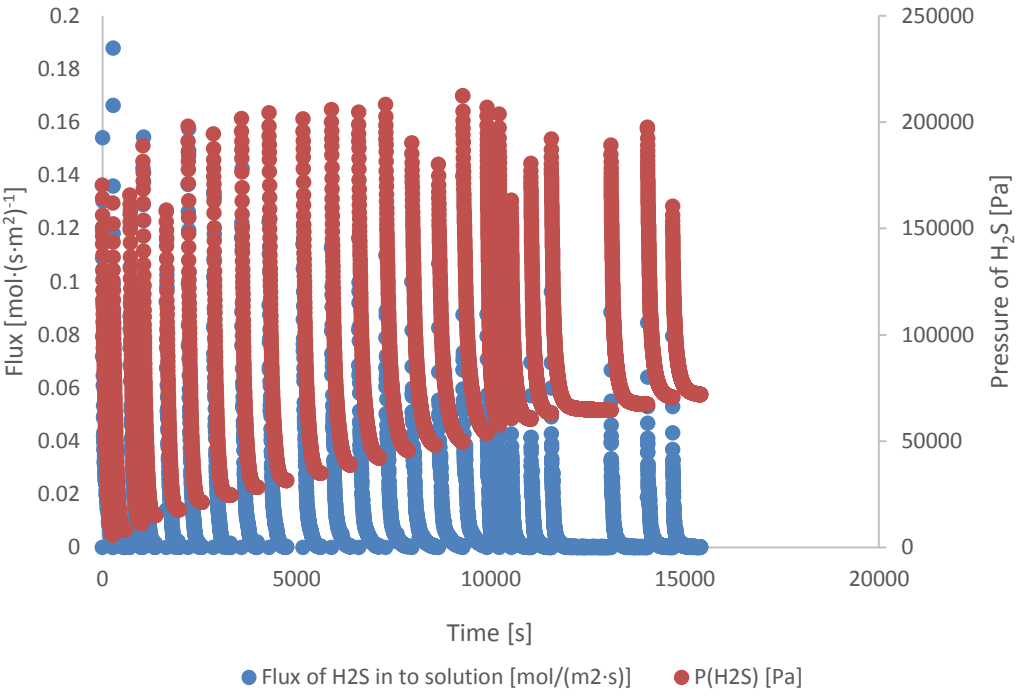

Figure 38. Flux of H_2S and Pressure of H_2S as a function of elapsed time at 319 K

10 Analysis of results

10.1 MDEA+CO_2

The differences in our cell in comparison to Pani et al. (1997a, 1997b) cell come from the diameter of the interfacial area between the gas and liquid layers as well as the difference in the mixer type used for the gas phase. They used a propeller for gas phase and Rushton turbine for liquid phase whereas our cell uses a Rushton turbine for both phases. The difference in the interfacial area can be taken in to account by comparing the flux of gas through the interface in $mol \cdot m^{-2} \cdot s^{-1}$. This was done for validation runs 1 and 4 to 8 and can be seen in figure 39.

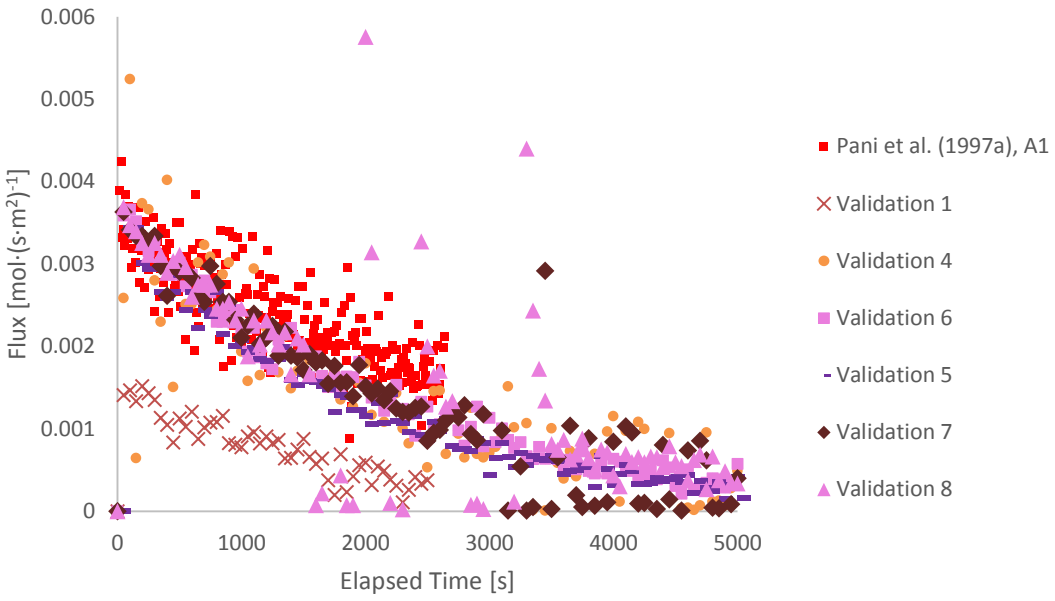

Figure 39. Validation runs at 296 K

It can be clearly seen that the data has a lot of scatter. The reason for this behavior is the condensation problem discussed earlier. However when a 2nd degree polynomial model was fitted to the data, all datasets except for the first one seemed to follow the trend of the values and data in literature quite well. These models are shown in figure 40. Validation 8 polynomial curve shows strange behavior due to the observed condensation in the pressure line.

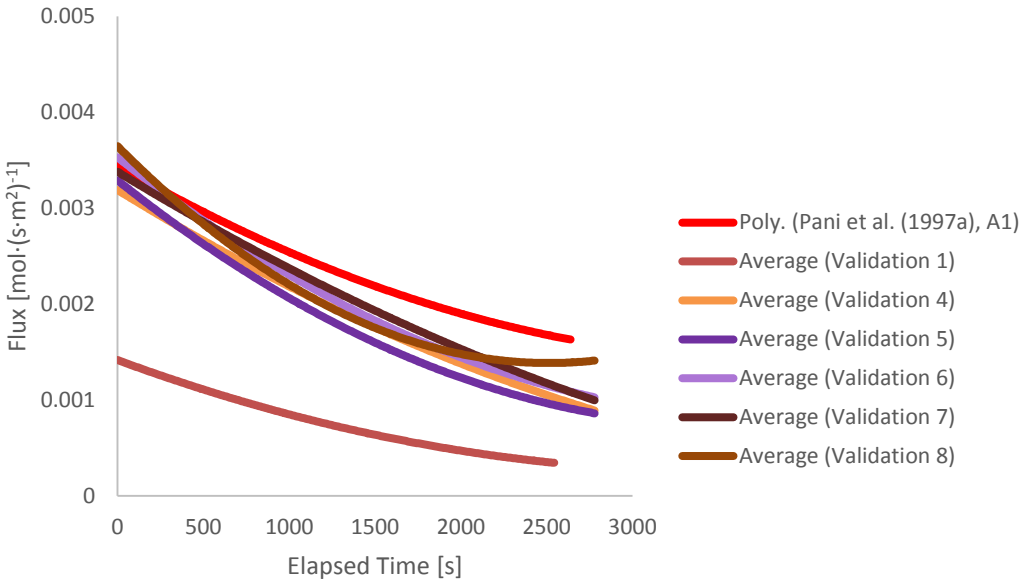

Figure 40. Polynomials of validation runs at 296 K

Validation 9 had very large scatter in the flux assessment and was dismissed. After the exchange from the capillary tube (ID 0.2 mm) to a larger internal diameter tube (ID 1 mm), two runs were made in 318 K and the fit from these curves and the earlier validation run 9 are available in figure 41. The figure shows, that the new runs correlate with our previous run better than they do with literature and their behavior does not show the condensation observed earlier.

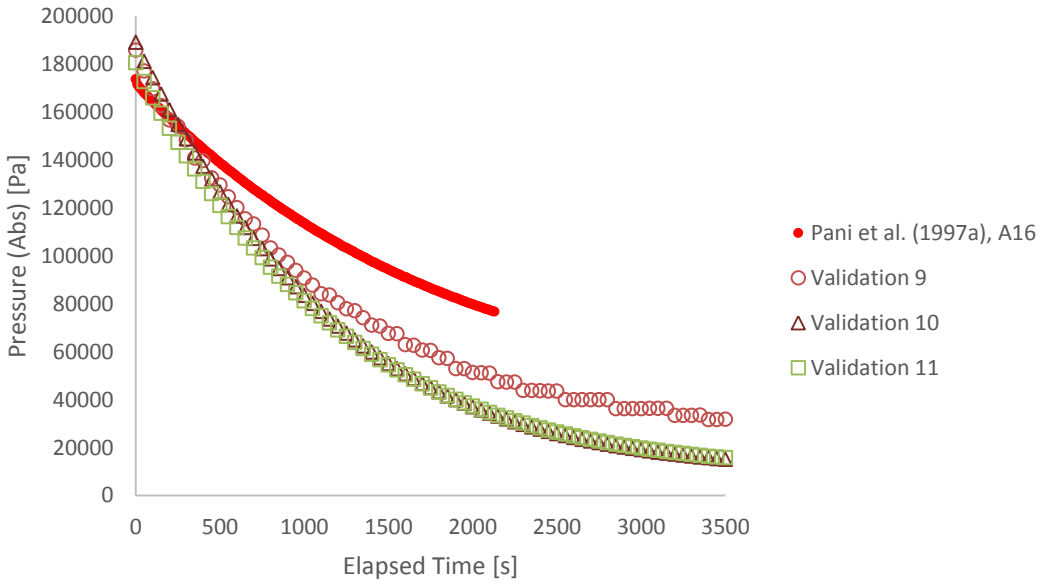

Figure 41. Validation runs in 318 K

Last run in 296 K, Validation 12, is shown in figure 42. In addition 2nd polynomial models for the average values of all the validation runs in 296 K are shown in figure 43.

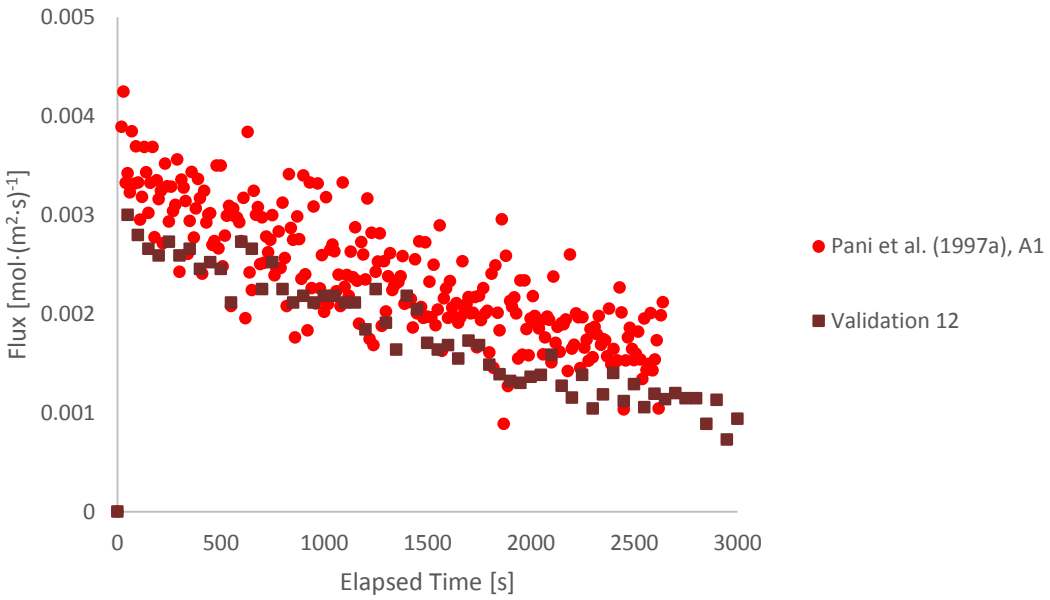

Figure 42. Last validation run against literature in 296 K

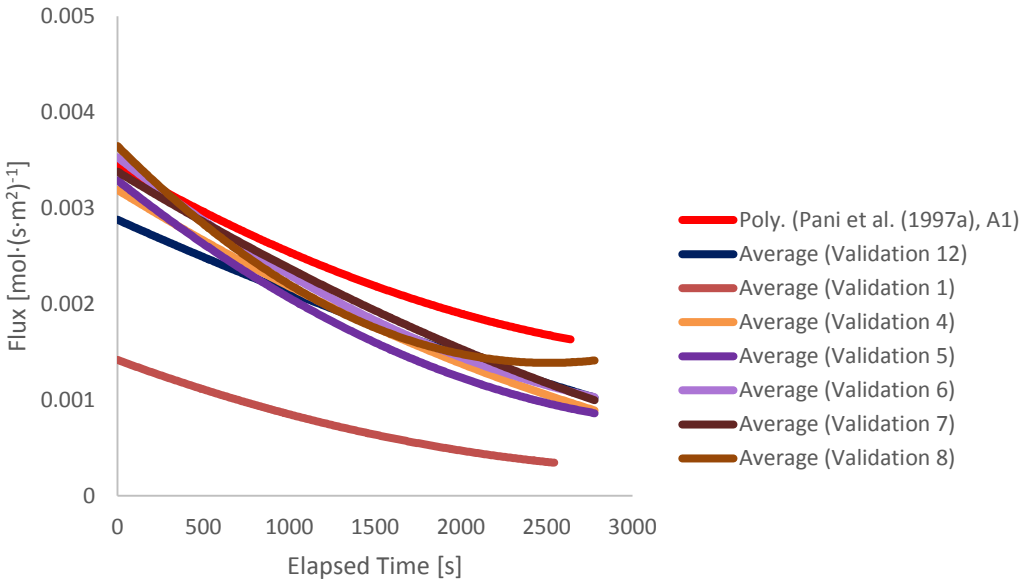

Figure 43. Comparison of all polynomial curves against literature for runs in 296 K

In addition to comparing the flux of gas through the interface, we calculated the reaction rate coefficient from our data with the model for MDEA and CO_2 explained earlier and compared it to the Arrhenius equation created by Pani et al. (1997a). The comparison and deviation in percent can be seen in table 16 and table 18. It can be seen that in 318 K Pani et al. (1997a) measurements also differentiate from their correlation significantly at this MDEA concentration. We also calculated the kinetic reaction rate for CO_2 at the early stages of absorption (5 kPa drop from initial pressure) on the interface. Equation (14) was used for the rate calculation on the interface with concentrations for MDEA from equation (16) and for CO_2 with Henry's law. These are also available in the tables. table 17 shows the constants and kinetic rates for validation runs 2 and 3.

Table 16. Comparison of reaction coefficients for Validation runs 1 and 4 to 8 against Pani et al. (1997a) literature values. (Slope is from equation (10), k_{cal} is calculated from equation (18), k_{eq} is calculated from the Arrhenius equation (21) and deviation is calculated from the difference between the two k values. Kinetic rate is calculated from equation (14) and difference in rate is calculated from Pani et al. (1997a) literature data)

Measurement	*Lit. A1*	*Valid. 1*	*Valid. 4*	*Valid. 5*	*Valid. 6*	*Valid. 7*	*Valid. 8*	*Valid. 12*
Temperature [K]	295.85	295.96	295.92	295.95	295.97	295.91	296.15	296.32
Slope, eq. (10) [$\cdot 10^3$]	-0.59	-0.59	-0.46	-0.51	-0.47	-0.44	-0.41	-0.39
k_{cal}, eq (18) $\cdot 10^3$ [$m^3 \cdot mol^{-1} \cdot s^{-1}$]	4.87	5.34	3.69	4.74	4.06	3.46	3.09	2.37
k_{eq}, eq (21) $\cdot 10^3$ [$m^3 \cdot mol^{-1} \cdot s^{-1}$]	4.51	4.54	4.53	4.53	4.54	4.52	4.59	4.64
Deviation in rate coef. [%]	8.1	17.6	-18.5	4.5	-10.5	-23.5	-32.8	-49.0
Kinetic rate [$mol \cdot (m^3 \cdot s)^{-1}$]	151.81	86.73	152.86	178.60	176.78	155.94	153.28	114.59
Deviation in rate [%]	0.0	-42.9	0.7	17.7	16.5	2.7	1.0	-24.5

Table 17. Reaction coefficients for Validation runs 2 and 3. (Slope is from equation (10), k_{cal} is calculated from equation (18), k_{eq} is calculated from the Arrhenius equation (21) and kinetic rate is calculated from equation (14))

Measurement	*Validation 2*	*Validation 3*
Temperature [K]	301.08	300.76
Slope, eq. (10) [$\cdot 10^3$]	-0.37	-0.58
k_{cal}, eq (18) $\cdot 10^3$ [$m^3 \cdot mol^{-1} \cdot s^{-1}$]	2.16	5.74
k_{eq}, eq (21) $\cdot 10^3$ [$m^3 \cdot mol^{-1} \cdot s^{-1}$]	6.21	6.09
Kinetic rate [$mol \cdot (m^3 \cdot s)^{-1}$]	40.49	108.87

Table 18. Comparison of reaction coefficients for Validation runs 9, 10 and 11 against Pani et al. (1997a) literature values. (Slope is from equation (10), k_{cal} is calculated from equation (18), k_{eq} is calculated from the Arrhenius equation (21) and deviation in rate coefficient is calculated from the difference between the two k values. Kinetic rate is calculated from equation (14) and difference in rate is calculated from Pani et al. (1997a) literature data)

Measurement	*Literature A16*	*Validation 9*	*Validation 10*	*Validation 11*
Temperature [K]	317.75	317.90	318.28	318.22
Slope, eq. (10) [$\cdot 10^3$]	-0.47	-0.52	-0.87	-0.89
k_{cal}, eq (18) $\cdot 10^3$ [$m^3 \cdot mol^{-1} \cdot s^{-1}$]	11.73	5.22	18.68	18.38
k_{eq}, eq (21) $\cdot 10^3$ [$m^3 \cdot mol^{-1} \cdot s^{-1}$]	16.08	16.21	16.55	16.49
Deviation in rate coef. [%]	-27.03	-67.82	12.92	11.47
Kinetic rate [$mol \cdot (m^3 \cdot s)^{-1}$]	250.35	258.02	734.47	721.82
Deviation in rate [%]	0.00	3.06	193.37	188.32

As is seen in the tables, despite apparent condensation seen in figure 28 for validation 9, the kinetic rate is very close to the values obtained by Pani et al. (1997a) for 318 K. This same behavior is also visible in table 16, where validations 4, 7 and 8 have very small deviations from the rates obtained by Pani et al. The kinetic rates for 296 K are displayed in figure 44 and for 318 K in figure 45. Figure 46 shows the calculated reaction coefficients from our work as well as those from multiple authors available in literature (Versteeg and van Swaaij, 1988, Rinker et al., 1995, Pani et al., 1997a, Ko and Li, 2000).

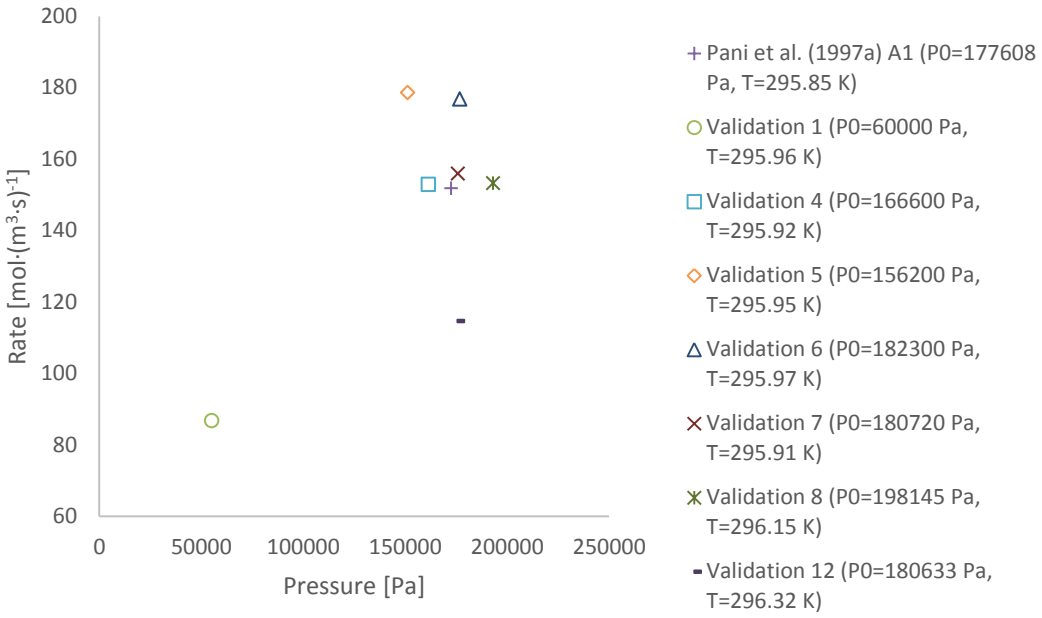

Figure 44. Kinetic rates in 296 K

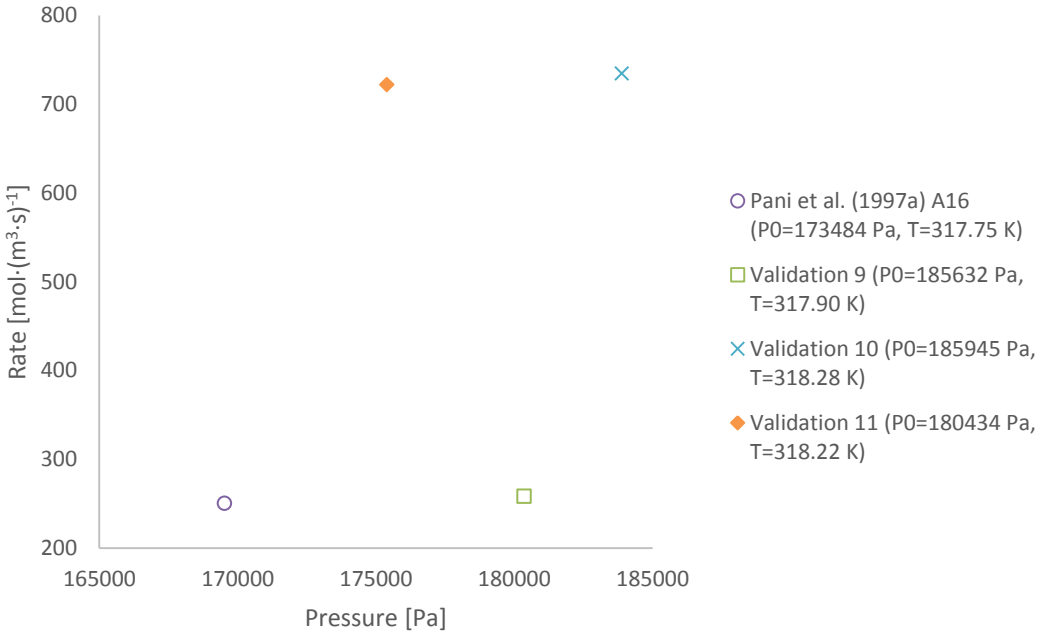

Figure 45. Kinetic rates in 318 K

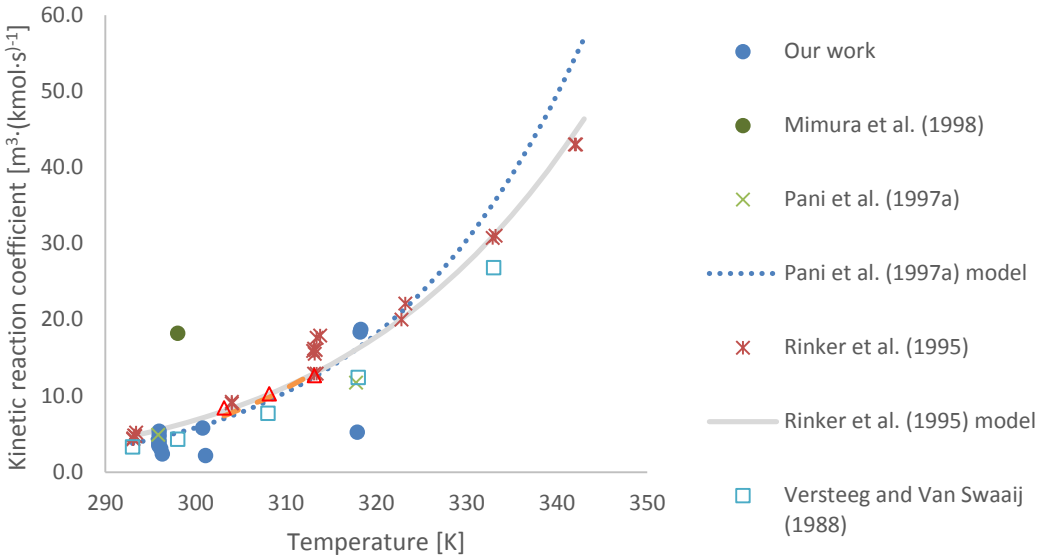

Figure 46. Our reaction rate coefficients compared with literature data

As can be seen from the figures for reaction rates, some measurements (validation 1 and 12) in 296 K have higher deviation from literature and the same is visible for validations 10 and 11 in 318 K. This behavior is more severe in high temperature, as the rate is about three times the literature value. Validation 1 can be disregarded as initial pressure has a strong effect in the absorption rate and therefore also the kinetic rate. Validation 1 had only 60 kPa initial pressure where as other runs had ~170 kPa initial pressures. Errors in validations 5 and 6 were assumed to be caused by subsequent loadings of gas in to the same amine solution and error in validation 12 was assumed to be caused by operator error. For validations 10 and 11 the results are much higher than those seen in literature and would merit further studies for better understanding of their behavior.

In figure 46 however, the kinetic constant that match the model by Pani et al. (1997a) and experiments found in literature are for validation runs 1, 3, 5, 6, 10 and 11. All the measurements are below the model proposed by Rinker et al. (1995). These two methods to check the validity of our results therefore do not correlate, as with comparison with kinetic rate validations 4, 7, 8 and 9 seem reasonable and when comparing the kinetic constant none of these are correlating with literature.

Despite none of the validation runs meeting both criteria for the reaction rate and the kinetic constant, it was decided that there is enough consistency with the results to validate the measurement equipment. It was still decided that the mass transfer correlation seen in equation (11) should be checked against literature using nitrous oxide and MDEA.

Data were also fitted with an exponential decay curve to have better idea of pressure decay over time during the absorption. This makes it possible to estimate the length of the runs when equilibrium pressure is known in measured temperatures. The model is shown in equation (68) and was fitted with the data from Validation runs at 296 K and 318 K.

$$\mathrm{P}(\mathrm{CO}_2, t) = \mathrm{P}(\mathrm{CO}_2, initial) \cdot e^{(-\lambda \cdot \mathrm{t} + \mathrm{B})} \tag{68}$$

The values fitted are shown in table 19 and the model is shown against measurement points in figure 47 to figure 54.

Table 19. Exponential model lambda values

T	*296 K*	*318 K*
λ [·10³]	0.457	0.797
B [·10³]	2.025	4.040

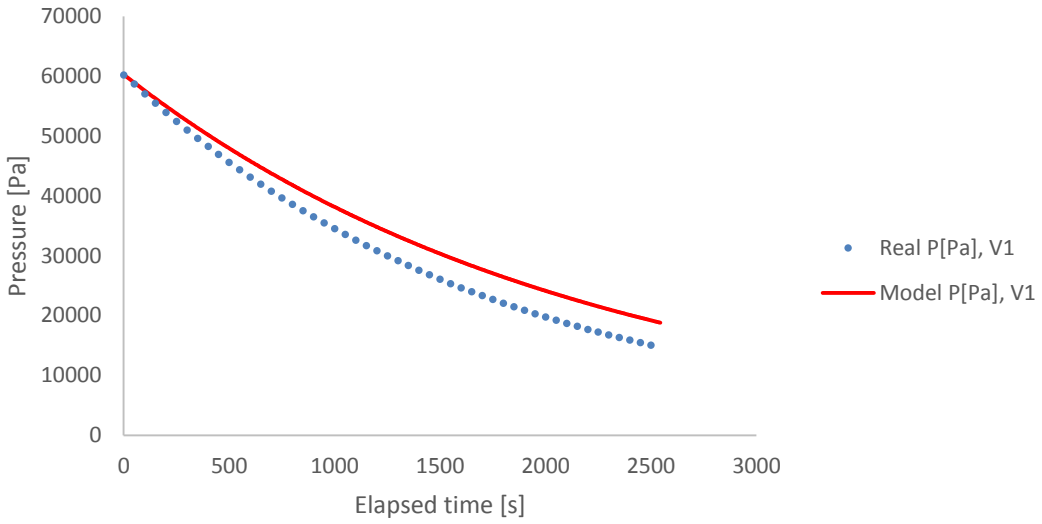

Figure 47. Exponential model against Validation 1 at 296 K

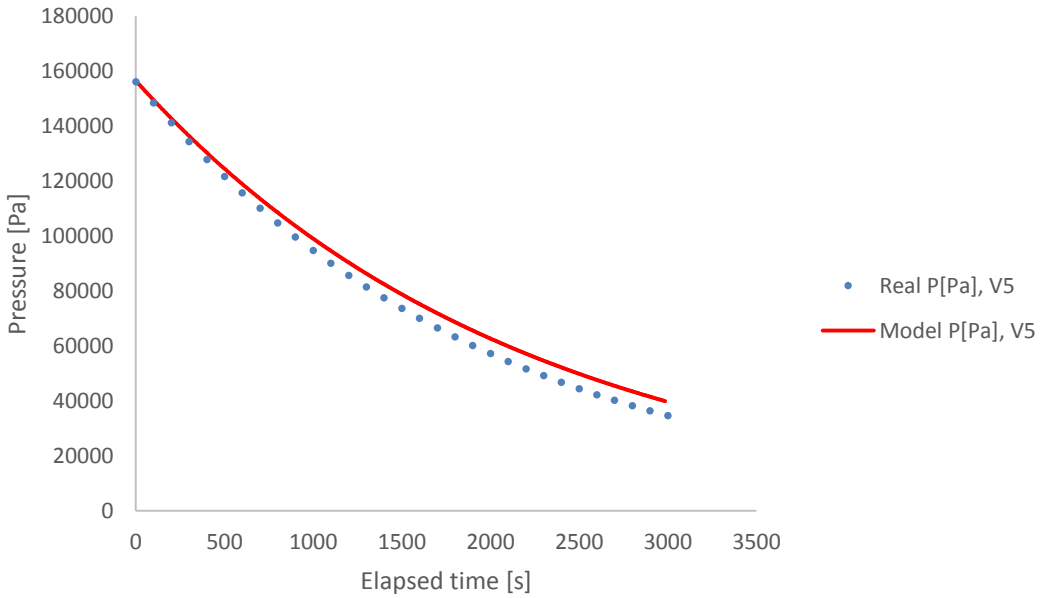

Figure 48. Exponential model against Validation 5 at 296 K

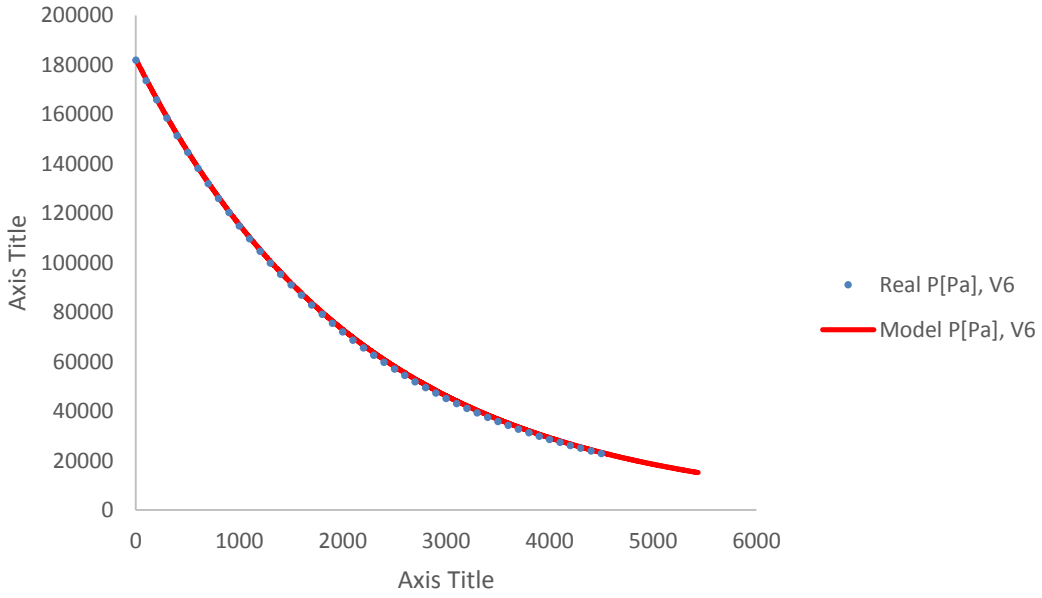

Figure 49. Exponential model against Validation 6 at 296 K

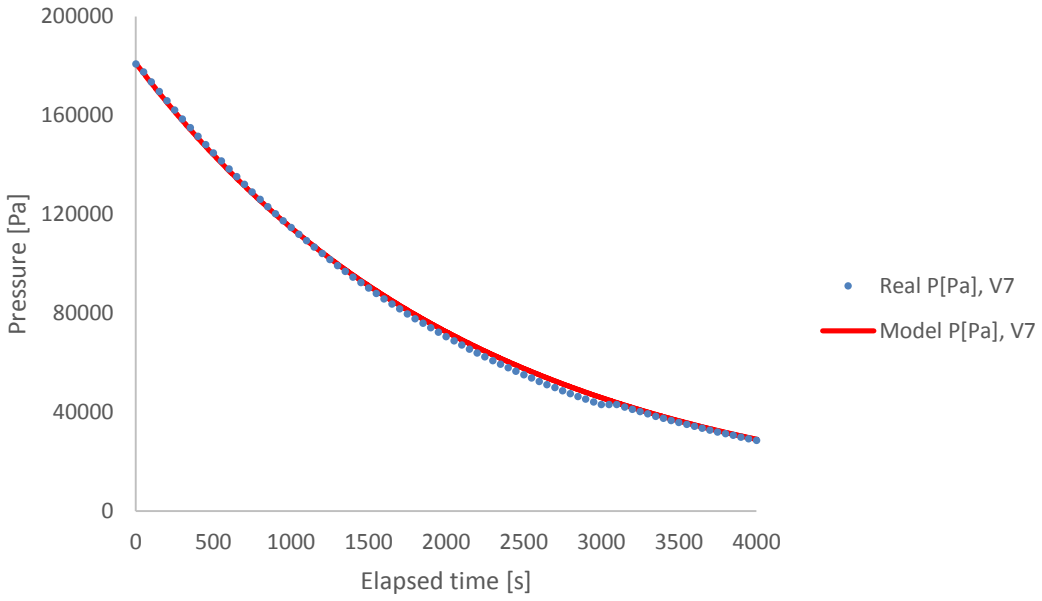

Figure 50. Exponential model against Validation 7 at 296 K

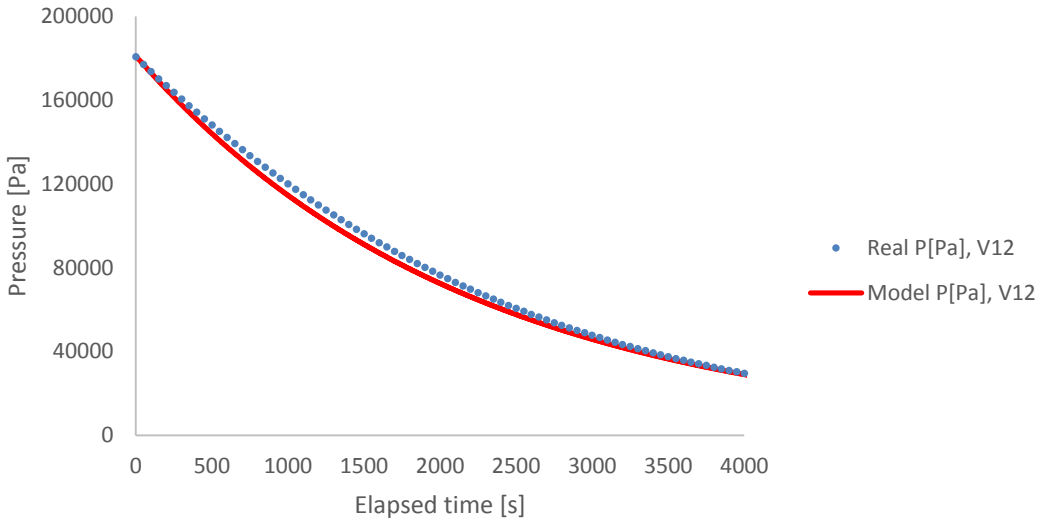

Figure 51. Exponential model against Validation 12 at 296 K

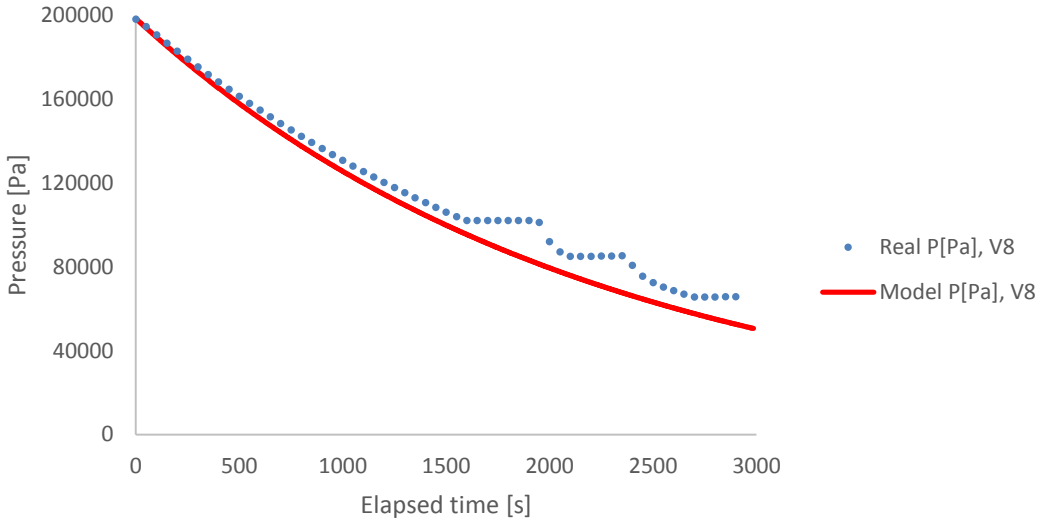

Figure 52. Exponential model against Validation 8 at 296 K

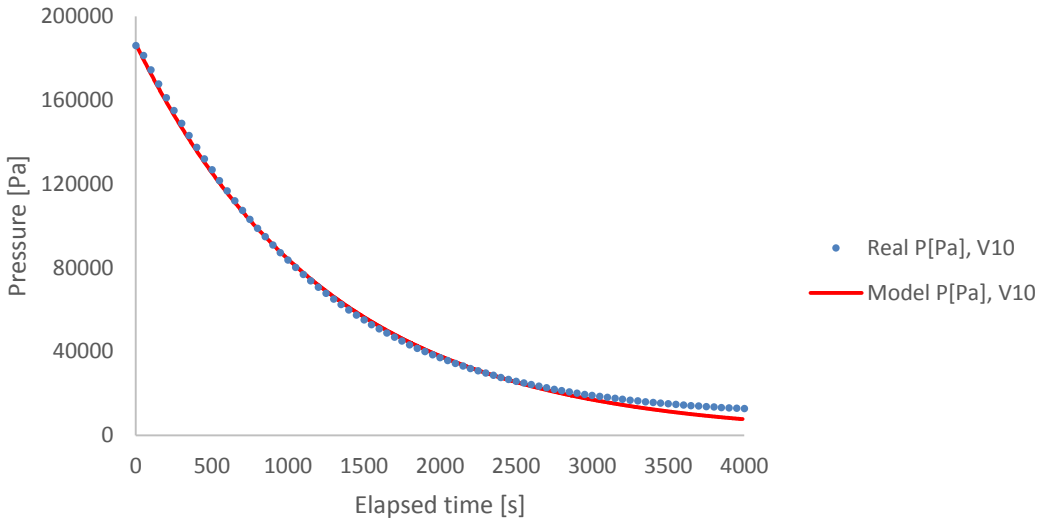

Figure 53. Exponential model against Validation 10 at 296 K

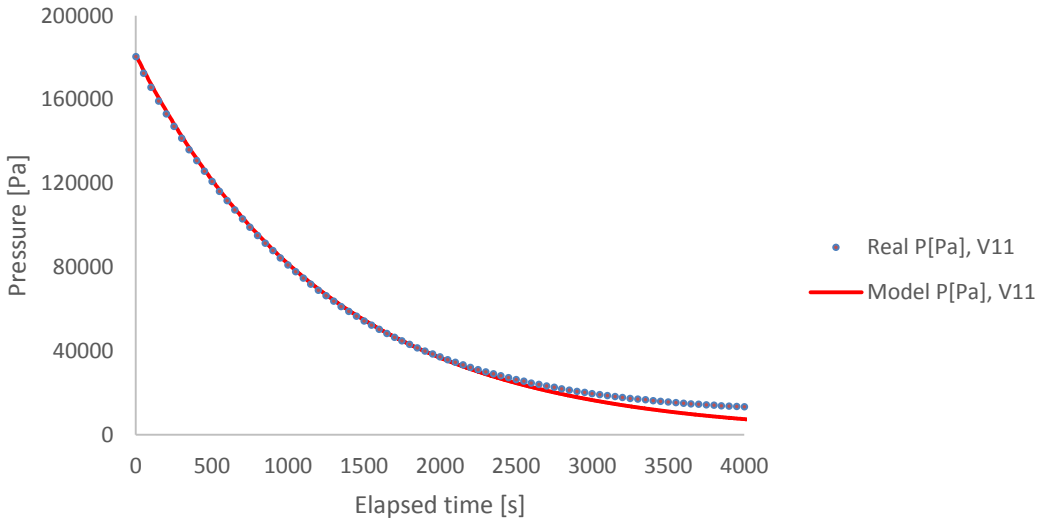

Figure 54. Exponential model against Validations 10 & 11 at 318 K

10.2 MDEA+N_2O

The measurement values for the mass transfer coefficient ($k_{L,\ calc}$) were calculated with equation (41) using the data shown earlier. Experiments lasted from 100 min to 133 min. Their comparison to the literature value ($k_{L,\ corr}$) obtained from the correlation used by Pani et al. (1997a, 1997b) can be seen in table 20. Specific calculations are available in Appendix H.

Table 20. Measurements with N_2O. (Re = impeller Reynolds number from equation (8), Sc = Schmidt number from equation (9) and Sh = Sherwood number from equation (10), X = multiplier calculated for equation (11), Diff = difference between k_L calculated from correlation and measurement data)

Temp. [K]	w_{MDEA}	*kL corr. [m·s^{-1}]*	*kL calc. [m·s^{-1}]*	*Re*	*Sc*	*D(N_2O) [m^2·s^{-1}]*	*Sh*	*X*	*Diff. [%]*
298.4	0.10	2.02E-05	1.70E-05	4353	896	1.39E-09	733	0.29	16.11
305.1	0.10	2.24E-05	2.21E-05	4529	629	1.68E-09	788	0.34	1.19
318.2	0.11	3.19E-05	3.23E-05	6343	353	2.33E-09	834	0.34	-1.28
305.1	0.20	1.60E-05	1.43E-05	3089	1241	1.24E-09	692	0.30	10.74
318.2	0.20	2.35E-05	2.24E-05	4445	626	1.80E-09	749	0.32	4.76
298.1	0.20	1.34E-05	1.24E-05	2680	1877	9.94E-10	746	0.31	7.83

As can be seen, only two of the values of constants used in equation (11) (X in table 20) correspond perfectly to literature correlation and therefore we decided to optimize the parameter in the mass transfer correlation (equation (11)) to improve the correlation with respect to our measurements. We optimized it based on the calculated values for the constants and got a value of approximately 0.318 for the constant. This value was used when analyzing the validation measurement results for the cell.

10.3 MAPA+DEEA+CO_2

In order to find out how the split into two liquid phases in the 5D2M solution affects the absorption rate, experiments were run at 318 K and at 308 K. Data from those experiments was plotted for flux dependency on loading. The values for flux were taken at three distinct pressures: 105 kPa, 74 kPa and 64 kPa.

The idea was that as the initial pressure of gas is the same between runs, the effect of the difference in the driving force in absorption would be small and thus we would see the effect of loading in the absorption speed. In addition the visual identification of the phase split during absorption experiments is shown and a second order polynomial was fitted to the data to show the average value and the trend better. The graphs for loading dependency are shown in figure 55 to figure 60.

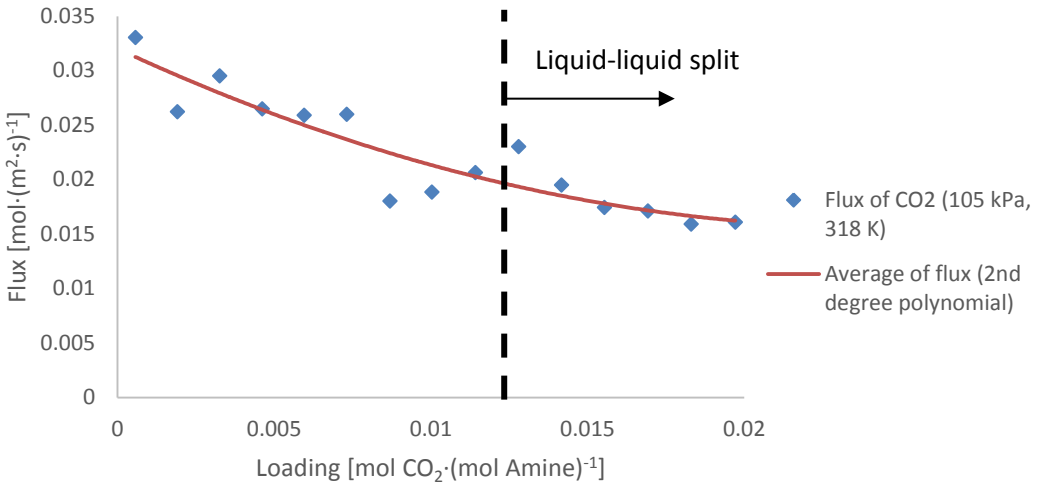

Figure 55. Flux of CO_2 as a function of loading in 105kPa and 1st run at 318 K

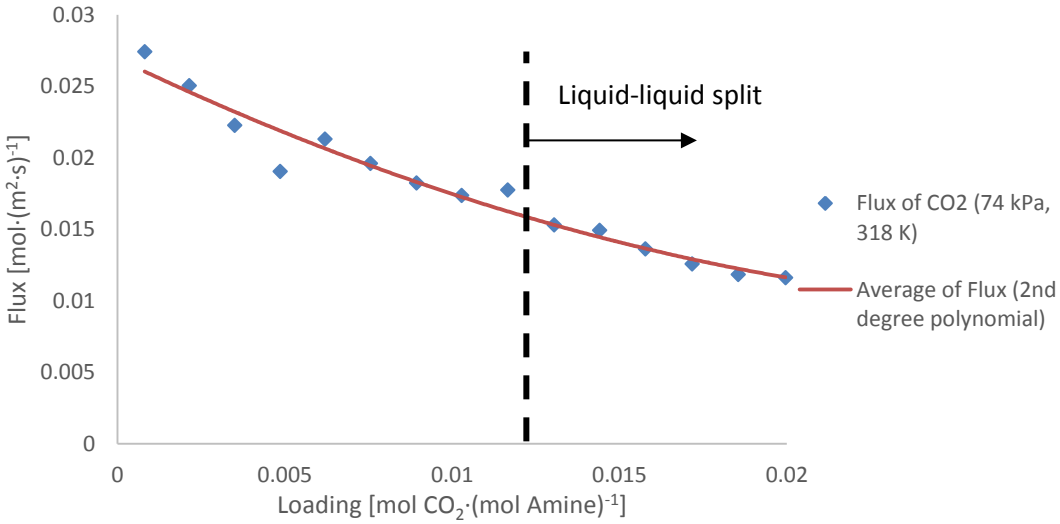

Figure 56. Flux of CO_2 as a function of loading in 74kPa and 1st run at 318 K

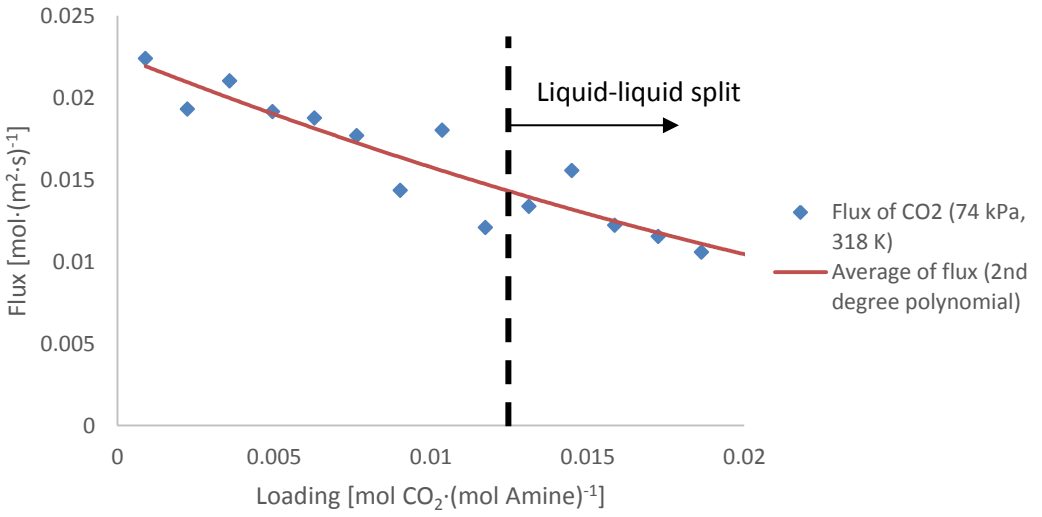

Figure 57. Flux of CO_2 as a function of loading in 64kPa and 1st run at 318 K

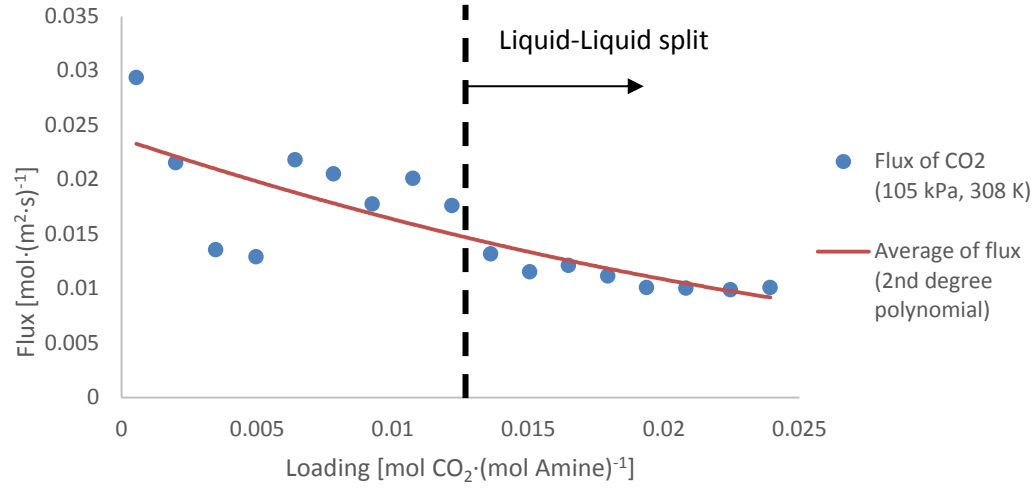

Figure 58. Flux of CO_2 as a function of loading in 105kPa and 2nd run at 308 K

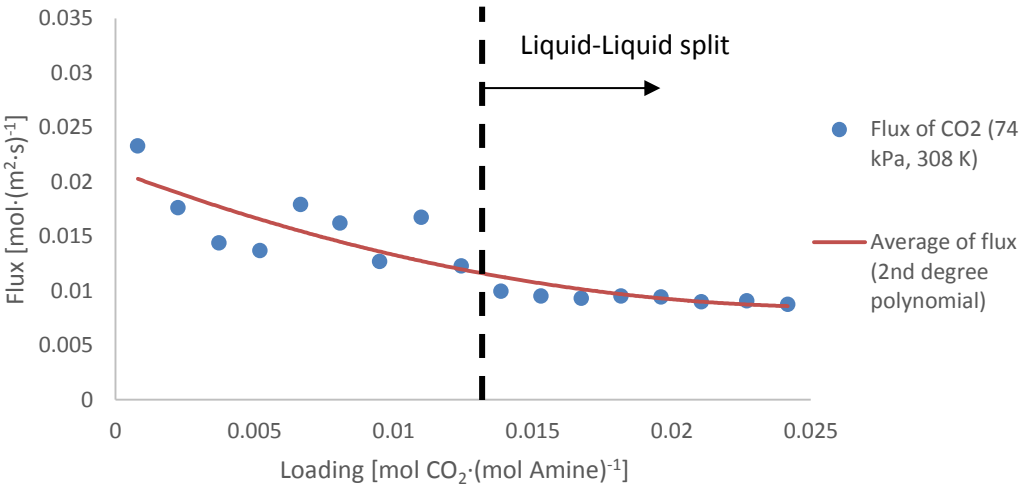

Figure 59. Flux of CO_2 as a function of loading in 74kPa and 2nd run at 308 K

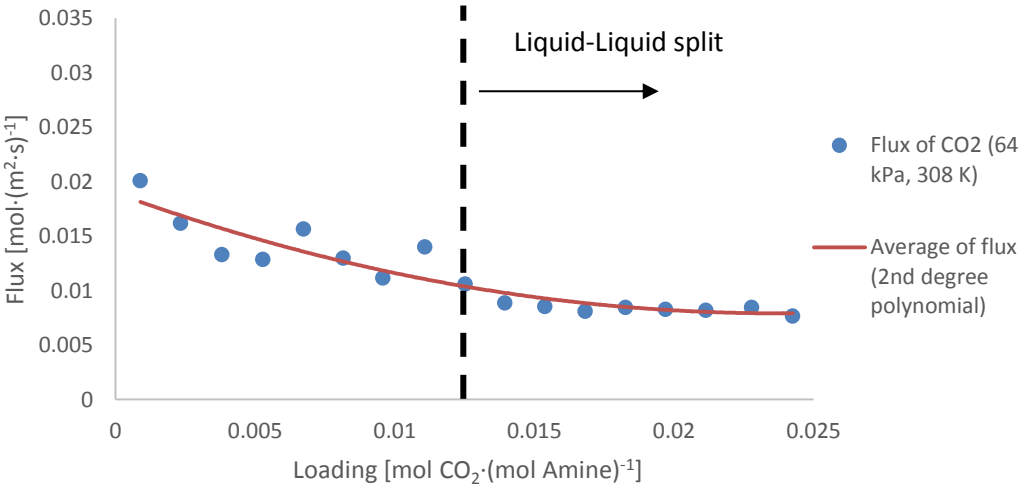

Figure 60. Flux of CO_2 as a function of loading in 64kPa and 2nd run at 308 K

First three graphs show that in 318 K there is no clear effect on the flux with such low loadings. In the first run in 318 K at 74 kPa, flux shows a slope to a slower absorption rate without reaching a stable rate at any point. Same trend can be seen for the 105 kPa and 64 kPa graphs, despite some outliers in the data. At 64 kPa the rate however does seem to slow down to a stable rate around 0.016 mol CO_2·(mol Amine)$^{-1}$ loading.

The three following graphs showing the effect in 308 K show some effect however. These experiments show a slow decrease in the rate of absorption until the split happens. Once the split is seen, a clear trend of stable absorption speed is observed. For the 2nd run there is clear scatter in the data during the earlier experiments, but all three graphs show that after formation of the phase split in the 10th-11th absorption run, the absorption rate stays relatively stable. The stable absorption is reached at 0.014 – 0.016 mol CO_2·(mol Amine)$^{-1}$ loading in these graphs. This scatter behavior is assumed to be due to MAPA reactivity in the solution. As MAPA is spent the rate decreases, however there is some transfer between DEEA and MAPA in the liquid which can cause MAPA to be released and for the rate to speed up again.

To further analyze the temperature effect on the absorption speed, graphs showing the flux in both temperatures in all three studied pressures were drawn and can be seen in figure 61, figure 62 and figure 63.

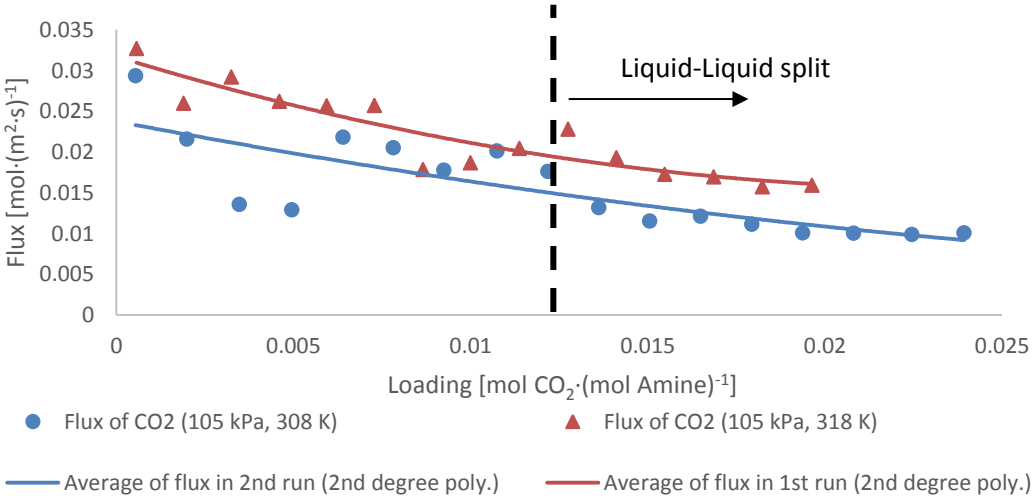

Figure 61. Flux of CO_2 in to Amine as a function of loading in 105 kPa

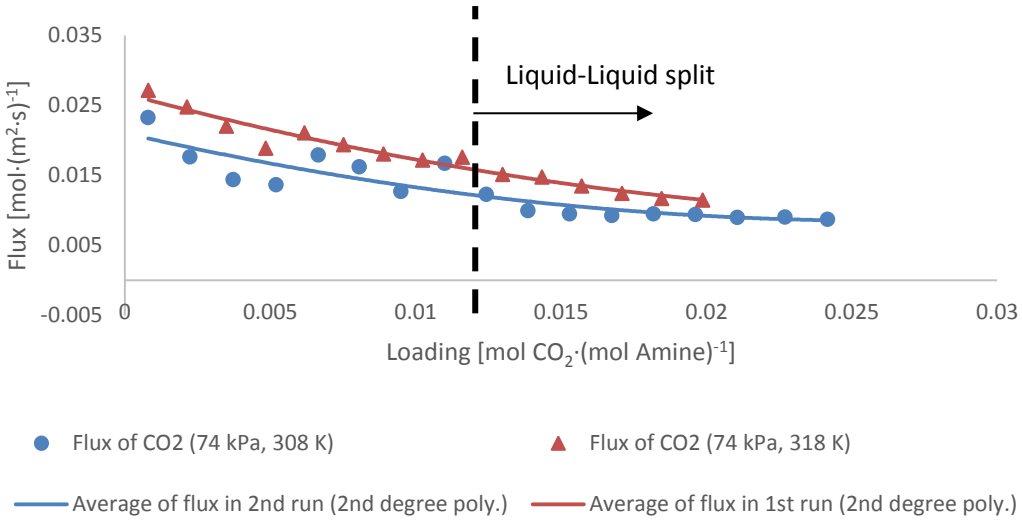

Figure 62. Flux of CO_2 in to Amine as a function of loading in 74 kPa

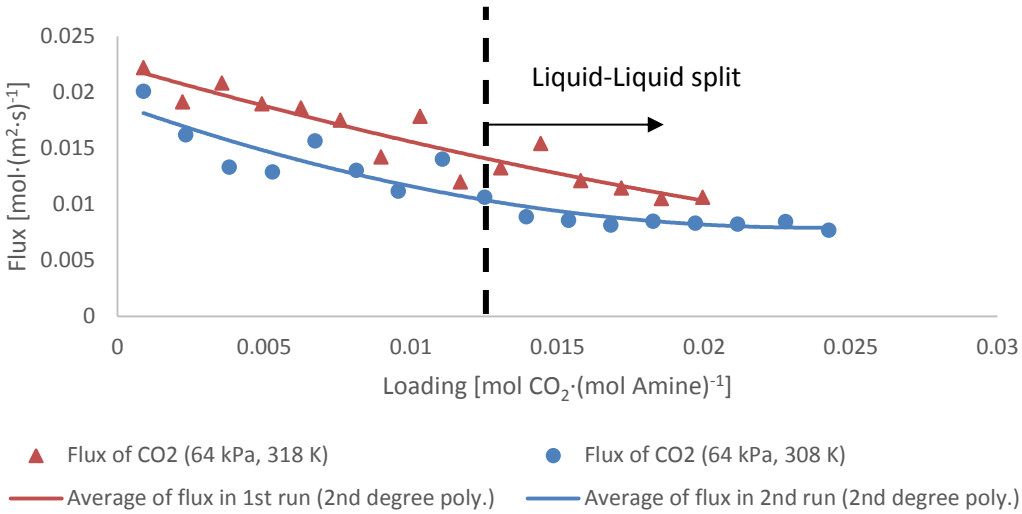

Figure 63. Flux of CO_2 in to Amine as a function of loading in 64 kPa

From these figures it is apparent that the temperature has some effect on the absorption rate, however the effect diminishes as the two liquid phases appear. It was also of interest to review the final pressures in the cell after each experiment. These values are usually available in articles regarding phase equilibrium measurements and can therefore be compared to our data. figure 64 and figure 65 show the final pressures logged in each absorption test of runs 1 and 2. These figures also show the pure amine solution vapor pressure as estimated with pure component vapor

pressures from DIPPR Project 801 (Design Institute for Physical Properties, 2014) and Hartono et al. (2013) for use with Raoult's law.

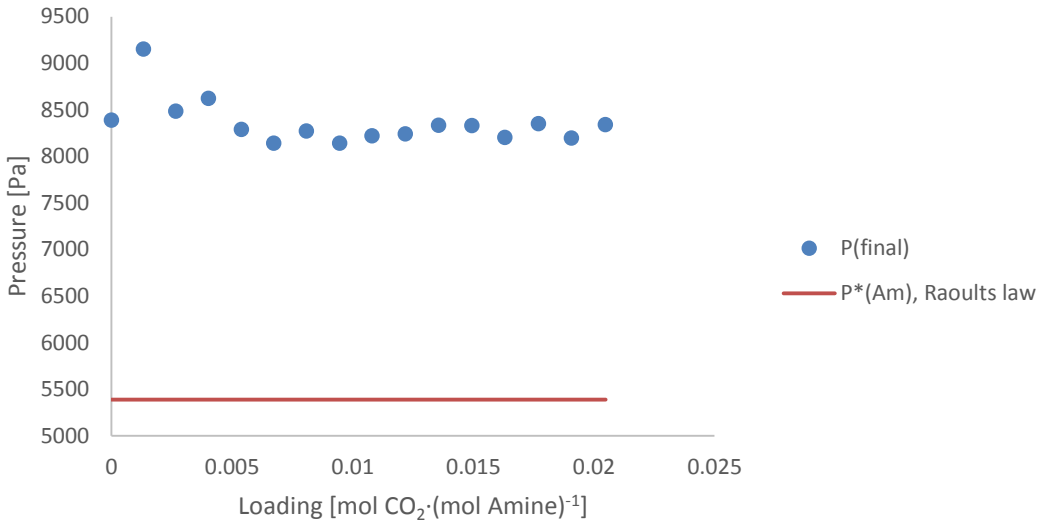

Figure 64. Final pressures of the cell after each absorption in run 1 in 318 K

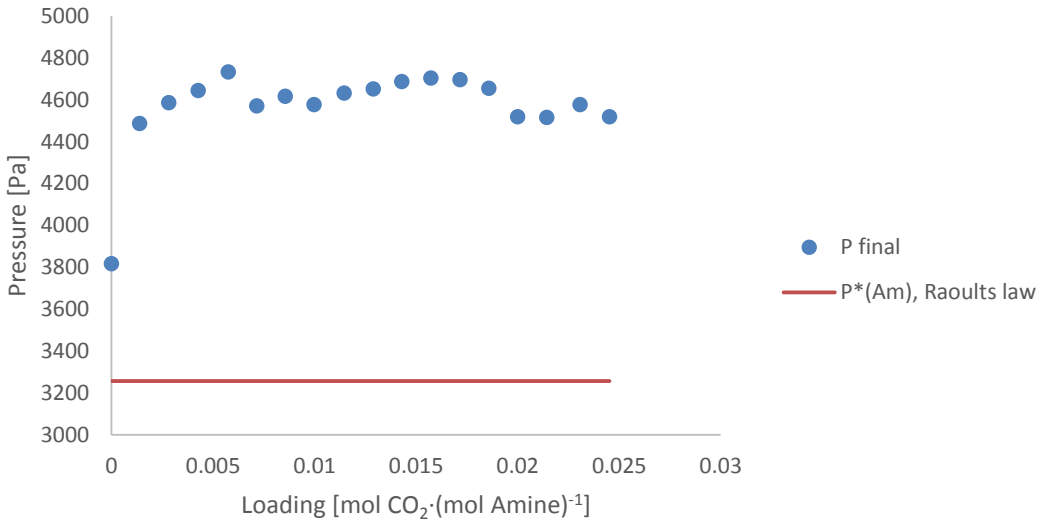

Figure 65. Final pressures of the cell after each absorption in run 2 in 308 K

It would be ideal to compare the pressures of CO_2 in the gas phase, but this is not possible, as the vapor pressure of the amine solution changes with loading and this change is not well documented. However there is literature data (Arshad et al., 2014) available at 313 K to 393 K from loadings of 0.3 to 0.7 mol CO_2·(mol Amine)$^{-1}$ for both the final pressure of the system and the equilibrium pressure of CO_2. The closest loading value close to our loadings in their data is 0.3 mol CO_2·(mol Amine)$^{-1}$, for

which the final pressure was 11.4 kPa. In figure 66 our final pressures of the system at 318 K were compared to the values obtained by this team for 313 K as well as the pure vapor pressure of the amine (~5380 Pa) in 318 K.

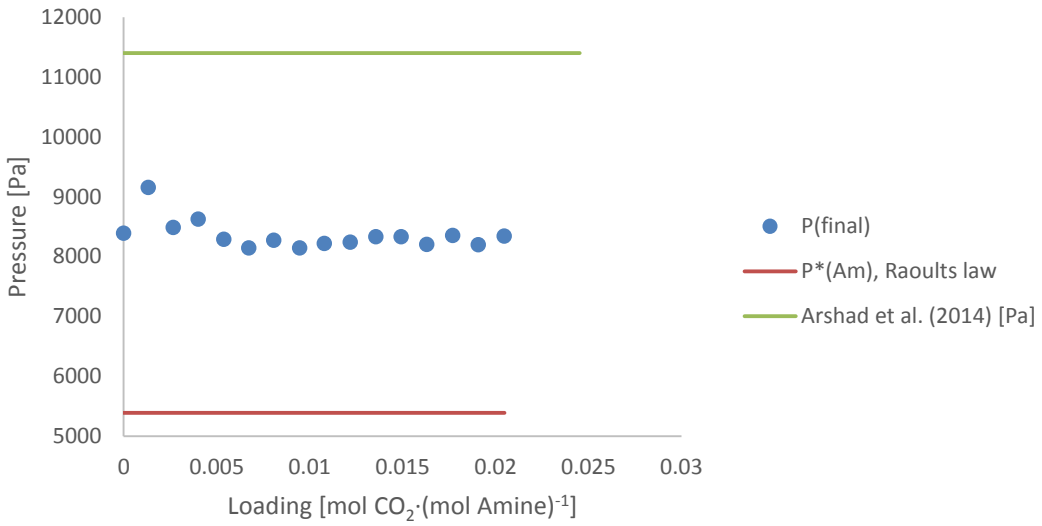

Figure 66. Comparison of final pressures at 318 K

From the figure we can see, that when compared with the final pressure at 0.3 mol CO_2·(mol Amine)$^{-1}$ loading, our pressures show a logical trend. More experiments towards a higher loading value would be beneficial. It would allow for better understanding on the effect of loading on the amine absorption rate.

Analysis of the absorption experiments around the formation of the two phase split was also of interest, as it could possibly point out the loading in which the split happens with this solution. Absorptions 10 to 15 in the 1st run as a function of loading can be seen in figure 67 and Absorptions 10 to 17 in the 2nd run as a function of loading can be seen in figure 68.

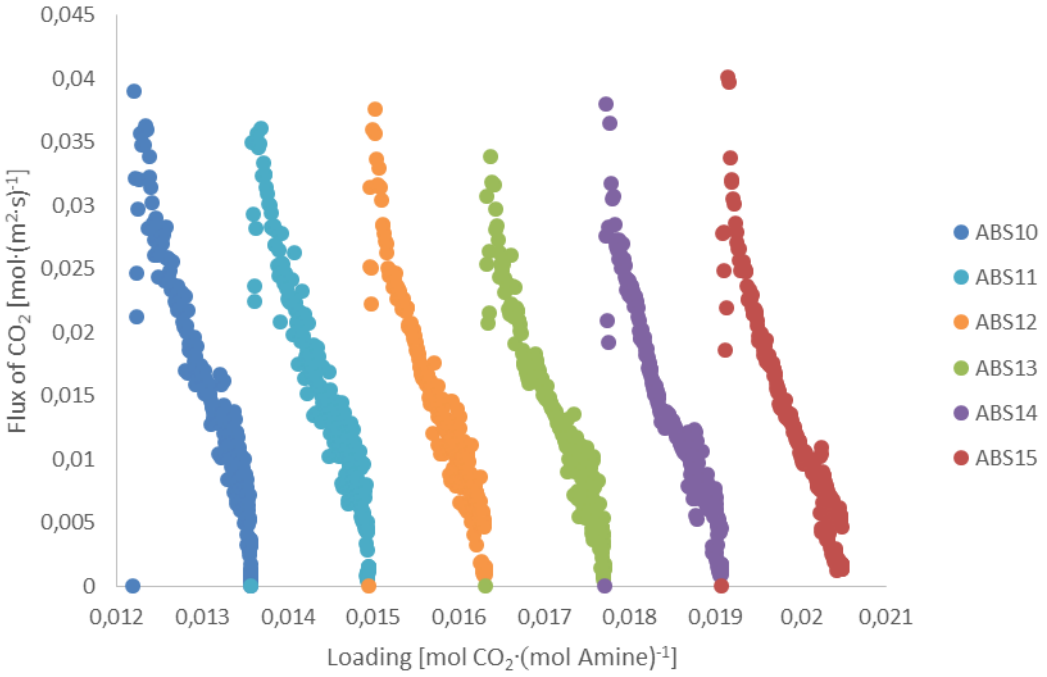

Figure 67. Flux as a function of loading. 1st run. Absorptions 10-15 in 318 K

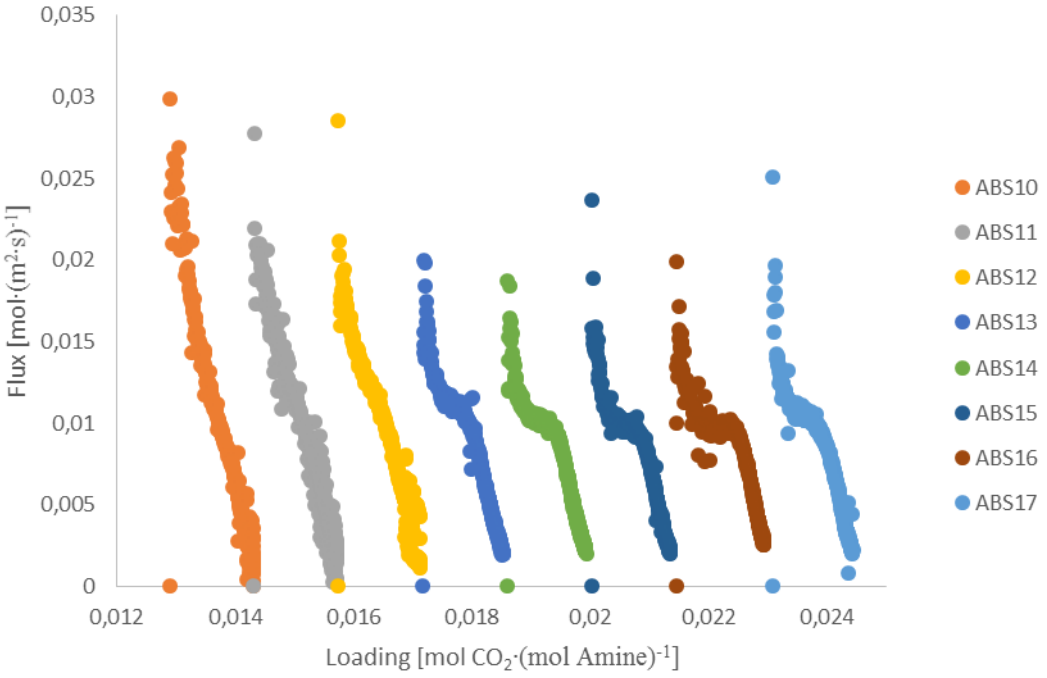

Figure 68. Flux as a function of loading, 2nd run, Absorptions 10-17 in 308 K

As can be seen from the figures, the absorption in 318 K seems to continue in the same trend regardless of loading where as in 308 K it starts to show a trend of stable area already in absorption 10. As the loading increases the trend becomes more and more visible. During these absorption runs it was also observed that the viscose layer, or the gas rich layer, increased in volume as more gas absorbed. It can be concluded that once all MAPA has been spent in the amine solution, the absorption rate will stabilize to about 0.01 mol·(m2·s)$^{-1}$ at 308 K as long as the driving force is sufficient. It was also of interest to analyze the flux as a function of pressure, to determine which pressure range would be suitable to cause the stable absorption rate. These plots can be seen in figure 69 and figure 70.

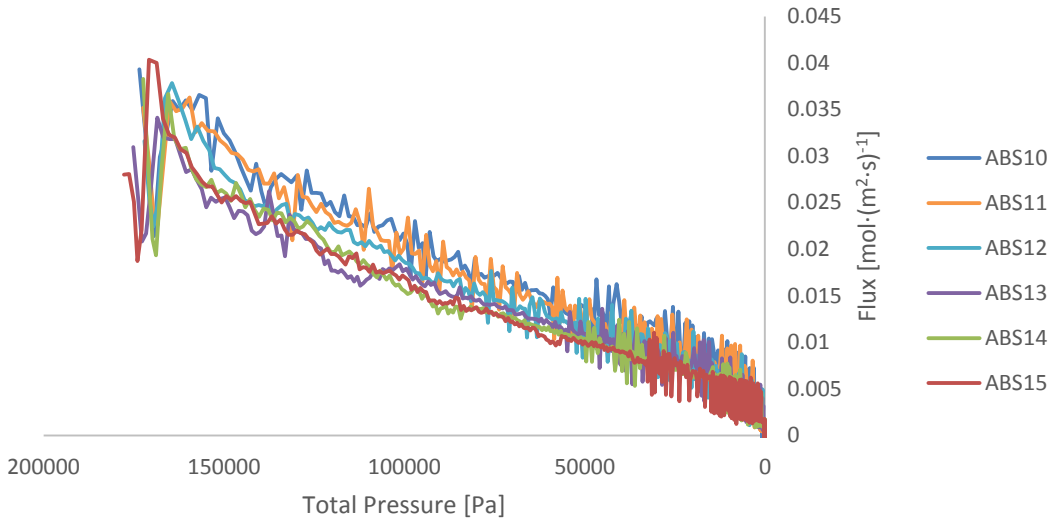

Figure 69. Flux as a function of pressure in absorption runs 10 to 15 of run 1 in 318 K

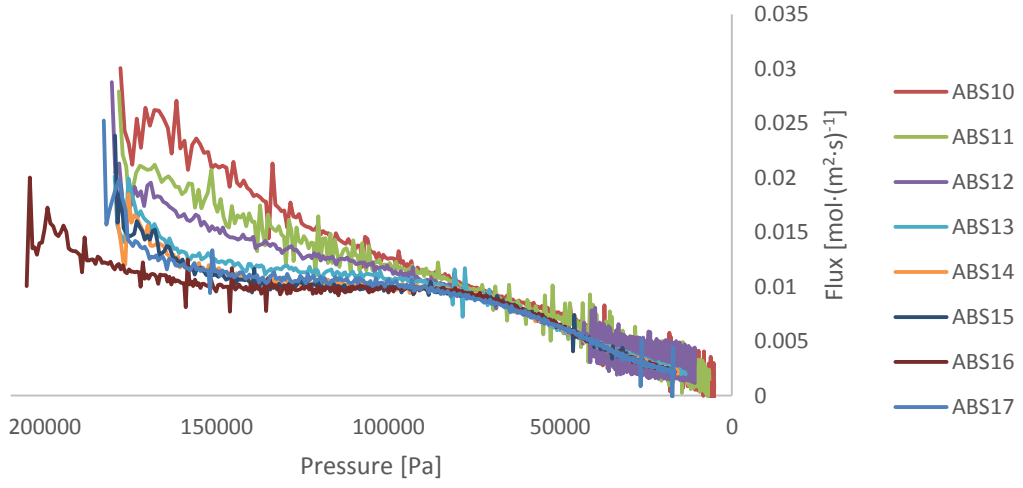

Figure 70. Flux as a function of pressure in absorption runs 10 to 17 of run 2 in 308 K

For temperature 308 K figure 70 shows that when the phase split has formed and the pressure of CO_2 is in the range of 150000-80000 Pa the flux of gas is effectively 0.01 mol·(m2·s)$^{-1}$. There is a deviation of 0.005 mol·(m^2·s)$^{-1}$ in the flux value between loadings of 0.013 and 0.025 mol CO_2·(mol Amine)$^{-1}$. It seems, that when the phase split forms around the loading of 0.014-0.016 mol CO_2·(mol Amine)$^{-1}$ the absorption rate stabilizes at 0.01 mol·(m2·s)$^{-1}$. In the higher temperature tested, 318 K, this trend is not noticeable at all. This can be due to the higher viscosity of the 2nd, CO_2 rich, phase at lower temperature and therefore slower settling of this layer to the bottom of the cell and consequently slower refreshment speed of the interface layer or then from a difference in the absorption energy. Latter possibility would suggest, that the higher absorption temperature is more industrially interesting, as it should be able to handle higher loading values without a decrease in the flux.

10.4 MDEA vs MAPA+DEEA in CO_2 capture

To show the large difference in absorption rates of these two compounds, figures were plotted to show the flux of gas as a function of CO_2 pressure in the cell. Slowest absorption rates observed with high loading for MAPA+DEEA at the end of the 1st run. The comparison with only earlier MDEA measurements is problematic, as the concentration used in our validation runs was in the range of 0.84 M and the total amine concentration of the MAPA+DEEA solution is around 6.8 M. To take this in to account literature data from Pani et al. (1997a) was used at 4.324 M (Literature 21) and 3.436 M (Literature 20). The comparison for these is shown in figure 71.

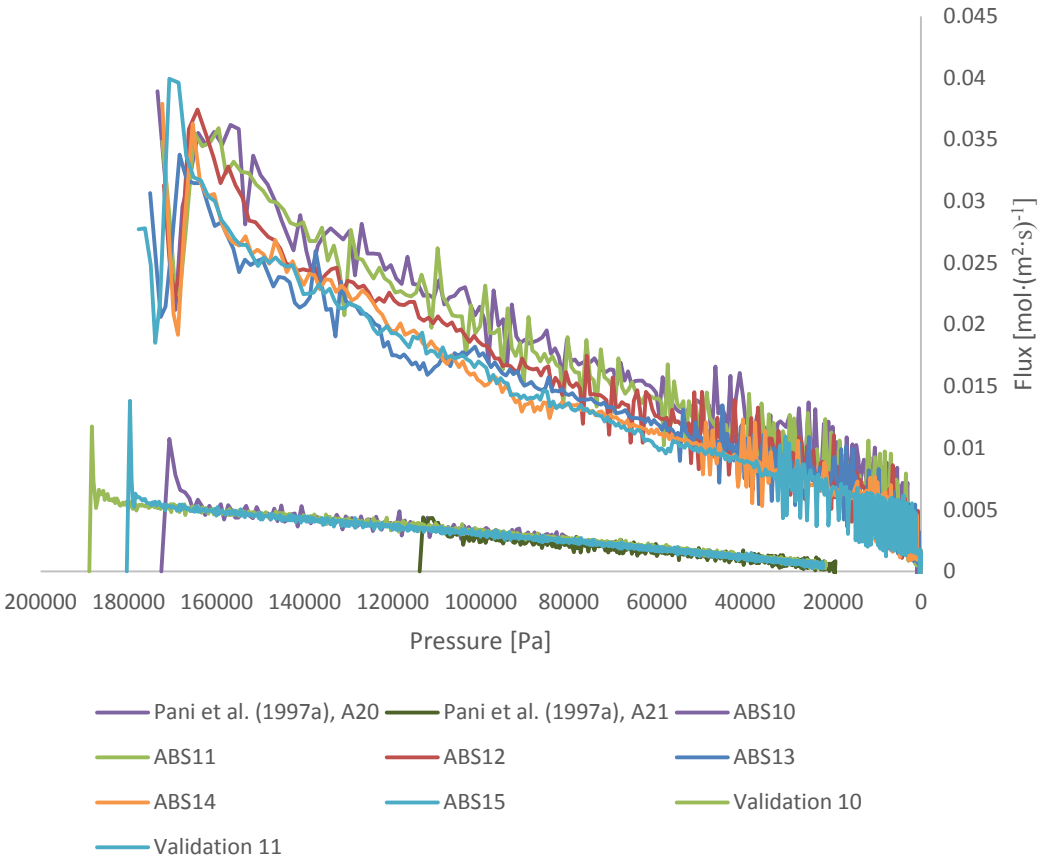

Figure 71. Comparison of fresh MDEA and loaded MAPA+DEEA absorbents in 318 K

The absorption rate of CO_2 from the same initial pressures to nearly same final pressure is considerably higher for MAPA+DEEA. As can be seen, the flux of these literature data correlates very well to our validation runs, showing that with MDEA, the solvent concentration does not seem to influence the flux observed in low loadings. To further illustrate this difference, a comparison of the initial absorption rate of unloaded and slightly loaded amines were also plotted. It is visible in figure 72.

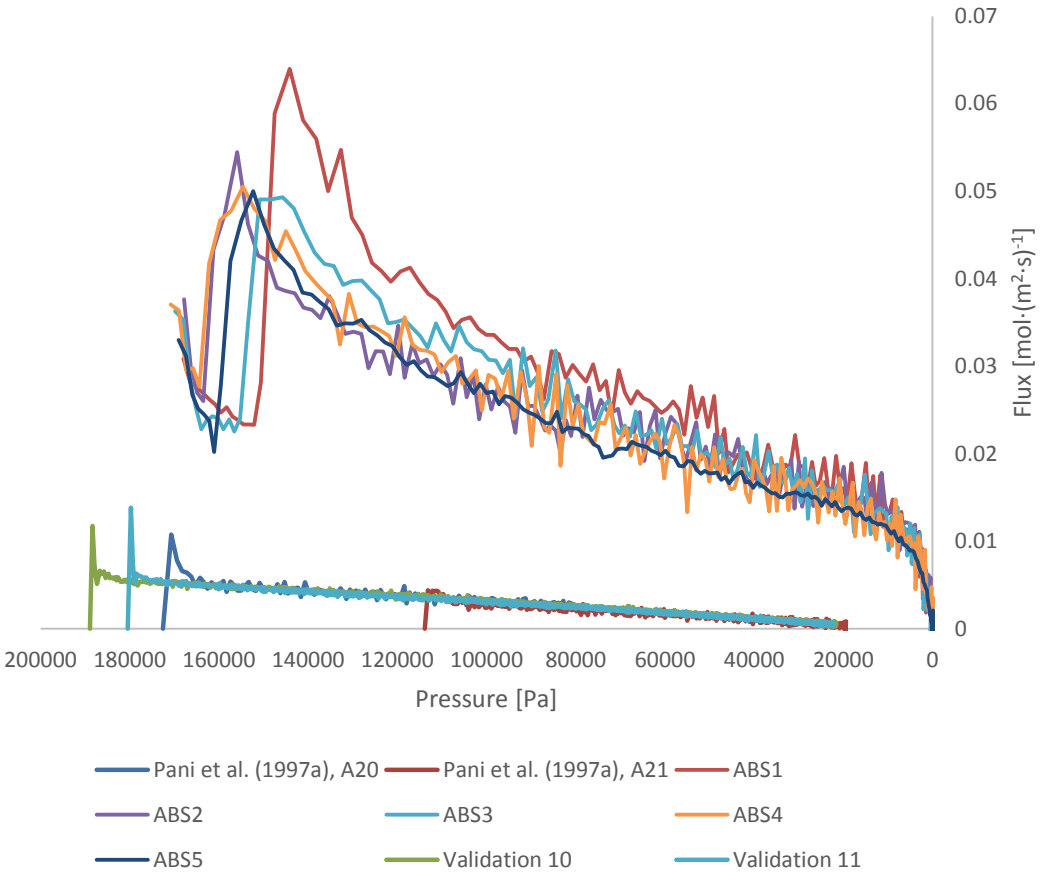

Figure 72. Comparison of the CO_2 flux in fresh MDEA and fresh MAPA+DEEA absorbents in 318 K

Figure 72 clearly shows how much these two absorbents differ when they are both unloaded. The 1st absorption run with MAPA+DEEA, ABS1, reaches up to 0.06 mol·(m^2·s)$^{-1}$ whereas the unloaded MAPA reaches absorption rates below 0.01 mol·(m^2·s)$^{-1}$ in the same temperature. These results are of course not conclusive, as the only MDEA solution that was used by our validation was of 0.84 M concentration and the used MAPA+DEEA solution contains a total amine concentration of 6.8 M. Comparison to Pani et al. (1997a) literature values seems to indicate however that the concentration of the amine solution is not influencing the flux of gas at low loadings.

10.5 DEEA+MAPA+H_2S

During the 24 runs, it was observed that there is a clear equilibrium pressure forming unlike with CO_2. The rate of absorption was again analyzed as a function of loading

and is shown in three different pressures in figure 73, figure 74 and figure 75.The final pressure of the cell is displayed against loading in figure 76.

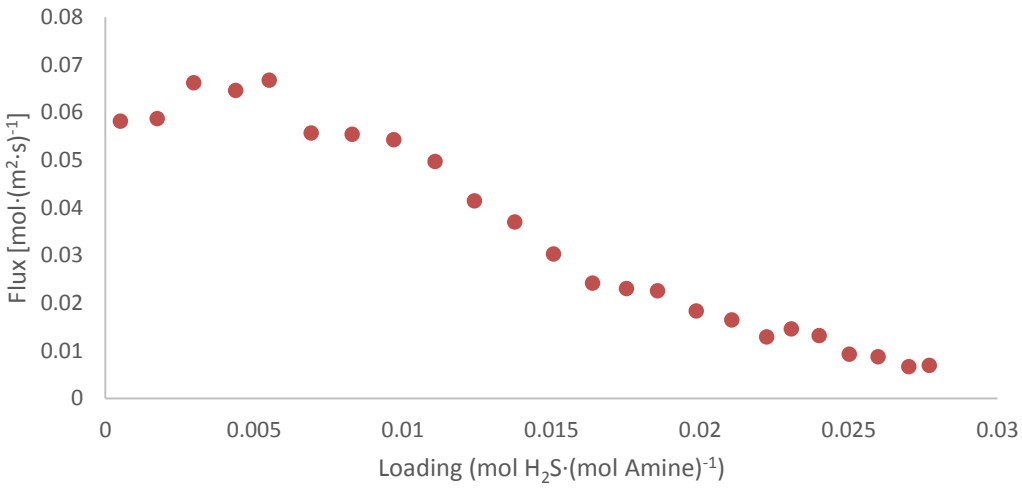

Figure 73. Flux of H2S as a function of loading at 105 kPa and 319 K

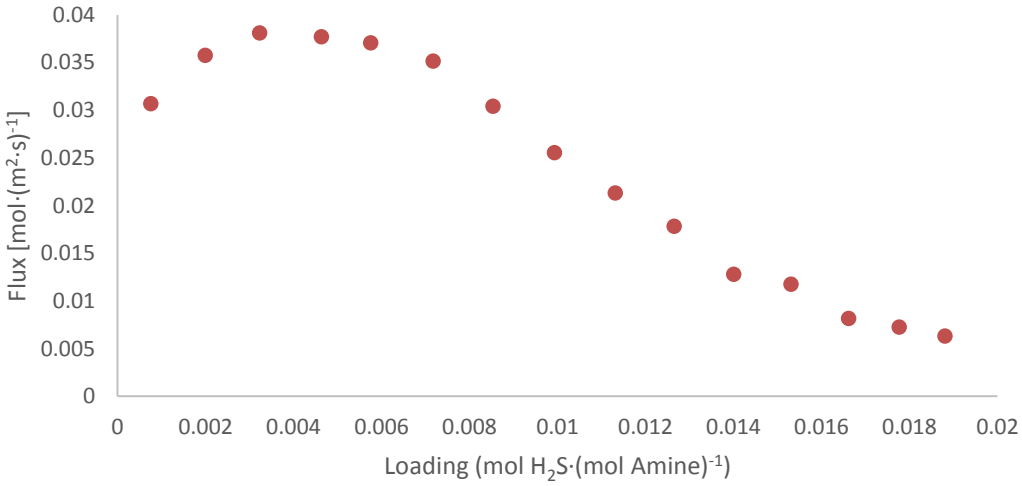

Figure 74. Flux of H_2S as a function of loading at 74 kPa and 319 K

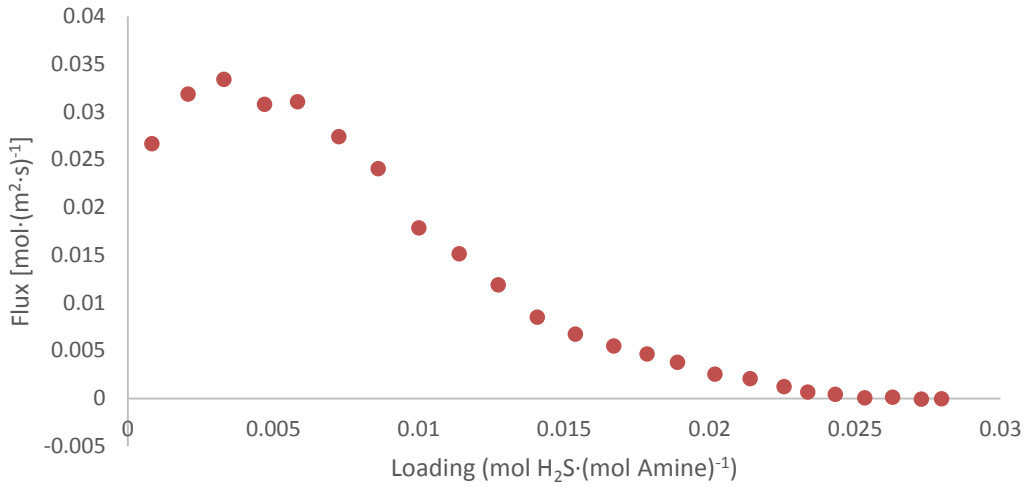

Figure 75. Flux of H_2S as a function of loading at 64 kPa and 319 K

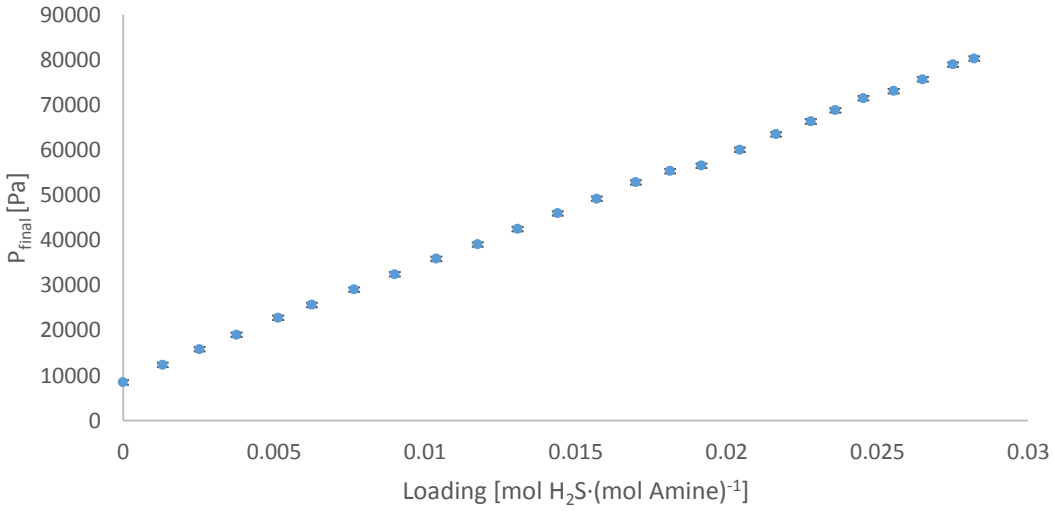

Figure 76. Final pressures of the cell as a function of amine loading at 319 K

In figure 76 the 0 loading value is the vapor pressure of the solution before any gas was added to the cell. It can be observed that as the equilibrium pressure rises, the driving force logically decreases and therefore so does the rate of absorption. In addition no liquid-liquid split was observed, which also explains the rise in equilibrium pressure.

10.6 MAPA+DEEA, H_2S vs CO_2

To compare the effectiveness of the phase change solvent studied in H_2S and CO_2 absorption, a graph showing the rate of absorption as a function of time in the first absorption was studied. This graph is shown in figure 77.

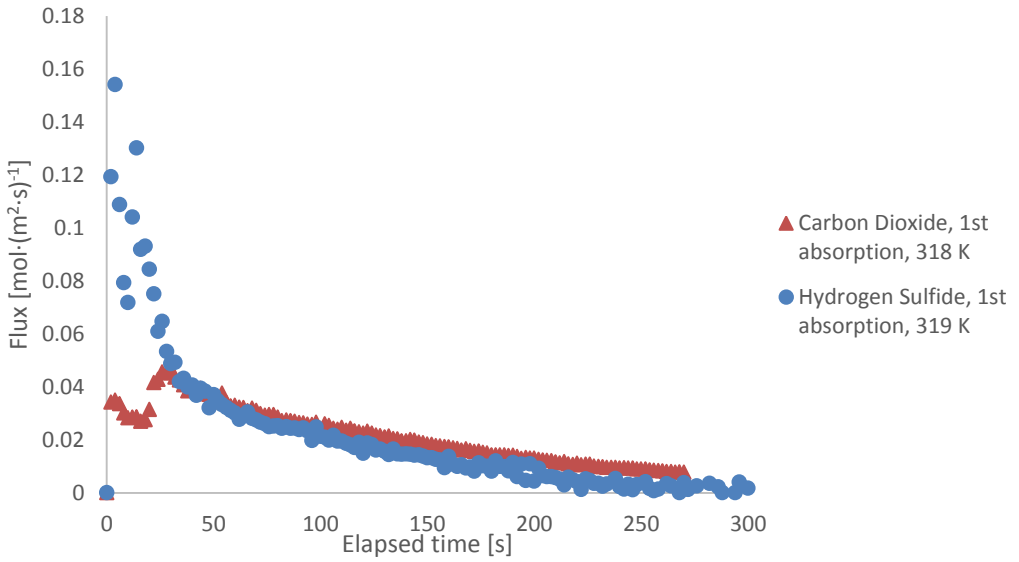

Figure 77. Comparison of H_2S and CO_2 absorption in to MAPA+DEEA, 1st absorptions

In figure 77, figure 78 and figure 79 the initial slow absorption seen for CO_2 is due to a delay in the mixer start. When mixing is not on, the absorption is considerably slower as the solvent on the interface is not refreshed effectively. This behavior is further discussed in improvement ideas. As can be seen, the behavior of H_2S rate of absorption is similar to that of CO_2 in to MDEA as was observed earlier. The absorption is considerably faster in the beginning of the run, but as the equilibrium pressure in the cell rises, the rate decreases. This is more evident later in the 10th absorption seen in figure 78 and even more so on the comparison of the last absorptions of both runs in figure 79.

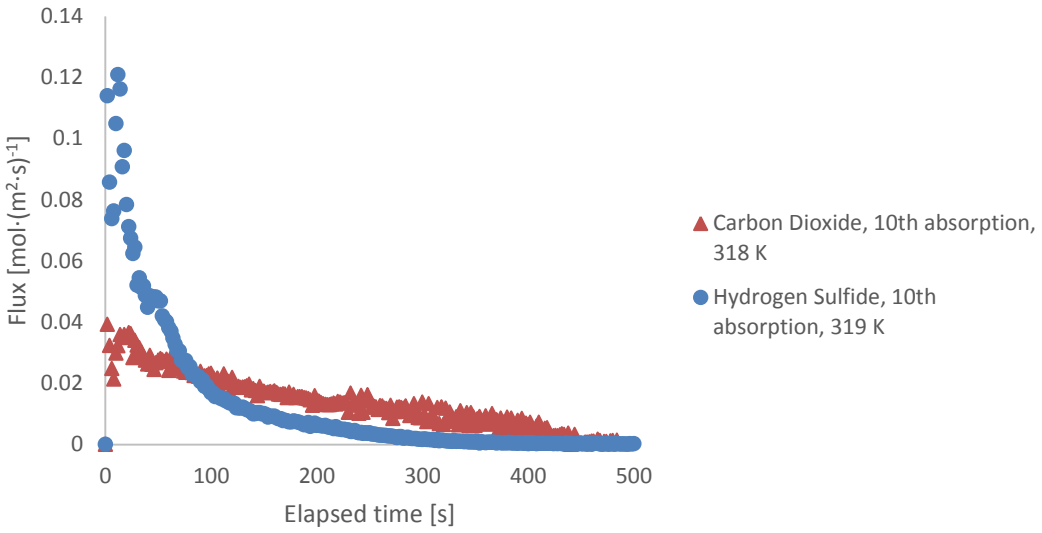

Figure 78. Comparison of H_2S and CO_2 absorption in to MAPA+DEEA, 10th absorptions

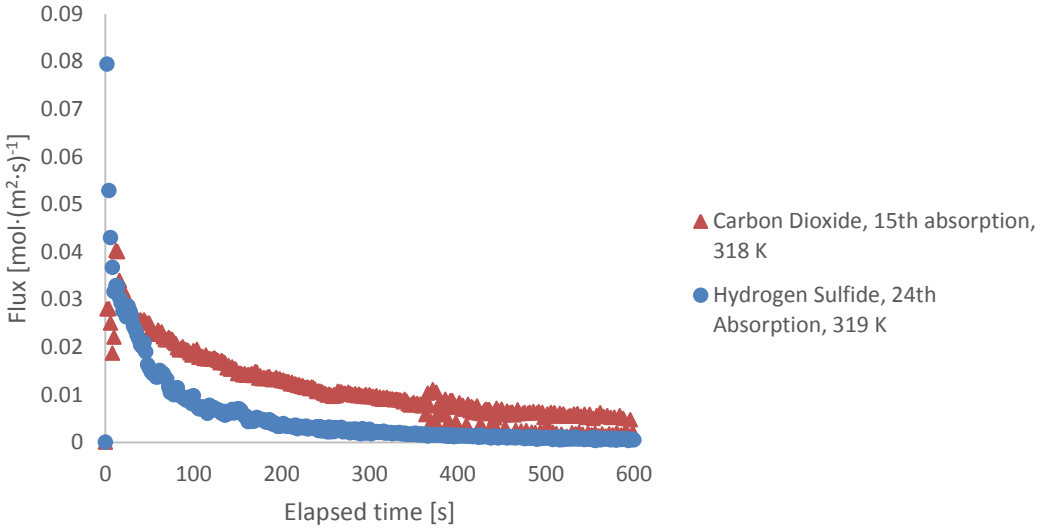

Figure 79. Comparison of H2S and CO2 absorption in to MAPA+DEEA, final absorptions

To better illustrate the difference in flux, a figure showing the ΔFlux (H_2S – CO_2) as a function of time during the measurements was drawn and is seen in figure 80.

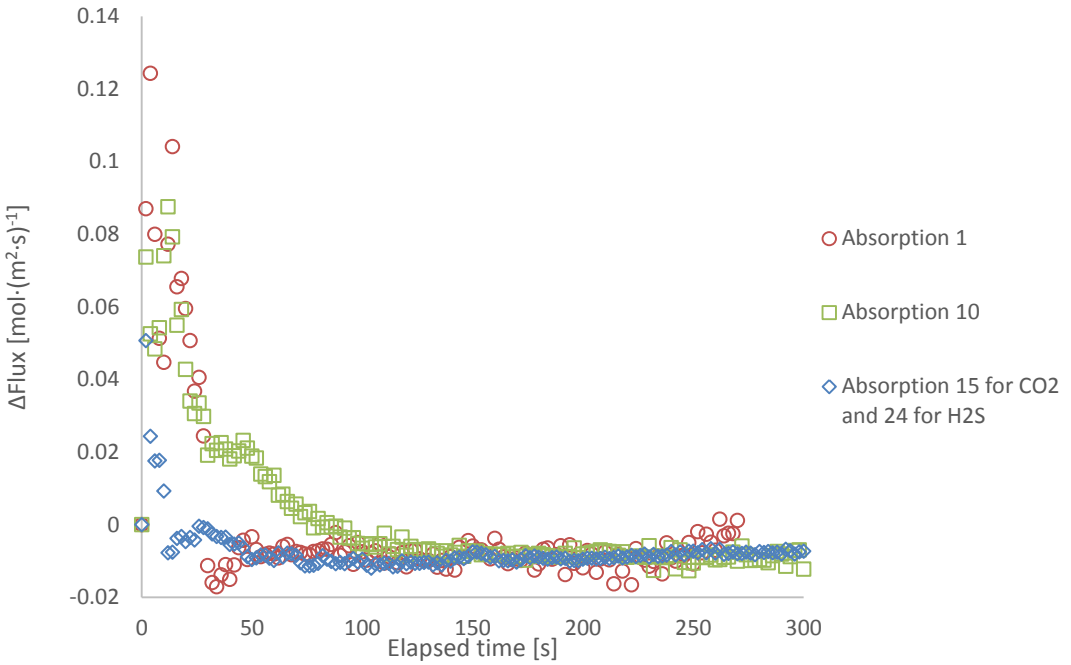

Figure 80. Comparison of ΔFlux between CO_2 and H_2S at 318 K

As can be seen, the rate of absorption for H_2S is highly dependent on the amine loading. This, along with a high equilibrium pressure, suggests that this composition of the absorbent is not suitable for H_2S capture alone.

A comparison of final pressures in the cell after each absorption run was also made to illustrate the difference between the behaviors of these two gases. In addition Raoult's law was used to determine the pure mixture vapor pressure in experimental temperature (318 K). This comparison is available in figure 81.

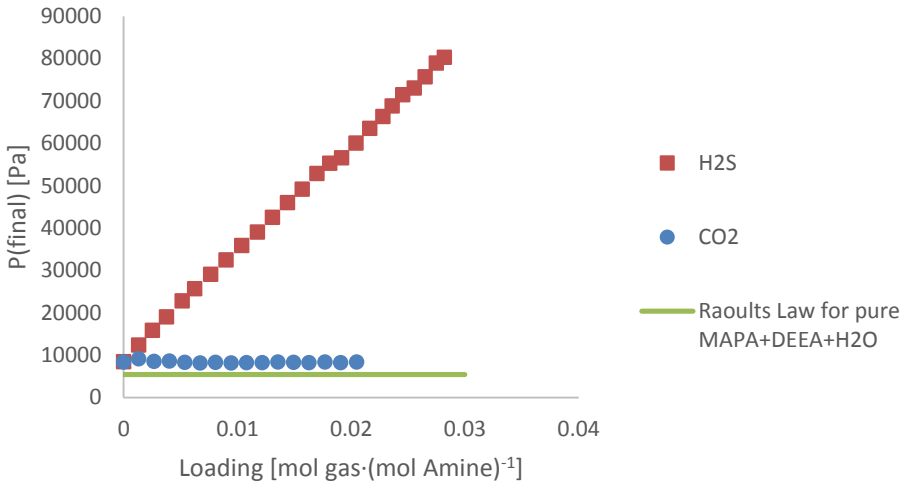

Figure 81. Pure vapor pressure and final pressure comparison

11 Ideas for further research and improvements

11.1 Ideas for further research

For carbon dioxide absorption runs it is suggested that more mixtures with different concentrations should be tested. In addition allowing for more time to stabilize between measurements might provide better reliability for the estimation of CO_2 final pressure at the end of each experiment. It could also be of interest to obtain more flux data as it is not published for most of the studied amine solutions. Only MDEA has this data directly available from the research done by Pani et al. (1997a). A study of activated mixtures of MDEA could provide better understanding in regard to the flux of MAPA+DEEA solutions and if their absorption rate really is superior to others.

To further increase the usefulness of the obtained results from this thesis, a study of equilibrium constants between hydrogen sulfide or carbon dioxide and aqueous MAPA and DEEA would be beneficial. The reaction paths for both DEEA and MAPA are equilibrium reactions and therefore require some amount of time in the column or vessel to reach said equilibrium. It would be beneficial to also analyze this with further research as it is industrially important when designing such absorption units. It would also be useful to study the Henry's law coefficients and physical

properties of these combinations, as most of the equations presented in this thesis also rely on those and are therefore not useable for this alkanolamine solution at the time.

From the measurements done with hydrogen sulfide on MAPA and DEEA it seems that the absorbent is not viable for the capture of H_2S alone, at least in the studied concentrations. However it would be of interest to study how the liquid-liquid split affects the absorption rates and equilibrium pressures of hydrogen sulfide in the solution. With CO_2 it was observed that as the liquid-liquid split forms, there is no equilibrium pressure for CO_2 seen in the low loadings reached within our work. Therefore an experiment with CO_2 loaded aqueous solution of MAPA and DEEA is proposed for H_2S absorption.

11.2 Improvement ideas for the equipment

During the measurements, it was noted that the transfer of gas from the gas feed tank to the cell should be faster. The current line size is too small as it was evident that small amount of the gas was already absorbing in to the liquid before mixing was started. This can be seen in figure 82 taken during the measurements with MAPA+DEEA as small white droplets falling from the interface layer.

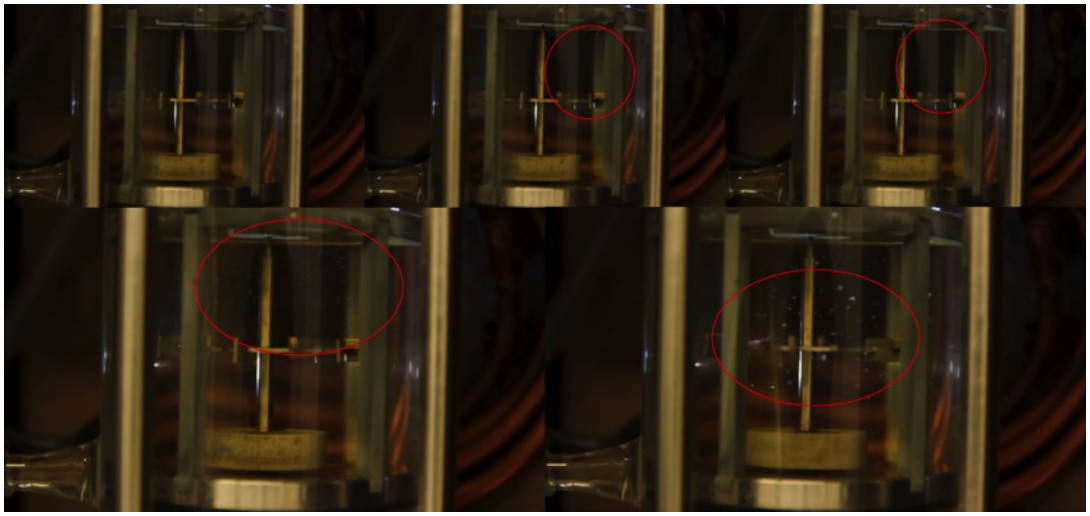

Figure 82. Evidence of absorption prior to stirring the cell

Due to this issue it is suggested that the feeding line for gas from the GFT to the equipment be upgraded to a larger diameter one. While this is done, it is also suggested that one of the valves between the gas tank and the cell be removed as it creates more dead volume. There is one more connection available in the cell and it is suggested that the gas be fed there directly from valve 5 and the current feed line along with valve 6 be used for possible gas evacuation. This is illustrated in figure 83.

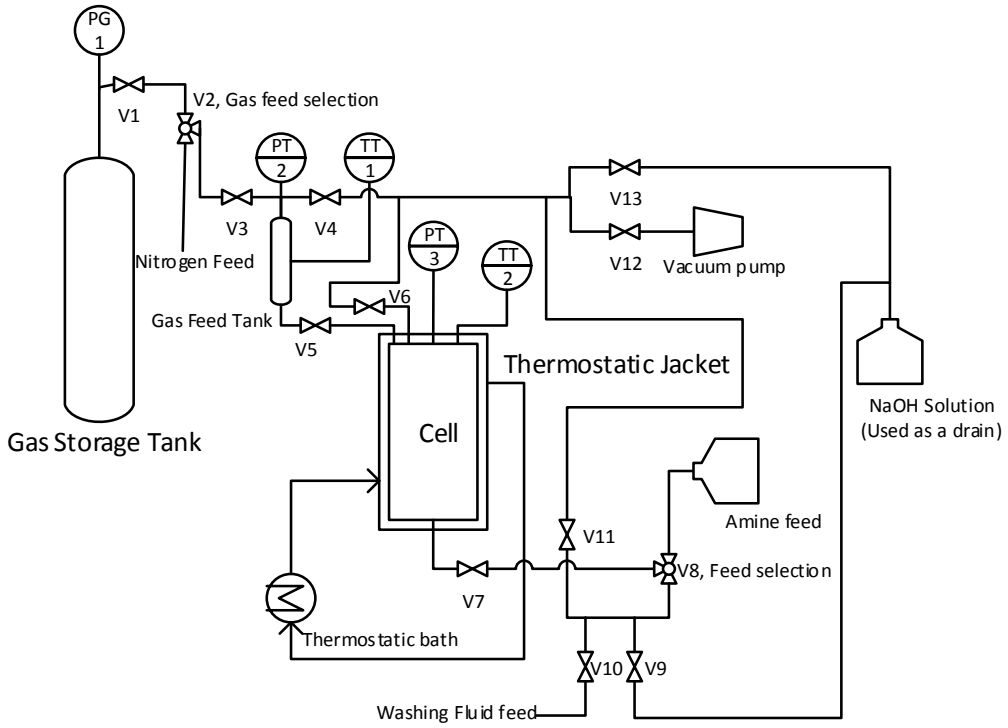

Figure 83. Setup suggested for further experiments

For better documenting of results, a camera system should be installed permanently on the apparatus, taking video of the cell during measurements. Another improvement idea for the cell would be to add a light in to the oven. As can be seen from the pictures taken from a video shot during the measurement, the light is scarce in the equipment and therefore the video and pictures are hard to make out. During these runs a small led lamp located behind the cell was used to light the white particles. However it is proposed that a led strip is added to both bottom and top of the cell to provide proper lightning for the measurements.

In addition it was observed that the mixer motors were not holding the speed set to them very well, as they were repurposed old rotavapor motors. It is therefore suggested that for more accurate measurements these motors would be upgraded to units that allow the user to set the rotating speed accurately at least within ± 1 rpm. This upgrade was already scheduled for the equipment after the thesis was completed.

To allow the use of higher temperatures, it is also suggested that the internal parts of the cell, now made out of PVC, would in the future be machined out of stainless steel. The current construction is limited to temperatures below 50 °C and a stainless steel construction would allow for temperatures up to 100 °C. This would potentially make desorption tests using the same cell possible. This would allow for better understanding of solvent behavior in temperatures that are more attractive from industrial viewpoint.

In some other studies the gas tanks have also been thermostated to the same temperature as the solution. This might also be worth considering, as it would remove another uncertainty or a source of error in the calculations from the system. The cell only monitors the liquid temperature and in some cases the gas has been as much as 10-20 degrees colder than the liquid when it was introduced. Thermostating the GFT would effectively reduce this problem.

12 Conclusions

During this thesis a literature survey in to carbon dioxide and hydrogen sulfide absorption methods was conducted. Survey focused on the reaction kinetics used to evaluate gas flux to absorbent. New measurement equipment, a Lewis type kinetic cell along with all required measuring instrumentation, was set up in the Chemical Engineering laboratories of Aalto University. The equipment was validated with carbon dioxide and aqueous solution of MDEA and compared with prior literature values obtained from Pani et al. (1997a, 1997b).

After validation, measurements were made to find out carbon dioxide absorption rate in to aqueous solution of MAPA and DEEA. This rate proved to be substantially higher than that observed during validation runs with MDEA. This combination of amine solvents could provide advantages over currently used solvents. Experiments on H_2S absorption in to MAPA and DEEA were also conducted and a linear trend of equilibrium pressure vs loading was noticed. MAPA and DEEA seems to be an unsuitable solvent for the H_2S capture alone in light of the results obtained, as in order to reach reasonable loading values in solvent, high partial pressures for the sour gas are required. These are not generally available in the industry.

New research targets to better understand the solvent and its physical properties along with improvement ideas for the equipment as well as new absorption experiments for both CO_2 and H_2S studies were also suggested.

References

Aboudheir, A., Tontiwachwuthikul, P., Chakma, A. and Idem, R., 2004. Novel Design for the Nozzle of a Laminar Jet Absorber. *Ind. Eng. Chem. Res.,* 43(10), pp. 2568-2574. DOI: 10.1021/ie0341606.

Aboudheir, A., Tontiwachwuthikul, P., Chakma, A. and Idem, R., 2003. Kinetics of the reactive absorption of carbon dioxide in high CO_2-loaded, concentrated aqueous monoethanolamine solutions. *Chemical Engineering Science,* 58(23–24), pp. 5195-5210. ISSN: 0009-2509. DOI: 10.1016/j.ces.2003.08.014.

Ahlqvist, M., Litmanen, R. and Ahonen, A., 2014. *Imatran, Lappeenrannan ja Svetogorskin ilmanlaatu vuonna 2013.* Imatra: Imatran kaupunki, Ympäristö- ja tutkimusyksikkö.

Al-Ghawas, H.A., Hagewiesche, D.P., Ruiz-Ibanez, G. and Sandall, O.C., 1989. Physicochemical properties important for carbon dioxide absorption in aqueous methyldiethanolamine. *J. Chem. Eng. Data,* 34(4), pp. 385-391. DOI: 10.1021/je00058a004.

Argirova, M., Jayasuriya, G., Kappus, H., Katz, M., Rolfe, K., Savolainen, H., Smith, R.P., Tarkowski, S., Tolivia, E. and Vashkova, V.V., 1981. ENVIRONMENTAL HEALTH CRITERIA 19, Hydrogen Sulfide. ISSN: ISBN 92 4 154079 6.

Arshad, M.W., Svendsen, H.F., Fosbøl, P.L., von Solms, N. and Thomsen, K., 2014. Equilibrium Total Pressure and CO_2 Solubility in Binary and Ternary Aqueous Solutions of 2-(Diethylamino)ethanol (DEEA) and 3-(Methylamino)propylamine (MAPA). *Journal of Chemical & Engineering data,* 59(3), pp. 764-772. DOI: dx.doi.org/10.1021/je400886w.

Arshad, M.W., von Solms, N., Thomsen, K. and Svendsen, H.F., 2013. Heat of Absorption of CO_2 in Aqueous Solutions of DEEA, MAPA and their Mixture. *Energy Procedia,* 37, pp. 1532-1542. DOI: 10.1016/j.egypro.2013.06.029.

Baker Hughes Incorporated, 2011. White Paper: Hydrogen Sulfide Management. *Baker Hughes Incorporated,* [23.5.2014]. Available : http://assets.cmp.bh.mxmcloud.com/system/423d7d28b39df28c79a3819b9039d5fa_28859-sulfix-h2s-white-paper-print-0311.pdf.

Ballerat-Busserolles, K., Coulier, Y., Majer, V. and Coxam, J., 2013. Liquid-liquid equilibria in demixing amines: a thermodynamic approach, *XXXIX JEEP – 39th Edition of the Joint European Days on Equilibrium Between Phases*, 01.7.2013 2013, MATEC Web of Conferences.

BASF - The Chemical Company, 2014. Diethylethanolamine. *BASF - The Chemical Company,* [23.5.2014]. Available : https://www.basf.com/group/corporate/en/brand/DIETHYLETHANOLAMINE.

Brian, P.L.T., Hurley, J.F. and Hasseltine, E.H., 1961. Penetration theory for gas absorption accompanied by a second order chemical reaction. *AIChE Journal,* 7(2), pp. 226-231. DOI: 10.1002/aic.690070212.

Cadours, R., Zhao, J., Weiss, C. and Shah, V., 2012. HySWEET. *Techno Hub,* Processes, pp. 22-30.

Centers for Disease Control and Prevention, 2007. 2-Diethylaminoethanol. *NIOSH POCKET GUIDE TO CHEMICAL HAZARDS.* 1st edition. Centers for Disease Control and Preventation, pp. 107.

Chen, X., Closmann, F. and Rochelle, G.T., 2011. Accurate screening of amines by the Wetted Wall Column. *Energy Procedia,* 4, pp. 101-108. ISSN: 1876-6102. DOI: 10.1016/j.egypro.2011.01.029.

Crowley, T.J., 2000. Causes of Climate Change Over the Past 1000 Years. *Science,* 289(5477), pp. 270-277. DOI: 10.1126/science.289.5477.270.

DESIGN INSTITUTE FOR PHYSICAL PROPERTIES, 2014. *DIPPR Project 801 - Full Version.* Design Institute for Physical Property Research/AIChE.

Dieck, R.H., 2007. Unit 7. Applied Considerations. *Measurement Uncertainty - Methods and Applications (4th Edition).* Fourth edition. United States of America: ISA, pp. 169-171.

DiGuilio, R.M., Lee, R.J., Schaeffer, S.T., Brasher, L.L. and Teja, A.S., 1992. Densities and Viscosities of the Ethanolamines. *J. Chem. Eng. Data,* 37(2), pp. 239-242. DOI: 10.1021/je00006a028.

Donaldson, T.L. and Nguyen, Y.N., 1980. Carbon dioxide reaction kinetics and transport in aqueous amine membranes. *Ind. Eng. Chem. Fundamen.,* 19(3), pp. 260-266. DOI: 10.1021/i160075a005.

EPA, 2014. Carbon Dioxide Emissions. *United States Environmental Protection Agency,* [2.6.2014]. Available : http://www.epa.gov/climatechange/ghgemissions/gases/co2.html.

EPA, 1995. Chapter 5.3: Natural Gas Processing. *AP 42, Compilation of Air Pollutant Emission Factors, Volume 1: Stationary Point and Area Sources.* Fifth edition. United States: Environmental Protection Agency, Office of Air Quality Planning and Standards

EUROPEAN COMMISSION, 2009. *COMMISSION DIRECTIVE 2009/161/EU of 17 December 2009 establishing a third list of indicative occupational exposure limit values in implementation of Council Directive 98/24/EC and amending Commission Directive 2000/39/EC.* Directive edition. European Union.2009/161/EU.

Falkowski, P., Scholes, R.J., Boyle, E., Canadell, J., Canfield, D., Elser, J., Gruber, N., Hibbard, K., Högberg, P., Linder, S., Mackenzie, F.T., Moore III, B., Pedersen, T., Rosenthal, Y., Seitzinger, S., Smetacek, V. and Steffen, W., 2000. The Global Carbon Cycle: A Test of Our Knowledge of Earth as a System. *Science,* 290(5490), pp. 291-296. DOI: 10.1126/science.290.5490.291.

Ferrando, N., Mougin, P., Defiolle, D. and Vermesse, H., 2008. Absorption of H_2S and CO_2 in Alkanolamine Aqueous Solution: Experimental Data and Modelling with the Electrolyte-NRTL Model. *Oil & Gas Science and Technology,* 63(3), pp. 343-351. DOI: 10.2516/ogst:2008009.

Geankoplis, C.J., 2008. Stage and Continous Gas-Liquid Separation Processes. *Transport Processes and Spearation Process Principles.* Fourth edition. United States: Pearson Education LTD, pp. 625-696.

Glasscock, D.A., 1990. *Modeling and experimental study of carbom dioxide absorption into aqueous alkanolamines*, The University of Texas. Austin.

Godini, H.R. and Mowla, D., 2008. Selectivity study of H_2S and CO_2 absorption from gaseous mixtures by MEA in packed beds. *Chemical Engineering Research and Design,* 86(4), pp. 401-409. DOI: DOI: 10.1016/j.cherd.2007.11.012.

Haimour, N. and Sandall, O.C., 1987. Absorption of H_2S into Aqueous Methydiethanolamine. *Chemical Engineering Communications,* 59(1-6), pp. 85-93.

Hartono, A., Saleem, F., Arshad, M.W., Usman, M. and Svendsen, H.F., 2013. Binary and ternary VLE of the 2-(diethylamino)-ethanol (DEEA)/3-(methylamino)-propylamine (MAPA)/water system. *Chemical Engineering Science,* 101, pp. 401-411. DOI: 10.1016/j.ces.2013.06.052.

Hartono, A. and Svendsen, H.F., 2009. Kinetics reaction of primary and secondary amine group in aqueous solution of diethylenetriamine (DETA) with carbon dioxide. *Energy Procedia,* 1(1), pp. 853-859. DOI: 10.1016/j.egypro.2009.01.113.

Kamps, A.P., Balaban, A., Jödecke, M., Kuranov, G., Smirnova, N.A. and Maurer, G., 2001. Solubility of Single Gases Carbon Dioxide and Hydrogen Sulfide in Aqueous Solutions of N-Methyldiethanolamine at Temperatures from 313 to 393 K and Pressures up to 7.6 MPa: New Experimental Data and Model Extension. *Ind. Eng. Chem. Res.,* 40(2), pp. 696-706. DOI: 10.1021/ie000441r.

Kennard, M.L. and Meisen, A., 1984. Solubility of carbon dioxide in aqueous diethanolamine solutions at elevated temperatures and pressures. *J. Chem. Eng. Data,* 29(3), pp. 309-312. DOI: 10.1021/je00037a025.

Kent, R.L. and Eisenberg, B., 1976. Better data for amine treating. *Hydrocarbon Processing,* 55(2), pp. 87-90.

Ko, J. and Li, M., 2000. Kinetics of absorption of carbon dioxide into solutions of N-methyldiethanolamine+water. *Chemical Engineering Science,* 55(19), pp. 4139-4147. ISSN: 0009-2509. DOI: http://dx.doi.org/10.1016/S0009-2509(00)00079-8.

Kohl, A.L. and Nielsen, R.B., 1997. 2. Alkanolamines for Hydrogen Sulfide and Carbon Dioxide Removal. *Gas Purification.* 5th Edition edition. Gulf Professional Publishing, pp. 41-174.

Kriebel, M., 2008. Absorption, 2. Design of Systems and Equipment. *Ullmann's Encyclopedia of Industrial Chemistry.* Weinheim: Wiley-VCH Verlag GmbH & Co. KGaA, .

Liao, C.-., Leron, R.B. and Li, M., 2014. Mutual diffusion coefficients, density, and viscosity of aqueous solutions of new polyamine CO_2 absorbents. *Fluid Phase Equilibria,* 363, pp. 180-188. ISSN: 0378-3812. DOI: 10.1016/j.fluid.2013.11.028.

Liebenthal, U., Pinto, D.D.D., Monteiro, J.G.M.-., Svendsen, H.F. and Kather, A., 2013. Overall Process Analysis and Optimisation for CO_2 Capture from Coal Fired Power Plants based on Phase Change Solvents Forming Two Liquid Phases. *Energy Procedia,* 37, pp. 1844-1854. DOI: 10.1016/j.egypro.2013.06.064.

Liss, P.S. and Slater, P.G., 1974. Flux of Gases across the Air-Sea Interface. *Nature,* 247, pp. 181-184. DOI: 10.1038/247181a0.

Mandal, M. and Bandyopadhyay, S.S., 2006. Simultaneous absorption of CO_2 and H_2S into aqueous blends of N-methyldiethanolamine and diethanolamine. *Environ. Sci. Technol.,* 40(19), pp. 6076-6084. DOI: 10.1021/es0606475.

Mazloumi, S.H., Haghtalab, A., Jalili, A.H. and Shokouhi, M., 2012. Solubility of H_2S in Aqueous Diisopropanolamine + Piperazine Solutions: New Experimental Data and Modeling with the Electrolyte Cubic Square-Well Equation of State. *J. Chem. Eng. Data,* 57(10), pp. 2625-2631. DOI: 10.1021/je2005243.

MDH, 2013. Carbon Dioxide (CO_2). *Minnesota Department of Health,* [2.6.2014]. Available : http://www.health.state.mn.us/divs/eh/indoorair/co2/.

Monteiro, J.G.M.-., Pinto, D.D.D., Luo, X., Knuutila, H., Hussain, S., Mba, E., Hartono, A. and Svendsen, H.F., 2013b. Activity-based Kinetics of the Reaction of Carbon Dioxide with Aqueous Amine Systems. Case Studies: MAPA and MEA. *Energy Procedia,* 37, pp. 1888-1896. DOI: 10.1016/j.egypro.2013.06.069.

Monteiro, J.G.M.-., Pinto, D.D.D., Zaidy, S.A.H., Hartono, A. and Svendsen, H.F., 2013a. VLE data and modelling of aqueous N,N-diethylethanolamine (DEEA) solutions. *International Journal of Greenhouse Gas Control,* 19, pp. 432-440. DOI: 10.1016/j.ijggc.2013.10.001.

OSHA, 2005. OSHA Fact Sheet, Hydrogen Sulfide. *Occupational Safety and Health Administration,* [23.5.2014]. Available : https://www.osha.gov/OshDoc/data_Hurricane_Facts/hydrogen_sulfide_fact.pdf.

Pacheco, M.A. and Rochelle, G.T., 1998. Rate-Based Modeling of Reactive Absorption of CO_2 and H_2S into Aqueous Methyldiethanolamine. *Ind. Eng. Chem. Res.,* 37(10), pp. 4107-4117. DOI: 10.1021/ie980123g.

Pani, F., Gaunand, A., Cadours, R., Bouallou, C. and Richon, D., 1997a. Kinetics of Absorption of CO_2 in Concentrated Aqueous Methyldiethanolamine Solutions in the Range 296 K to 343 K. *J. Chem. Eng. Data,* 42(2), pp. 353-359. DOI: 10.1021/je960251g.

Pani, F., Gaunand, A., Richon, D., Cadours, R. and Bouallou, C., 1997b. Absorption of H_2S by an Aqueous Methyldiethanolamine Solution at 296 and 343K. *J. Chem. Eng. Data,* 42(5), pp. 865-870. DOI: 10.1021/je970062d.

Pinto, D.D.D., Monteiro, J.G.M.-., Johansen, B., Svendsen, H.F. and Knuutila, H., 2014a. Density measurements and modelling of loaded and unloaded aqueous solutions of MDEA (N-methyldiethanolamine), DMEA (N,N-dimethylethanolamine), DEEA (diethylethanolamine) and MAPA (N-methyl-1,3-diaminopropane). *International Journal of Greenhouse Gas Control,* 25, pp. 173-185. DOI: 10.1016/j.ijggc.2014.04.017.

Pinto, D.D.D., Zaidy, S.A.H., Hartono, A. and Svendsen, H.F., 2014b. Evaluation of a phase change solvent for CO_2 capture: Absorption and desorption tests. *International Journal of Greenhouse Gas Control,* 28, pp. 318-327. DOI: 10.1016/j.ijggc.2014.07.002.

Raynal, L., Alix, P., Bouillon, P., Gomez, A., le Febvre de Nailly, M., Jacquin, M., Kittel, J., di Lella, A. and Mougin, P.T.,J., 2011. The DMX™ process: An original solution for lowering the cost of post-combustion carbon capture. *Energy Procedia,* 4, pp. 779-786. DOI: 10.1016/j.egypro.2011.01.119.

Rinker, E.B. and Sandall, O.C., 2000. Physical solubility of hydrogen sulfide in several aqueous solvents. *The Canadian Journal of Chemical Engineering,* 78(1), pp. 232-235. DOI: 10.1002/cjce.5450780130.

Rinker, E.B., Sami, S.A. and Sandall, O.C., 1995. Kinetics and modelling of carbon dioxide absorption into aqueous solutions of N-methyldiethanolamine. *Chemical Engineering Science,* 50(5), pp. 755-768. ISSN: 0009-2509. DOI: http://dx.doi.org/10.1016/0009-2509(94)00444-V.

Santa Cruz Biotechnology, I., 2014. 3-(Methylamino)propylamine (CAS 6291-84-5). *Santa Cruz Biotechnology, Inc.,* [28.5.2014]. Available : http://www.scbt.com/datasheet-256422-3-methylaminopropylamine.html.

Seo, D.J. and Hong, W.H., 2000. Effect of Piperazine on the Kinetics of Carbon Dioxide with Aqueous Solutions of 2-Amino-2-methyl-1-propanol. *Ind. Eng. Chem. Res.,* 39(6), pp. 2062-2067. DOI: 10.1021/ie990846f.

Sigma-Aldrich Co. LLC., 2014b. 2-(Diethylamino)ethanol. *Sigma-Aldrich Co. LLC.,* [23.5.2014]. Available: http://www.sigmaaldrich.com/catalog/product/aldrich/471321.

Sigma-Aldrich Co. LLC., 2014a. N-Methyldiethanolamine. *Sigma-Aldrich Co. LLC.,* [13.6.2014]. Available: http://www.sigmaaldrich.com/catalog/product/aldrich/471828.

Snijder, E.D., te Riele, M.J.M., Versteeg, G.F. and van Swaaij, W.P.M., 1993. Diffusion coefficients of several aqueous alkanolamine solutions. *J. Chem. Eng. Data,* 38(3), pp. 475-480. DOI: 10.1021/je00011a037.

Solomon, S., Plattner, G., Knutti, R. and Friedlingstein, P., 2009. Irreversible climate change due to carbon dioxide emissions. *Proceedings of the National Academy of Sciences of the United States of America,* 106(6), pp. 1704-1709. DOI: 10.1073/pnas.0812721106.

Sutar, P.N., Vaidya, P.D. and Kenig, E.Y., 2013. Activated DEEA solutions for CO_2 capture - A study of equilibrium and kinetic characteristics. *Chemical Engineering Science,* 100, pp. 234-241. DOI: 10.1016/j.ces.2012.11.038.

Sweeney, A., 2014. *Monthly Energy Review.* United States: Total Energy Experts.

Tamimi, A., Rinker, E.B. and Sandall, O.C., 1994. Diffusion Coefficients for Hydrogen Sulfide, Carbon Dioxide, and Nitrous Oxide in Water over the Temperature Range 293-368 K. *J. Chem. Eng. Data,* 39(2), pp. 330-332. DOI: 10.1021/je00014a031.

TGM, 2010. Amine Technology. *Technology Center Mongstad,* [4.9.2014]. Available: http://www.tcmda.com/en/Technology/Amine-technology/.

U.S. Energy Information Administration, 2014. U.S. Sulfur Content of Crude Oil Input to Refineries. *U.S. Energy Information Administration,* [23.5.2014]. Available: http://www.eia.gov/dnav/pet/hist/LeafHandler.ashx?n=PET&s=MCRS1US2&f=A.

Vaidya, P.D. and Kenig, E.Y., 2007a. Gas-liquid reaction kinetics: A review of determination methods. *Chemical engineering communications,* 194(12), pp. 1543-1565. ISSN: 0098-6445. DOI: 10.1080/00986440701518314.

Vaidya, P.D. and Kenig, E.Y., 2007b. Reactive Absorption of CO_2 into Aqueous Solutions of N-N,Diethylethanolamine. *Chemical Engineering Transactions,* 12, pp. 73-78. ISSN: 88-901915-4-6.

van Krevelen, D.W. and Hoftijzer, P.J., 1948. Sur la solubilité des gaz dans les solutions aqueuses, *Chimie et industrie: numéro spécial du XXIe Congrés International de Chimie Industrielle* 1948, Brussels, s. 168-173.

Versteeg, G.F. and Swaaij, W.V., 1988. Solubility and diffusivity of acid gases (carbon dioxide, nitrous oxide) in aqueous alkanolamine solutions. *J. Chem. Eng. Data,* 33(1), pp. 29-34. DOI: 10.1021/je00051a011.

Versteeg, G.F. and van Swaaij, W.P.M., 1988. On the kinetics between CO2 and alkanolamines both in aqueous and non-aqueous solutions—II. Tertiary amines. *Chemical Engineering Science,* 43(3), pp. 587-591. ISSN: 0009-2509. DOI: http://dx.doi.org/10.1016/0009-2509(88)87018-0.

Voice, A.K., Vevelstad, S.J., Chen, X., Nguyen, T. and Rochelle, G.T., 2013. Aqueous 3-(methylamino)propylamine for CO_2 capture. *International Journal of Greenhouse Gas Control,* 15, pp. 70-77. DOI: 10.1016/j.ijggc.2013.01.045.

Wang, X., Kang, K., Wang, W. and Tian, Y., 2013. Volumetric Properties of Binary Mixtures of 3-(Methylamino)propylamine with Water, *N*-Methyldiethanolamine, *N*,*N*-Dimethylethanolamine, and *N*,*N*-Diethylethanolamine from (283.15 to 363.15) K. *J. Chem. Eng. Data,* 58(12), pp. 3430-3439. DOI: 10.1021/je400679k.

Weil, E.D., Sandler, S.R. and Gernon, M., 2006. Sulfur Compounds. *Kirk-Othmer Encyclopedia of Chemical Technology.* 5 edition. John Wiley and Sons, Inc, pp. 9-16.

Weiland, R.H., Chakravarty, T. and Mather, A.E., 1993. Solubility of carbon dioxide and hydrogen sulfide in aqueous alkanolamines. *Ind. Eng. Chem. Res.,* 32(7), pp. 1419-1430. DOI: 10.1021/ie00019a016.

WHO, Edited: F. Theakston, 2000. Chapter 6.6 - Hydrogen Sulfide. *Air Quality Guidelines.* 2nd edition. Copenhagen, Denmark: WHO Regional Office for Europe, pp. 1-7.

Appendix A. Calibration data for the PT1 UNIK 5000 sensor

Calibration data for the Channel 21 pressure transducer, PT1, UNIK 5000 transducer with the serial number 4143746, is shown in Table A - 1. The data is shown also in Figure A - 1. The correlation between obtained mA vs Pa data is shown in Table A - 2 and in equation (A - 1).

Table A - 1. Calibration dataset for PT1

P(Beamex)	*mA(GFT)*	*P(Beamex)*	*mA(GFT)*
440	4.077	51485	7.347
440	4.076	52980	7.444
520	4.082	55355	7.596
530	4.082	57640	7.742
1160	4.122	61215	7.971
2040	4.178	63860	8.141
3120	4.248	66780	8.329
3980	4.303	69795	8.521
5150	4.378	74550	8.826
6020	4.434	78770	9.096
6950	4.493	81660	9.282
8110	4.567	85550	9.531
9900	4.682	89480	9.782
9900	4.682	92730	9.991
10830	4.742	94430	10.100
13940	4.940	97590	10.303
15330	5.030	100020	10.459
18170	5.212	114510	11.387
20950	5.390	126850	12.178
24070	5.590	136140	12.772
26720	5.760	144180	13.288
28920	5.901	156100	14.052
31770	6.084	164980	14.621
35280	6.308	176720	15.372
39190	6.559	185510	15.936
41950	6.736	194200	16.492
44820	6.920	205420	17.211
48580	7.162	215590	17.862

Appendix A. Calibration data for the PT1 UNIK 5000 sensor

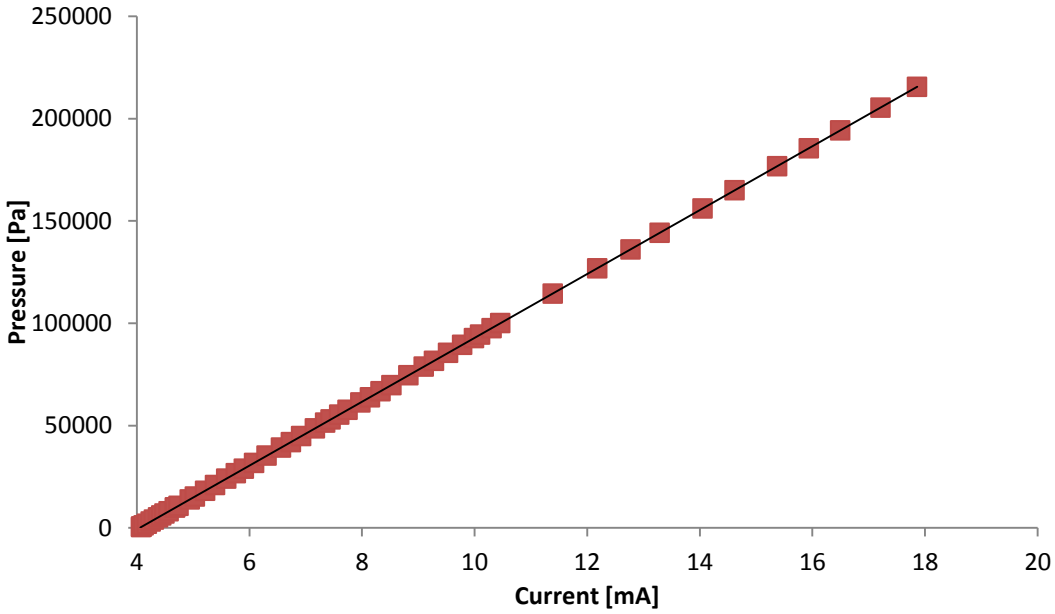

Figure A - 1. Calibration dataset for PT1

Table A - 2. Correlation data for PT1

	CH21 nr 4143746
Slope	15604.7
Intercept	-63168.1
RSQ	1

$$(Pa)_{GFT} = 15604.6 * I(mA)_{PT1} - 63167.5 \quad \text{(A - 1)}$$

Maximum error between the measured pressure values and model was 0.0121 Pa, which was calculated for the first measurement point at 440 Pa. The data points themselves have a maximum error of ±150 Pa.

Appendix B. Calibration data for the PT2 UNIK 5000 sensor

Calibration data for the Channel 22 pressure transducer, PT2, a UNIK 5000 transducer with serial number 4178684, is shown in Table B - 1. The data is shown also in Figure B - 1. The correlation between obtained mA vs Pa data is shown in Table B - 2 and in equation (B - 1).

Table B - 1. Calibration data for PT2

P(Beamex)	*mA(CELL)*	*P(Beamex)*	*mA(CELL)*
670	4.049	59600	7.827
660	4.049	59610	7.828
15800	5.017	59610	7.828
15870	5.021	66520	8.271
15970	5.028	66650	8.279
15990	5.029	66720	8.284
16000	5.030	66740	8.285
18850	5.213	74480	8.782
19000	5.222	74640	8.791
19180	5.233	74770	8.elo
19250	5.238	74790	8.801
19310	5.242	78880	9.063
19340	5.244	79090	9.077
21850	5.406	79170	9.082
22080	5.420	83790	9.378
22170	5.425	84100	9.397
22220	5.429	84090	9.397
29090	5.868	87480	9.614
29180	5.874	87600	9.622
29250	5.879	87710	9.629
36300	6.332	91710	9.886
36320	6.333	91850	9.894
36320	6.334	91870	9.896
40900	6.627	95280	10.115
41050	6.636	95570	10.133
41170	6.645	98500	10.321
47030	7.030	98590	10.327
47200	7.031	98630	10.329
47410	7.045	99970	10.416
47410	7.046	100120	10.425

Appendix B. Calibration data for the PT2 UNIK 5000 sensor

53900	7.461
54610	7.507
54710	7.513
59590	7.826

100220	10.431
100360	10.440
100380	10.442
100390	10.442

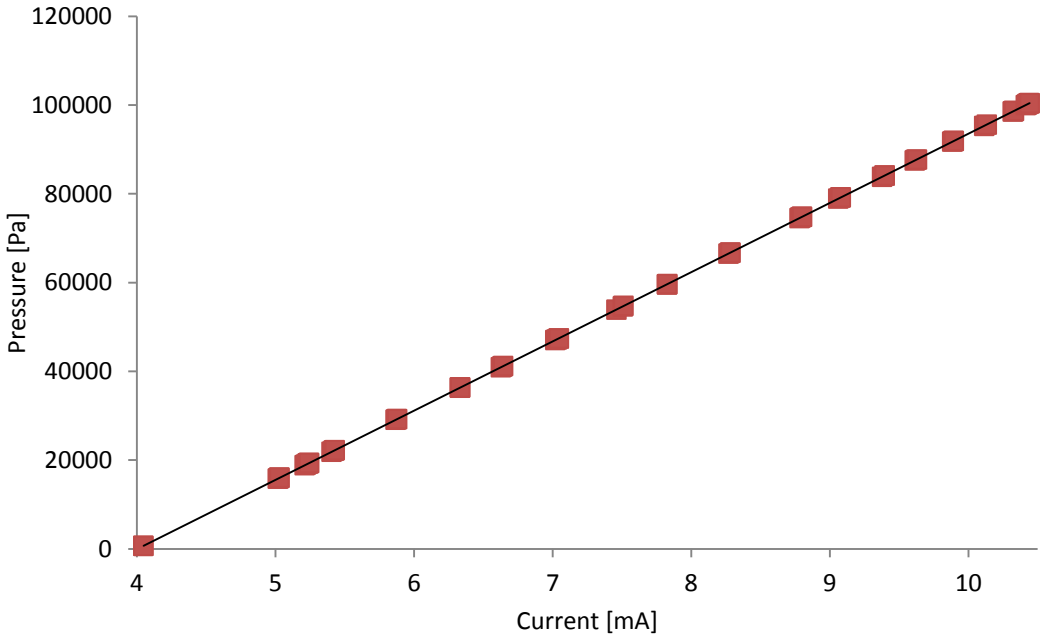

Figure B - 1. Calibration dataset for PT2

Table B - 2. Correlation data for PT2

	CH22 / nr 4178684
Slope	15592.3
Intercept	-62432.1
RSQ	1

$$(Pa)_{Cell} = 15592.3 * I(mA)_{PT2} - 62432.1 \quad \text{(B - 1)}$$

Maximum error between the measured pressure values and model was 0.051 Pa, which was calculated for the first measurement point at 670 Pa. The data points themselves have a maximum error of ±150 Pa.

Appendix C. Calibration data for PT100 units TT1 and TT2

The temperature probes were calibrated against a PT100 probe calibrated by the Centre for Metrology and Accreditation in Finland. The obtained temperature dataset is shown in Table C - 1. The dataset is also shown in Figure C - 1. The correlations for TT1 and TT2 are shown in Table C - 2 and in equations (C - 1) and (C - 2).

Table C - 1. Calibration dataset for TT1 and TT2

Calibrated Unit [K]	*TT1 [K]*	*TT2 [K]*	*Calibrated Unit [K]*	*TT1 [K]*	*TT2 [K]*
273.25	273.21	274.15	291.06	291.18	292.19
273.25	273.21	274.15	291.11	291.22	292.23
273.26	273.24	274.18	291.23	291.34	292.35
273.32	273.23	274.16	291.35	291.46	292.47
273.33	273.23	274.17	291.61	291.73	292.73
274.40	274.37	275.36	294.08	294.12	295.15
278.44	278.01	279.28	295.71	295.85	296.83
278.66	278.46	279.70	295.83	295.91	296.90
279.26	279.18	280.23	296.27	296.46	297.43
279.54	279.54	280.54	296.87	297.09	298.05
280.50	280.76	281.53	297.31	297.39	298.40
280.77	281.05	281.80	297.59	297.63	298.69
281.01	281.31	282.04	304.71	305.23	306.18
281.68	282.01	282.71	305.12	305.09	306.11
283.83	284.20	284.87	305.78	305.76	306.76
284.23	284.58	285.26	305.82	306.86	307.76
286.25	286.41	287.38	306.23	306.27	307.27
286.34	286.51	287.47	306.85	306.86	307.87
287.87	288.04	289.03	307.62	307.63	308.62
287.99	288.16	289.16	309.10	309.05	310.10
288.06	288.22	289.22	310.61	310.54	311.63
288.25	288.41	289.40	312.73	312.73	313.77
288.86	289.00	290.01	314.62	314.66	315.70
289.00	289.13	290.14	317.05	317.02	318.11
289.08	289.22	290.23	322.17	322.22	323.21
289.21	289.34	290.35	323.80	323.93	324.84
289.40	289.52	290.53	334.27	334.47	335.28
289.48	289.60	290.62	346.08	346.51	347.15
290.70	290.80	291.81	348.46	348.96	349.45
290.75	290.87	291.88	351.69	352.06	352.78
290.83	290.94	291.96	354.87	355.19	356.21
290.94	291.05	292.07			

Appendix C. Calibration data for PT100 units TT1 and TT2

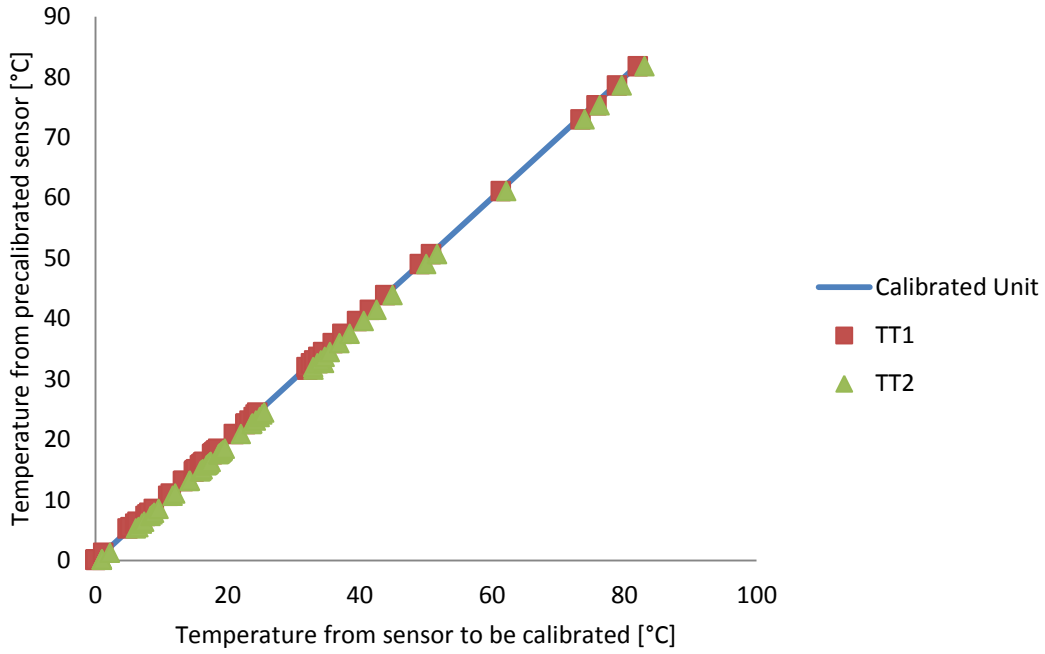

Figure C - 1. Calibration of temperature sensors

Table C - 2. Calibration data for TT1 and TT2

	Slope	*Intercept*
TT1	0.996	0.954
TT2	0.998	-0.564

$$T(K)_{TT1} = 0.996 * T(K) + 0.954 \quad \text{(C - 1)}$$

$$T(K)_{TT2} = 0.998 * T(K) - 0.564 \quad \text{(C - 2)}$$

Appendix D. Calibration data for the Huba Control pressure transducer

Calibration data for the Huba Control pressure transducer (Model number 692.919007141) is shown in Table D - 1. The data is shown also in Figure D - 1. The calibration was done against room pressure. Room pressure at calibration time was 99840 Pa. The correlation between obtained mA vs Pa data is shown in Table D - 2 and in equation (D - 1).

Table D - 1. Calibration data for PT1 / Huba Control

PT3 *[mA]*	P_{Beamex} *[Pa]*
15.137	420100
14.476	395600
13.597	362300
12.732	329300
11.644	288700
10.885	259700
9.906	223200
9.135	193900
8.373	164700
7.433	129300
6.753	103400
5.859	70100
5.005	37700
4.471	17900
4.107	3700
4.015	200

Appendix D. Calibration data for the Huba Control pressure transducer

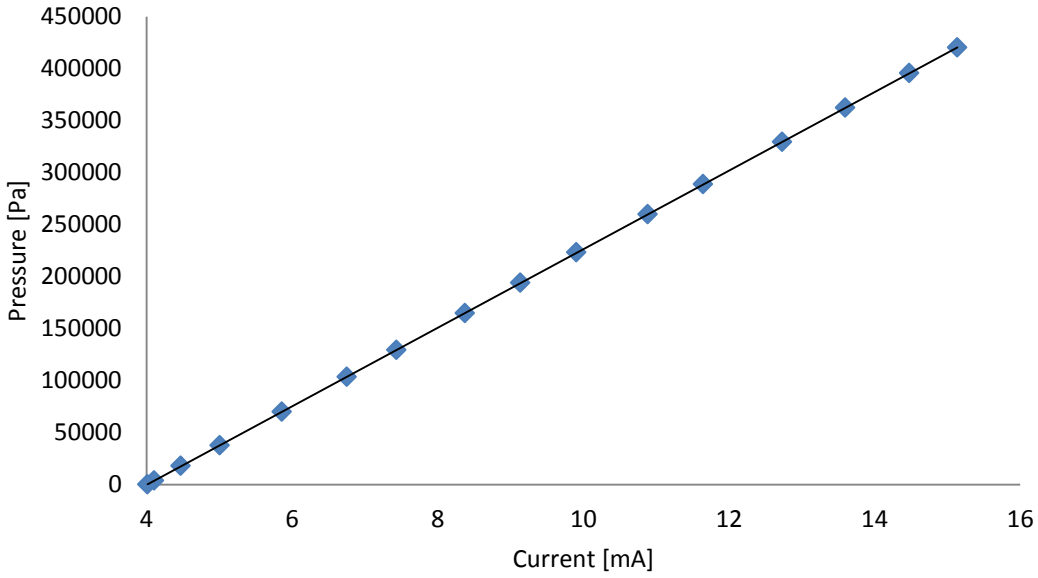

Figure D - 1. Calibration data for PT1 / Huba Control

Table D - 2. Correlation data for PT1 / Huba Control

	Intercept	*Slope*	*RSQ*
CH21 / 926.919007141	-151291	37766.36	0.999997

$$(\mathrm{Pa})_{\mathrm{GFT}} = 37766.36 * \mathrm{I}(\mathrm{mA})_{\mathrm{PT1,Huba}} - 151291 \qquad \text{(D - 1)}$$

Maximum error between the measured pressure values and model was 0.633 Pa, which was calculated for the first measurement point at 200 Pa. The data points themselves have a maximum error of ±150 Pa.

Appendix E. Calibration data for Trafag NAH 6A series pressure transducer

Calibration data for the Trafag NAH 6A series pressure transducer (Serial number 387694-001) is shown in Table E - 1. The data is shown also in Figure E - 1. The calibration was done against room pressure. Room pressure at calibration time was 101190 Pa. The correlation between obtained mA vs Pa data is shown in Table E - 2 and in equation (E - 1).

Table E - 1. Calibration data for Trafag NAH 6A

P(Beamex) [Pa]	*PT1 [mA]*
524000	17.921
498100	17.234
469200	16.462
425500	15.296
425400	15.297
356450	13.459
308700	12.186
259300	10.868
236200	10.251
190450	9.030
151150	7.980
131700	7.461
103200	6.700
76600	5.988
52200	5.336
32700	4.815
16800	4.393
6300	4.113
1800	3.993

Appendix E. Calibration data for Trafag NAH 6A series pressure transducer

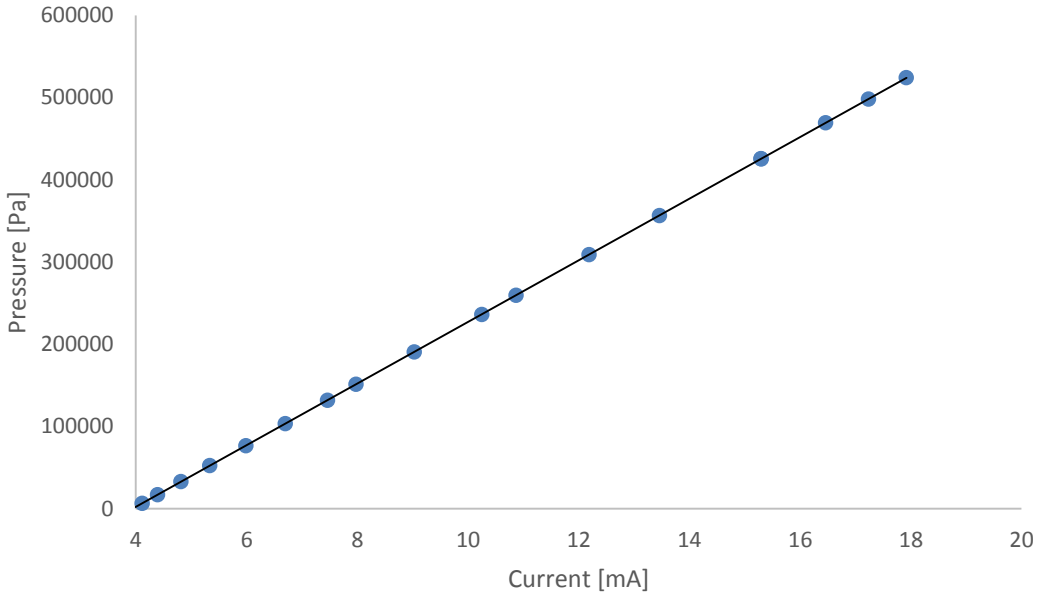

Figure E - 1. Calibration data for Trafag NAH 6A

Table E - 2. Correlation data for Trafag NAH 6A

Intercept	*Slope*	*RSQ*
-147901	37481.5	1

$$(\mathrm{Pa})_{\mathrm{GFT}} = 37481.5 * \mathrm{I(mA)}_{\mathrm{PT1,Trafag}} - 147901 \qquad \text{(E - 1)}$$

Maximum error between the measured pressure values and model was 0.021 Pa, which was calculated for the first measurement point at 1800 Pa. The data points themselves have a maximum error of ±150 Pa.

Appendix F. Gas Feed Tank volume measurements

Gas tank volume was measured eight times. First two tests were done with a 50 ml Isco-pump and the other 6 were done with a 500 ml Isco-pump. The standard error and deviation determination method of Thompson Tau was used to determine which measurements to discard. Four measurement sets were found to be in error and were discarded. Standard error for the volume was calculated and the result is shown below in Table F - 1.

Table F - 1. Gas Feeding Tank volume measurements

Gas Feeding Tank volume							
(V2->V4) : Isco-pump feeding with 10 ml/min until 20 ml left -> then 5ml/min until 5ml left -> then 1ml/min							
Measurement 1 (Disqualified)		Measurement 2 (Disqualified)		Measurement 3 (Disqualified)		Measurement 4	
Distilled water (Isco 100DM)		Distilled water (Isco 100DM)		Degassed water (Isco 100DM)		Degassed water (Isco 260D)	
V1 [cm^3]	102.4	V1 [cm^3]	102.45	V1 [cm^3]	102.39	V1 [cm^3]	506.32
V2 [cm^3]	20.51	V2 [cm^3]	37.69	V2 [cm^3]	17.43	V2 [cm^3]	345.75
V3 [cm^3]	103.06	V3 [cm^3]	103.06	V3 [cm^3]	103.06	V3 [cm^3]	
V4 [cm^3]	36.56	V4 [cm^3]	55.29	V4 [cm^3]	27.14	V4 [cm^3]	
V5 [cm^3]	80.6	V5 [cm^3]	103.06	V5 [cm^3]		V5 [cm^3]	
V6 [cm^3]	64.03	V6 [cm^3]	54.58	V6 [cm^3]		V6 [cm^3]	
Volume [cm^3]	164.96	Volume [cm^3]	161.01	Volume [cm^3]	160.88	Volume [cm^3]	160.57
Measurement 5 (Disqualified)		Measurement 6		Measurement 7		Measurement 8	
Degassed water (Isco 260D), Leak		Degassed water (Isco 260D)		Degassed water (Isco 260D),		Degassed water (Isco 260D),	
V1 [cm^3]	504.99	V1 [cm^3]	506.43	V1 [cm^3]	506.37	V1 [cm^3]	506.4
V2 [cm^3]	343.62	V2 [cm^3]	345.86	V2 [cm^3]	345.71	V2 [cm^3]	345.87
V3 [cm^3]		V3 [cm^3]		V3 [cm^3]		V3 [cm^3]	
V4 [cm^3]		V4 [cm^3]		V4 [cm^3]		V4 [cm^3]	
V5 [cm^3]		V5 [cm^3]		V5 [cm^3]		V5 [cm^3]	
V6 [cm^3]		V6 [cm^3]		V6 [cm^3]		V6 [cm^3]	
Volume [cm^3]	161.37	Volume [cm^3]	160.57	Volume [cm^3]	160.66	Volume [cm^3]	160.53
Average volume for the tank				160.5825 ± 0.24834			cm^3
Average volume for the tank				0.0001605825 ± 0.00000024834			m^3

After the change of pressure transducer from UNIK 5000 to the Trafag unit, the volume of GFT was measured again using a previously determined 25 ml gas bomb and a high pressure. The gas was released from the bomb to the GFT and the pressure change from initial to final was logged. This allowed us to determine the volume of GFT very accurately. Measurement setup can be seen in Figure F - 1.

Appendix F. Gas Feed Tank volume measurements

Measurements were repeated 9 times and the measurement results are available in Table F - 2.

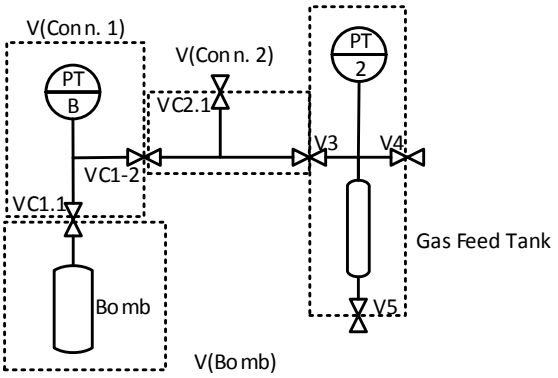

Figure F - 1. GFT volume measurement through Gas Pressure

Table F - 2. Gas based volume measurement for GFT, C1 and C2 denote connections 1 and 2 as seen in Figure F - 1

Measurement 1 with gas		Measurement 2 with gas		Measurement 3 with gas	
P(1) [Pa]	801400	P(1) [Pa]	800600	P(1) [Pa]	800800
P(2) [Pa]	6800	P(2) [Pa]	6200	P(2) [Pa]	3000
P(3) [Pa]	74600	P(3) [Pa]	745600	P(3) [Pa]	746400
P(4) [Pa]	725600	P(4) [Pa]	725300	P(4) [Pa]	826200
P(5) [Pa]	111400	P(5) [Pa]	111100	P(5) [Pa]	111300
V(BOMB) [$\cdot 10^{-4}$ m^3]	0.2507	V(BOMB) [$\cdot 10^{-4}$ m^3]	0.2507	V(BOMB) [$\cdot 10^{-4}$ m^3]	0.2507
V(B+C1) [$\cdot 10^{-5}$ m^3]	2.93814	V(B+C1) [$\cdot 10^{-5}$ m^3]	2.69348	V(B+C1) [$\cdot 10^{-5}$ m^3]	2.69046
V(B+C1+C2) [$\cdot 10^{-5}$ m^3]	2.77137	V(B+C1+C2) [$\cdot 10^{-5}$ m^3]	2.76952	V(B+C1+C2) [$\cdot 10^{-5}$ m^3]	2.42965
V(B+C1&2+GFT) [$\cdot 10^{-4}$ m^3]	1.90446	V(B+C1&2+GFT) [$\cdot 10^{-4}$ m^3]	1.89853	V(B+C1&2+GFT) [$\cdot 10^{-4}$ m^3]	1.8468
V(GFT) [$\cdot 10^{-4}$ m^3]	1.62732	V(GFT) [$\cdot 10^{-4}$ m^3]	1.62158	V(GFT) [m^3]	1.60384
Measurement 4 with gas		**Measurement 5 with gas**		**Measurement 6 with gas**	
P(1) [Pa]	800200	P(1) [Pa]	800000	P(1) [Pa]	802800
P(2) [Pa]	6600	P(2) [Pa]	7100	P(2) [Pa]	7100
P(3) [Pa]	746400	P(3) [Pa]	746400	P(3) [Pa]	749000
P(4) [Pa]	726200	P(4) [Pa]	726300	P(4) [Pa]	728800
P(5) [Pa]	111200	P(5) [Pa]	112400	P(5) [Pa]	112800
V(BOMB) [$\cdot 10^{-4}$ m^3]	0.2507	V(BOMB) [$\cdot 10^{-4}$ m^3]	0.2507	V(BOMB) [$\cdot 10^{-4}$ m^3]	0.2507
V(B+C1) [$\cdot 10^{-5}$ m^3]	2.68931	V(B+C1) [$\cdot 10^{-5}$ m^3]	2.68876	V(B+C1) [$\cdot 10^{-5}$ m^3]	2.6888
V(B+C1+C2) [$\cdot 10^{-5}$ m^3]	2.76481	V(B+C1+C2) [$\cdot 10^{-5}$ m^3]	2.7639	V(B+C1+C2) [$\cdot 10^{-5}$ m^3]	2.76406
V(B+C1&2+GFT) [$\cdot 10^{-4}$ m^3]	1.90206	V(B+C1&2+GFT) [$\cdot 10^{-4}$ m^3]	1.88775	V(B+C1&2+GFT) [$\cdot 10^{-4}$ m^3]	1.88725
V(GFT) [$\cdot 10^{-4}$ m^3]	1.62558	V(GFT) [$\cdot 10^{-4}$ m^3]	1.61136	V(GFT) [$\cdot 10^{-4}$ m^3]	1.61084

Appendix F. Gas Feed Tank volume measurements

Measurement 7 with gas		Measurement 8 with gas		Measurement 9 with gas	
P(1) [Pa]	813400	P(1) [Pa]	812200	P(1) [Pa]	804700
P(2) [Pa]	5700	P(2) [Pa]	6600	P(2) [Pa]	7700
P(3) [Pa]	758400	P(3) [Pa]	757400	P(3) [Pa]	750800
P(4) [Pa]	737900	P(4) [Pa]	737000	P(4) [Pa]	730400
P(5) [Pa]	112800	P(5) [Pa]	113400	P(5) [Pa]	113200
V(BOMB) [$\cdot 10^{-4}$ m^3]	0.2507	V(BOMB) [$\cdot 10^{-4}$ m^3]	0.2507	V(BOMB) [$\cdot 10^{-4}$ m^3]	0.2507
V(B+C1) [$\cdot 10^{-5}$ m^3]	2.69019	V(B+C1) [$\cdot 10^{-5}$ m^3]	2.68998	V(B+C1) [$\cdot 10^{-5}$ m^3]	2.68884
V(B+C1+C2) [$\cdot 10^{-5}$ m^3]	2.76551	V(B+C1+C2) [$\cdot 10^{-5}$ m^3]	2.76511	V(B+C1+C2) [$\cdot 10^{-5}$ m^3]	2.76474
V(B+C1&2+GFT) [$\cdot 10^{-4}$ m^3]	1.89067	V(B+C1&2+GFT) [$\cdot 10^{-4}$ m^3]	1.89105	V(B+C1&2+GFT) [$\cdot 10^{-4}$ m^3]	1.89391
V(GFT) [$\cdot 10^{-4}$ m^3]	1.61412	V(GFT) [$\cdot 10^{-4}$ m^3]	1.61454	V(GFT) [$\cdot 10^{-4}$ m^3]	1.61744

The volume was calculated to be 161.6 ml ± 0.6 ml.

Appendix G. Measurement Cell volume measurements

Cell volume was measured three times using liquid. The tests were done with a 500 ml Isco-pump. The standard error and deviation determination method of Thompson Tau was used to determine which measurements to discard. The measurements were found not to deviate too much from each other and they were all found to meet the Thompson Tau test. Measurement data is available in Table G - 1.

Table G - 1. Cell Volume measurements using liquid

Cell Volume						
Fed with 5ml / min until full. Vacuumed prior to feeding.						
Measurement 1		Measurement 2		Measurement 3		
V1 [cm^3]	473.42	V1 [cm^3]	413.28	V1 [cm^3]	478.62	
V2 [cm^3]	312.8	V2 [cm^3]	253.2	V2 [cm^3]	322.18	
V3 [cm^3]	300.18	V3 [cm^3]	242.3	V3 [cm^3]	307.57	
V4 [cm^3]	156.33	V4 [cm^3]	97.04	V4 [cm^3]	162.64	
V_{liq} [cm^3]	160.62	V_{liq} [cm^3]	160.08	V_{liq} [cm^3]	156.44	
V_i [cm^3]	12.62	V_i [cm^3]	10.9	V_i [cm^3]	14.61	
V_{gas} [cm^3]	143.85	V_{gas} [cm^3]	145.26	V_{gas} [cm^3]	144.93	
V_{cell} [cm^3]	317.09	V_{cell} [cm^3]	316.24	V_{cell} [cm^3]	315.98	
Average volume of whole cell				316.44	cm^3	
Average volume of liquid space				159.05	cm^3	
Average volume of interface				12.71	cm^3	
Average volume of gas space				144.68	cm^3	
Average volume for the Cell			316.44 ± 1.44			cm^3
Average volume for the liquid space			159.05 ± 5.64			cm^3
Average volume for the interface			12.71 ± 4.61			cm^3
Average volume for the gas space			144.68 ± 1.83			cm^3

As can be clearly seen from these results, the volume of the cell was not determined accurately enough as the error is almost 1.5 cm^3. Therefore a method using the gas tank and nitrogen gas was used to determine the volume. The GFT was pressurized at approximately 1.5 bars and then the pressure was released to the cell. The drop in GFT pressure was logged and the transferred gas amount calculated. From this logged pressure drop, and the pressure rise in the cell the volume of the cell could be determined. The calculation data is available in Table G - 2. The Thompson Tau test was again utilized and one measurement was discarded.

Table G - 2. Measurement results for Cell Volume with Pressure method

Measurement 1		Measurement 2 (Disqualified)		Measurement 3		Measurement 4		Measurement 5	
$P_{GFT,I}$ [Pa]	152243	$P_{GFT,I}$ [Pa]	146864	$P_{GFT,I}$ [Pa]	160190	$P_{GFT,I}$ [Pa]	157367	$P_{GFT,I}$ [Pa]	157268
$P_{GFT,e}$ [Pa]	105338	$P_{GFT,e}$ [Pa]	97634	$P_{GFT,e}$ [Pa]	88203	$P_{GFT,e}$ [Pa]	75963	$P_{GFT,e}$ [Pa]	80553
$P_{Cell,i}$ [Pa]	589	$P_{Cell,i}$ [Pa]	546	$P_{Cell,i}$ [Pa]	609	$P_{Cell,i}$ [Pa]	548	$P_{Cell,i}$ [Pa]	563
$P_{Cell,e}$ [Pa]	24764	$P_{Cell,e}$ [Pa]	25975	$P_{Cell,e}$ [Pa]	37762	$P_{Cell,e}$ [Pa]	42438	$P_{Cell,e}$ [Pa]	39988
V_{GFT} [m^3]	$1.61629 \cdot 10^{-4}$	V_{GFT} [m^3]	$1.61629 \cdot 10^{-4}$	V_{GFT} [m^3]	$1.61629 \cdot 10^{-4}$	V_{GFT} [m^3]	$1.61629 \cdot 10^{-4}$	V_{GFT} [m^3]	$1.61629 \cdot 10^{-4}$
T_{GFT} [K]	296.4	T_{GFT} [K]	296.6	T_{GFT} [K]	296.8	T_{GFT} [K]	298.4	T_{GFT} [K]	298.3
T_{Cell} [K]	300.7	T_{Cell} [K]	300.8	T_{Cell} [K]	300.8	T_{Cell} [K]	301.9	T_{Cell} [K]	301.3
n_{gas} [mol]	$3.076475 \cdot 10^{-3}$	n_{gas} [mol]	$3.226522 \cdot 10^{-3}$	n_{gas} [mol]	$4.714531 \cdot 10^{-3}$	n_{gas} [mol]	$5.304193 \cdot 10^{-3}$	n_{gas} [mol]	$5.000333 \cdot 10^{-3}$
V_{Cell} [m^3]	$3.181987 \cdot 10^{-4}$	V_{Cell} [m^3]	$3.172918 \cdot 10^{-4}$	V_{Cell} [m^3]	$3.173631 \cdot 10^{-4}$	V_{Cell} [m^3]	$3.178068 \cdot 10^{-4}$	V_{Cell} [m^3]	$3.177569 \cdot 10^{-4}$
Measurement 6		Measurement 7		Measurement 8		Measurement 9		Measurement 10	
$P_{GFT,I}$ [Pa]	157552	$P_{GFT,I}$ [Pa]	156939	$P_{GFT,I}$ [Pa]	156896	$P_{GFT,I}$ [Pa]	156295	$P_{GFT,I}$ [Pa]	155914
$P_{GFT,e}$ [Pa]	80803	$P_{GFT,e}$ [Pa]	79743	$P_{GFT,e}$ [Pa]	80228	$P_{GFT,e}$ [Pa]	76034	$P_{GFT,e}$ [Pa]	78970
$P_{Cell,i}$ [Pa]	504	$P_{Cell,i}$ [Pa]	572	$P_{Cell,i}$ [Pa]	552	$P_{Cell,i}$ [Pa]	547	$P_{Cell,i}$ [Pa]	504
$P_{Cell,e}$ [Pa]	39974	$P_{Cell,e}$ [Pa]	40496	$P_{Cell,e}$ [Pa]	40124	$P_{Cell,e}$ [Pa]	41859	$P_{Cell,e}$ [Pa]	40105
V_{GFT} [m^3]	$1.61629 \cdot 10^{-4}$	V_{GFT} [m^3]	$1.61629 \cdot 10^{-4}$	V_{GFT} [m^3]	$1.61629 \cdot 10^{-4}$	V_{GFT} [m^3]	$1.61629 \cdot 10^{-4}$	V_{GFT} [m^3]	$1.61629 \cdot 10^{-4}$
T_{GFT} [K]	298.3	T_{GFT} [K]	296.4	T_{GFT} [K]	297.0	T_{GFT} [K]	297.6	T_{GFT} [K]	297.5
T_{Cell} [K]	301.3	T_{Cell} [K]	300.9	T_{Cell} [K]	300.8	T_{Cell} [K]	300.9	T_{Cell} [K]	300.9
n_{gas} [mol]	$5.002546 \cdot 10^{-3}$	n_{gas} [mol]	$5.063376 \cdot 10^{-3}$	n_{gas} [mol]	$5.018982 \cdot 10^{-3}$	n_{gas} [mol]	$5.242517 \cdot 10^{-3}$	n_{gas} [mol]	$5.028784 \cdot 10^{-3}$
V_{Cell} [m^3]	$3.175392 \cdot 10^{-4}$	V_{Cell} [m^3]	$3.172389 \cdot 10^{-4}$	V_{Cell} [m^3]	$3.172235 \cdot 10^{-4}$	V_{Cell} [m^3]	$3.174352 \cdot 10^{-4}$	V_{Cell} [m^3]	$3.177164 \cdot 10^{-4}$

Appendix G. Rough results for MAPA+DEEA+H_2S measurements

Table G - 3. Volume of the Cell

Average volume of whole cell	317.49 ml	
Average volume for the Cell	317.49 ± 0.25	ml
Average volume for the Cell	0.00031749 ± 0.00000025	m3

As can be seen from Table G - 3, the measurements were considerably more accurate and the volume was found to be 317.5 ml ± 0.3 m